FORMATION AND DISSOLUTION OF MAGNETITE AT HIGH TEMPERATURE AND HIGH PRESSURE IN DIFFERENT ENVIRONMENTAL CONDITIONS

By
VIVEKANAND DUBEY
CHEM01201004019

Bhabha Atomic Research Centre, Mumbai, India

A thesis submitted to the
Board of Studies in Chemical Sciences
In partial fulfilment of requirements
for the Degree of
DOCTOR OF PHILOSOPHY
of
HOMI BHABHA NATIONAL INSTITUTE

February 2018

Certificate
Will be
Uploaded
Soon

STATEMENT BY AUTHOR

This dissertation has been submitted in partial fulfillment of requirements for an advanced degree at Homi Bhabha National Institute (HBNI) and is deposited in the Library to be made available to borrowers under rules of the HBNI.

Brief quotations from this dissertation are allowable without special permission, provided that accurate acknowledgement of source is made. Requests for permission for extended quotation from or reproduction of this manuscript in whole or in part may be granted by the Competent Authority of HBNI when in his or her judgment the proposed use of the material is in the interests of scholarship. In all other instances, however, permission must be obtained from the author.

Vivekanand Dubey

DECLARATION

I, hereby declare that the investigation presented in the thesis has been carried out by me. The work is original and has not been submitted earlier as a whole or in part for a degree / diploma at this or any other Institution / University.

Vivekanand Dubey

Publications in Refereed Journal:

1. "**Effect of cold working on oxidation behaviour and nature of oxide film formed on carbon steel**", Vivekanand Dubey, Supratik Roychowdhury and Vivekanand Kain, *Materials and Corrosion*, **https://doi.org/10.1002/maco.201709895.**
2. "**Synthesis of magnetite by co-precipitation and sintering and its characterization",** Vivekanand Dubey and Vivekanand Kain, *Materials and Manufacturing Processes*, **33(8), 835-839, 2018.**
3. "**Oxidation behaviour of carbon steel: effect of formation temperature and pH of the environment",** Vivekanand Dubey and Vivekanand Kain, *Journal of Materials Engineering and Performance, 26(11), 5312-5322, 2017.*
4. **"Effect of dissolved oxygen on the nature of oxide film on carbon steel",** Vivekanand Dubey and Vivekanand Kain, **Manuscript under preparation**

Conference/Symposium proceedings

1. **"Effect of dissolved oxygen on the corrosion behaviour of carbon steel in simulated reactor environment",** Vivekanand Dubey, Surabhi Bhadauria and Vivekanand Kain, *17th Acian Pacific Corrosion Control Conference (APCCC) 2017*, Paper No 17128.
2. **"Oxide film formed on carbon steel: Effect of pH of the environment",** Vivekanand Dubey and Vivekanand Kain, *Corrosion Conference (CORCON2016),*Paper No. **Paper No: PU16**
3. **"Characterization of oxide film on carbon steel: Effect of formation temperature",** Vivekanand Dubey, Jaskaran S. Boparai and Vivekanand Kain, *Corrosion Conference (CORCON2015),*Paper No. **Paper No: 109**
4. **"Effect of Cold Work on the Electrochemical Behavior of Carbon Steel",** Vivekanand Dubey, Sunil Kumar B, John T. John, Vivekanand Kain and A. V. R. Reddy**,** *Proceedings of ELAC-2013* organized by ISEAC during January 16-20, 2013 at Hyderabad.
5. **"Establishing the solubility limit of magnetite – Synthesis of Magnetite Powder and Effect of Cold Working on Magnetite Formation",** V. Dubey, V. Kain and A. V. R. Reddy, *International conference of FAC-FAC20,1* organized by EDF in cooperation with IAEA and WANO during May 21-24,2013 in Avignon, France.
6. **"Synthesis and characterization of magnetite and hematite powders for establishing solubility in high temperature water",** Vivekanand Dubey, Vivekanand Kain, and A. V. R. Reddy**,** *NMD-ATM 2013,* organized by Indian Institute of Metals Varanasi Chapter during 12-15 November 2013 at IIT (BHU), Varanasi
7. **"Oxidation of magnetite powder: Effect of crystallite size",** Vivekanand Dubey, Vivekanand Kain and A. V. R. Reddy, *organized by society for material chemistry during December 9-13, 2014* at BARC, Mumbai
8. **"Electrochemical Characterization of oxide film formed on the carbon steel: Effect of cold work",** Vivekanand Dubey, Sunil Kumar B., Vivekanand Kain and A. V. R. Reddy, NMT-ATM 2015 organized by IIM Pune Chapter during November 12-15, 2015

DEDICATED

To

My Parents

&

My lovely daughters

Aastha and Geetika

ACKNOWLEDGEMENTS

First, I would like to express my deep and sincere gratitude to my guide Professor and Outstanding Scientist **Dr Vivekanand Kain**, Head MP&CED, BARC for giving the opportunity to register the Ph.D. under him and for his all the support, invaluable guidance, constant encouragement, unstinted inspiration, keen interest and good wishes. His wide knowledge and his logical way of thinking on critical scientific problems have been of great value for me. I acknowledge his excellent input and insightful comments during the preparation of manuscript for journal publication and this thesis.

I am also thankful to **Dr Gautam Kumar Dey, Chairman and Dr P. K. Pujari, Dr A.K. Tyagi and Dr (Smt) Sangita D Kumar, member of Doctoral Committee** for their encouragement, enthusiasm and valuable advice and discussion.

I take this opportunity to thanks my friends in corrosion engineering section of MP&CED, BARC, **Dr Supratik Roychowdhury, Dr Kiran Kumar, Dr Geogy Abraham, Shri Sunil Kumar** and other colleagues for extending their support and help at various stages of this thesis work. Special thanks to **Shri M. J. Patil** for helping me in sample preparation.

I wish to thanks the **Dr Bhaskar Paul, Shri Nachiket Keskar, Shri Naveen Kumar, Shri Sanjay Kumar** for helping me in SEM-EDS work. I also thanks to **Dr Abhishek Mukherjee, Dr S. K. Ghosh and Smt Charu Srivastava** for helping me in XRD analysis.

I also thank to Shri Jaskaran S. Boparai and Ms. Surabhi Bhadauria, Students from PEC University of Technology, Chandigarh for their help during the project.

I also thank to **Dr John T. John** under whom I started my journey in BARC. I wish to thanks all my teachers during my schools and collages who nurtured and shaped my career.

I also take this opportunity to thanks the editor and reviewers of journal for their comments and suggestion in the published paper and also for speedy publication.

I express special thanks to my parents, my brother and my sisters for endless love and support, for being the inspiration my life, and for teaching me that “no adversity and setback is forever”. Last but not the least, I acknowledge and admire **Rajeshwari**, my lovely wife and best friend, for being supportive and compassionate, for believing in me and for all the good things in my life.

Vivekanand Dubey

CONTENTS

ABSTRACT

Flow accelerated corrosion (FAC) is major mode of degradation for carbon steel components in secondary circuit of pressurized heavy water reactors (PHWRs). For FAC the protectiveness of the oxide film formed on the internal surface of carbon steel components plays as important role. It is known that factors like temperature, dissolved oxygen (DO), pH, materials composition and hydrodynamics affect FAC by altering solubility of the oxide film and also affect mass transport in the boundary layer. Therefore the oxide film nature and its formation kinetics play a crucial role for FAC. In this thesis, effects of temperature, DO, pH and cold working of carbon steel on oxidation and nature of oxide film formed has been studied. The inference of the nature of oxide film formed at different parameters was made on the FAC behavior. Solubility of magnetite was studied in simulated secondary circuit parameters of Indian PHWRs.

Cold working of carbon steel was done up to 30% by thickness reduction by cold rolling. Oxidation of the specimens was done in an autoclave at 270 °C in alkaline deoxygenated water chemistry for up to 20 days. Change in the weight measured at different stages was measured to arrive at the kinetics of oxidation. Oxide film was characterized by X-ray diffraction (XRD), Raman Spectroscopy and scanning electron microscopy (SEM). Electrochemical impedance spectroscopy followed by Mott-Schottky analysis was used to establish the type of point defects and defects density present in the oxide film. It was observed that oxidation rate and defect density increased with extent of cold working. Hence it was inferred that the oxide film formed on cold worked material was less protective.

As received specimen were used to study the effect of temperature, pH and DO on oxidation behaviour and nature of oxide formed on carbon steel. Temperature was varied from 150 °C to 300 °C to study the effect of temperature, two pH values (7.0 and 9.5) were used to study the effect of pH and two DO (high DO and low DO) levels were used to study the effect of DO. Defect density in the oxide was found to decease with (a) increase in temperature, (b) increase in DO level and (c) increase in pH value (9.5). Hence the protectiveness of the oxide film was established to increase with increase in temperature, pH and DO level.

To study the solubility of magnetite, magnetite powder was synthesized by co-precipitation method. Co-precipitation gave the nano size of particles of magnetite which were found to easily oxidize to hematite during Raman spectroscopic characterization. Magnetite powder was sintered at 1100 °C for 2 h in an inert atmosphere and then crushed. A two stage sieving was done to get to get uniform and required size of magnetite powder. Characterization after sintering and sieving confirmed the formation of pure magnetite powder with ~ 100 µm size.

A high temperature and high pressure (HTHP) circulation loop was designed and fabricated. This high temperature and pressure circuit had all the wet and high temperature parts made of titanium to avoid interference during analysis for iron ions. Magnetite powder synthesized by the co-precipitation method was exposed in the autoclave in the HTHP circulation loop after getting the desired water chemistry (9.5 pH with ethanolamine). After reaching 150 °C, water sample after interaction with magnetite powder was collected after different durations of the test and analyzed by ion chromatography. Samples collected after 18 h of exposure gave the saturated value (47 ppb) of iron in the solution.

List of Figures

List of tables

List of Abbreviations

AR	As Received
ASTM	American Society for Testing and Materials
BCC	Body Centered Cubic
CS	Carbon Steel
CW	Cold worked
DM	De-mineralized
DO	Dissolved Oxygen
ECN	Electrochemical Noise
EDS	Energy Dispersive Spectroscopy
EIS	Electrochemical Impedance Spectroscopy
ETA	Ethanol Amine
FAC	Flow Accelerated Corrosion
FCC	Face Centered Cubic
GDOES	Glow Discharge Optical Emission Microscopy
GI-XRD	Grazing Angle X-Ray Diffraction
HDO	High Dissolved Oxygen
HTHP	High Temperature and High Pressure
HV	Vicker's Hardness
IC	Ion Chromatography
LDO	Low Dissolved Oxygen
MLRS	Micro Laser Raman Spectroscopy
MS	Mott-Schottky
OCP	Open Circuit Potential
PCR	Post Column Reagent
PDM	Point Defect Model
PHT	Primary Heat Transport System
PHWR	Pressurized Heavy Water Reactor
SCE	Saturated Calomel Electrode
SEM	Scanning Electron Microscope
SS	Stainless steel
XRD	X-Ray Diffraction

Chapter 1

INTRODUCTION

1.0 Introduction

Carbon steel is extensively used as structural material for a majority of components in the primary and secondary circuits of pressurized heavy water reactors (PHWRs) and also for other types of nuclear reactors. The feed water system of Indian PHWRs is made of carbon steel ASTM A106 Gr B [Kain et al., 2008, 2011, 2014]. The major mode of degradation of these secondary circuit components/pipelines is flow accelerated corrosion (FAC). FAC causes thinning of carbon steel components/pipelines carrying high velocity water/steam. The secondary circuit components are exposed to temperatures up to 200 °C and the process fluid is de-aerated alkaline water, pH adjusted by ethanolamine (ETA) or ammonia [Kain et al., 2008, 2011, 2014]. It is known that FAC is electrochemical dissolution of the protective magnetite film (formed on the internal surfaces of carbon steel pipelines/components) at a faster rate in a high velocity environment. It has been reported that FAC has caused a large number of failures in piping used in all types of fossil, industrial steam and nuclear power plants [Kain el al., 2011, Dooley el al., 2000, Moon el al., 2005].

During the operation of plants at high temperature and in low dissolved oxygen (DO) process fluid, magnetite (Fe_3O_4) film forms on the internal surface of the carbon steel pipings and components. The magnetite film protects the component from further corrosion. Hence the nature of this oxide film dictates the corrosion behaviour of the underneath material. FAC depends on parameters like hydrodynamics, temperature, dissolved oxygen content, pH of the environment, chemical used in the environment and material composition. It has been explained in the literature that these parameters affects FAC by affecting the (bulk) solubility of ionic species and their mass transport in the boundary layer [Dooley et al., 2000, Betova et al., 2010, Sweeton et al., 1970, Tremaine et al., 1980]. Temperature affects FAC by influencing two processes, namely, diffusion of ionic (dissolved) species and its solubility in the bulk water [Betova et al., 2010, Sweeton et al., 1970]. With increase in temperature diffusion increases while solubility decreases. Hence there is a temperature (150-170 °C) where a maximum rate of FAC is observed [Betova et al., 2010, Sweeton et al., 1970]. Therefore, any parameter that affects solubility of dissolving species plays a role in FAC behaviour.

Dissolved oxygen also affects FAC rate by altering the nature of the oxide film. Dissolved oxygen present in the process fluid also alters the solubility by changing the redox potential of the environment. Also, the nature of oxide formed due to different DO levels (haematite/magnetite) primarily affects FAC rate. Presence of DO converts the magnetite (Fe_3O_4) to hematite (Fe_2O_3) or γ-FeOOH that has a very low solubility compared to that of the former [Dooley et al., 2000]. The pH value affects FAC by affecting the solubility of magnetite. The solubility of magnetite is reported [Fujiwaraa et al., 2011] to be minimum in the pH range 8.8-9.3. In FAC process, the magnetite film dissolves reductively; hence, the chemicals used for maintaining the pH and dissolved oxygen play an important role. The chemicals having reducing nature facilitate faster dissolution; hence, increase FAC rate. Material parameters affecting FAC include alloying elements in the carbon steel e.g. Cr, Mo and Cu and possibly cold working in the material. Similarly bends/reducers made up of carbon steel are known to show accelerated effect of FAC mainly due to hydrodynamic aspects. However, if there is any role of cold working in forming an oxide layer, that inherently makes the carbon steel more prone to FAC, is not known.

Role of various parameters viz. pH, temperature, DO and materials condition (cold working) on solubility and mass transfer has been reported in literature to some extent. However, their role on the oxide film formation and its nature has not been clearly established.

The objective of the thesis is two-fold:- (a) to establish the effect of various environmental parameters., viz; temperature, pH, dissolved oxygen levels and extent of cold working on the oxidation kinetics and nature of oxide formed on carbon steel and (b) to synthesize magnetite powder by co-precipitation method and establish its solubility behavior in simulated secondary circuit environment.

1.1 Roadmap

The objectives of the thesis were achieved following the road map as described below.

a. Effect of cold working on oxidation behaviour and nature of oxide film formed on carbon steel

Most of the failure analyses in the secondary circuit of PHWRs and modeling reported so far showed that the location of turbulence like elbow, bends, expanders, reducers are susceptible to FAC. It was attributed to increased mass transport due to turbulence/velocity [Kain et al., 2008, Moon el al., 2005, Betova et al., 2010]. However, the nature of protective oxide film formed on these locations has not been studied. The aim of the present work is to establish the effect of cold working on oxidation behaviour of carbon steel and the nature of oxide film formed on such a cold worked material.

b. Effect of formation temperature and pH of the environment on oxidation behaviour of carbon steel

Effect of temperature and pH on FAC rate has been explained on the basis of solubility of the oxide film formed on the carbon steel. There is no study relating the nature of oxide film on the formation temperature and pH of the environment. The aim of the present work is to establish the effect of formation temperature and pH of the environment on oxidation behaviour of carbon steel and to characterize the oxide film.

c. Effect of dissolved oxygen on the corrosion behaviour of carbon steel

Presence of dissolved oxygen in the environment significantly reduces FAC rate. This is attributed to the conversion of magnetite to hematite by DO. Hematite has a lower solubility than magnetite. There is no systematic study regarding this conversion of hematite. Also very less knowledge is available regarding the nature of hematite layer converted due to high DO from the previously formed magnetite layer (formed in low DO conditions). The aim of the present work is to establish the effect of dissolved oxygen on corrosion/oxidation behaviour of carbon steel and characterize the oxide film.

d. Synthesis and Characterization of magnetite powder

To study the solubility of magnetite, magnetite powder of high purity and desired size is required. Magnetite powders used by researchers for solubility study were synthesized by using iron powder [Sweeton et al., 1970, Tremaine et al., 1980]. Magnetite powder synthesized by co-precipitation methods is reported to produce nano-crystalline powder used for some other applications [Martínez-Mera et al., 2007, Mamania et al., 2016, Petcharoen et al., 2012, Khoshnevisan et al., 2016]. Coarse magnetite powder synthesis by co-precipitation method has not been used by any researchers. The aim of the present work is to synthesize the required size of magnetite powder by co-precipitation method and characterize it for purity and size and uses it in the solubility study.

e. Solubility study of magnetite

Solubility of magnetite has been studied by a few researchers with respect to pH and temperature of the environment. The chemicals typically used to maintain the pH value are HCl, NaOH, ammonia etc. The pH developed at high temperature is a function of chemicals used to maintain pH. Depending on the dissociation behavior of the chemical, pH at high temperature would be different for solutions prepared by different chemicals having the same pH at room temperature. The pH has been clearly shown to affect FAC by altering solubility of corrosion products. Therefore the role of pH is studied to determine the pH level (using ETA) at which the solubility would be minimum. Hence in plants, such a determined pH level that results in low solubility of magnetite can be aimed and maintained to minimize FAC.

1.2 Structure of the thesis

The thesis comprises of nine chapters. The current *Chapter 1* gives introduction to the topic and key knowledge available on the topic of magnetite film formation. Gap areas in available knowledge are highlighted and objectives of the thesis are defined. *Chapter 2* gives a detailed review of the literature in the published domain on the topics relevant to this thesis. Each of the next five chapters (*Chapters 3-7*) deals with the experimental results/observations and their discussion on one particular aspect of the objectives as mentioned in section 1.1. *Chapter 3* gives the effect of cold working of carbon steel on oxidation behavior and the nature of the oxide film formed. The effect of cold work on kinetics of oxidation and defect densities in the oxide film were determined and correlated to FAC. *Chapter 4* gives the effect of temperature and pH on oxidation kinetics of carbon steel and nature of oxide film formed. The effect of temperature and pH on kinetics of oxidation and defect densities in the oxide film were determined and possible effects on FAC were indicated. *Chapter 5* gives the effect of dissolved oxygen levels in the water on corrosion/oxidation behavior of carbon steel. *Chapter 6* deals with the method for synthesis of coarse magnetite powder to be used for the solubility study. The magnetite powder was synthesized by co-precipitation method followed by sintering in an inert atmosphere and crushing and was then characterized. *Chapter 7* presents the results of the measurement of solubility of magnetite at given parameters using a high temperature and high pressure loop specially fabricated for the purpose. *Chapter 8* summarizes the overall conclusions drawn from the results obtained and analysis done in the doctoral project. Finally, *Chapter 9* of the thesis lists some of the additional research possibilities in this field.

Chapter 2

LITERATURE REVIEW

2.0 Carbon steel and its applications

2.1. Composition and phases: Carbon steel is a generic term used for the alloy of iron containing carbon less than 2% and only residual quantities of other elements. Aluminum is added for de-oxidation, with silicon and manganese limited to 0.6% and 1.65% respectively [Avner H. S., 1974]. The carbon content can vary depending on the grade, and mostly is between 0.005% and 2.0% by weight. As per American iron and steel institute (AISI) a steel is considered to be carbon steel when no minimum content is specified or required to be specified for Al, Cr, Co, Mo, Ni, Ti, W, V, Zr or any other element added to obtain a desired alloying effect and when the specified Cu (min) ≤ 0.40, & Cu (max) ≤ 0.60, Mn (max) ≤ 1.65, Si (max) ≤ 0.60. The commonly used classification of carbon steels is based on weldability and the need for pre or post weld heat treatments. Therefore low carbon steels have carbon content less than 0.30 wt% and do not require pre or post weld heat treatments. Medium carbon steels have carbon from 0.30 wt.% to 0.60 wt.% and require pre weld heat treatment. High carbon steels have carbon above 0.60 wt.% and require both pre and post weld heat treatments. Typical disadvantages of carbon steels are – (a) they cannot be strengthened beyond 690 MPa without substantial loss of ductility and impact strength, (b) large section thicknesses cannot be produced with martensite throughout (i.e. not deep hardenable), (c) low corrosion and oxidation resistance, (d) medium carbon steels need to be quenched very fast to get full martensite structure leading to distortion and cracking and (e) poor impact resistance at low temperatures.

Phase diagram of iron-carbon is important as it helps in arriving at parameters of heat treatments, phase composition, control of property and solid-state reactions [William et al.,2001]. In addition, phase diagram also provides information about melting, casting, recrystallization etc. Figure 2.1 shows the iron-carbon equilibrium diagram. Phases present in the phase diagram are:

(a) α-ferrite: Solid solution of carbon in body centered cubic (BCC) iron. This is stable form of iron and maximum amount of carbon present in this phase is 0.022% at 727 °C.

(b) γ-austenite: solid solution of carbon in face centered cubic (FCC) iron. Maximum solubility of carbon in this phase is 2.14%. It is not stable below 727 °C (eutectic temperature) unless cooled rapidly.

(c) δ-ferrite: Solid solution of carbon in BCC iron. This has the same structure as α-ferrite but is stable at high temperature, above 1395 °C.

(d) Cementite: this is an intermetallic compound of iron and carbon and also called as iron carbide (Fe_3C) and readily forms at 6.67 wt% C.

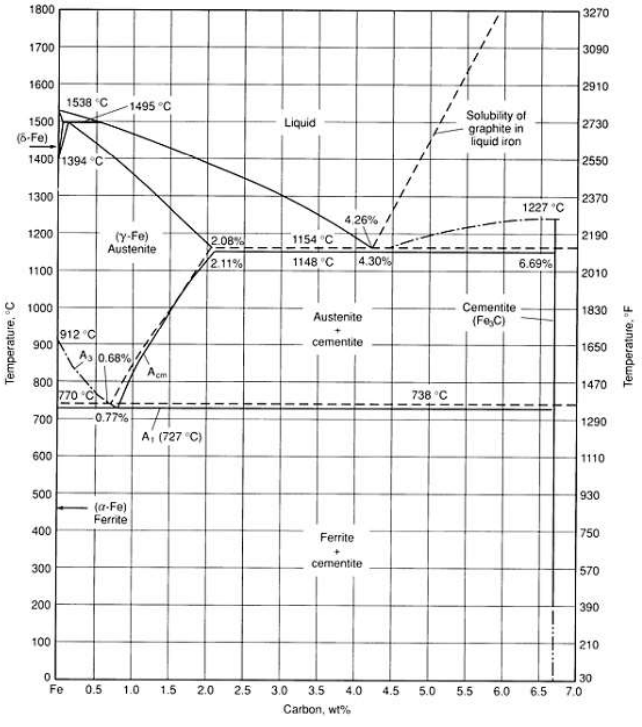

Figure 2.1 Iron-carbon phase diagram [ASM Hand book, vol. 1, 1990]

2.2 Microstructure of carbon steel

The phases present in the phase diagram can be classified based on their crystal structure. The structure of carbon steel depends on many parameters like concentration of each elements, temperature, cooling rate and the amount of cold work performed on the steel [Higgins 1994]. The different microstructural features in carbon steel are described below:

a. Ferrite: α-iron (crystal structure BCC)

b. Austenite: γ-iron (crystal structure FCC)

c. Delta Iron: δ-iron, (crystal structure BCC and exists at high temperature)

d. Cementite: iron carbide and most brittle phase, (crystal structure orthorhombic)

e. Pearlite: alternate platelets of ferrite and cementite

f. Martensite: This phase forms when austenite phase is rapidly cooled (crystal structure body centered tetragonal, BCT)

g. Bainite: If the steel is cooled such that formation of pearlite does not take by short range diffusion of iron, formation of bainite takes place.

A typical ferrite-pearlite structure is shown in figure 2.2.

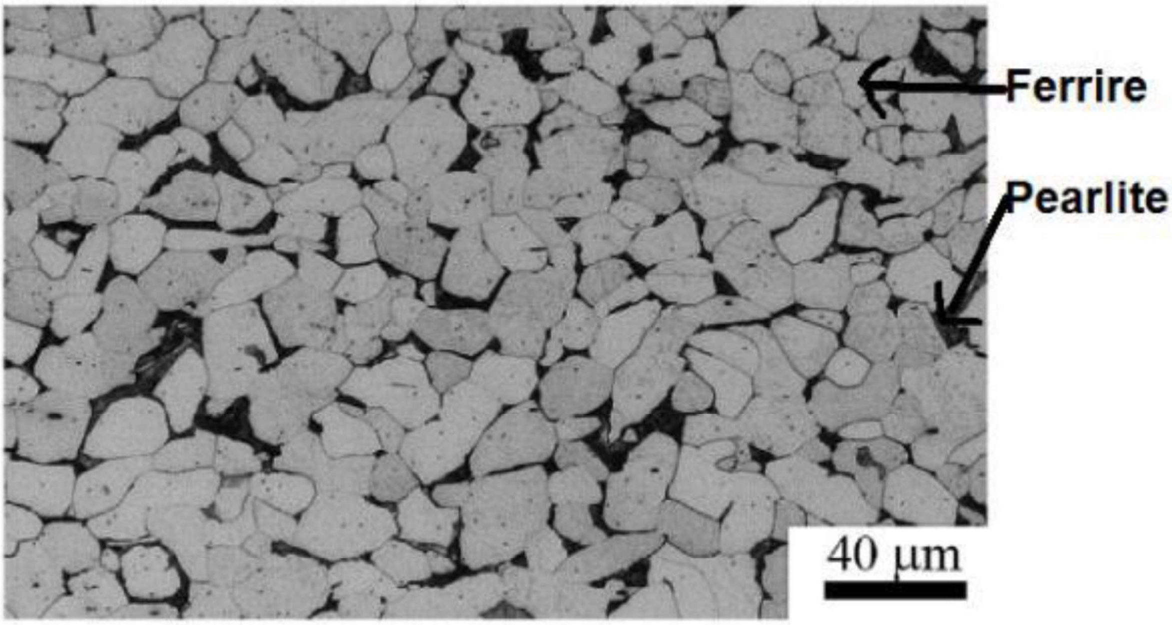

Figure 2.2 Typical ferrite-pearlite microstructure of carbon steel

2.3. Applications of carbon steel

Carbon steels have found many applications in day to day life. The pipelines used to carry domestic water are made of carbon steel. Carbon steel has found many applications in transport industries viz. trucks, trains, ships, anchor chain, jet engine components etc. Carbon steels are also used in construction industries, packaging industries, appliances industries. Carbon steel has a wide range of application in energy industries. All segments of energy sector including nuclear, wind power, thermal and fossil powder plants demand carbon steels for infrastructure and structural materials. Pipelines to carry high temperature and high pressure water in nuclear and fossil power plants are made of carbon steel.

In nuclear reactor, main materials of construction for recirculation pipelines in primary heat transport (PHT) system and secondary feed water system of pressurized heavy water reactor (PHWR) are carbon steel. In PHT, carbon steel components are exposed to the primary water environment, parameters of which are given in table 2.1 [Kiran Kumar at al. 2010]

Table 2.1: Typical water chemistry of PHT in 220 MWe PHWR

pH	10-10.3 by LiOH
DO	< 5 ppb
Temperature	249 – 292 °C

Secondary circuit of PHWR carrying feed water has the following water chemistry, given in table 2.2.

Table 2.2: Typical water chemistry of secondary circuit in PHWR

pH	8.8-9.5 by ethanol amine
DO	< 5 ppb
Temperature	90 – 250 °C
Hydrazine	50-200 ppb

The carbon steel components, during service, are exposed to high temperature and high pressure water and undergo oxidation leading to formation of a uniform oxide layer over the component surfaces. In low dissolved oxygen conditions, the oxide film formed in high temperature aqueous environment is magnetite [Kain et al., 2010]. This oxide film is adherent and protective, presence of which minimizes further corrosion of carbon steel. However, the oxide film also gets dissolved in the environment. The dissolution rate of this oxide film gets enhanced by flowing environment and electrochemical action. The enhancement of dissolution rate of the protective oxide film formed over surface of carbon steel is known as **flow accelerated corrosion (FAC).**

2.4 Flow Accelerated Corrosion

Flow accelerated corrosion is the dissolution of the protective oxide film formed on the internal surface of pipeline and components carrying high temperature water/wet-steam. FAC causes wall thinning (metal thickness loss) of carbon steel piping, tubing, elbow, bends, reducers and other components exposed to flowing water or wet steam. When the thickness of the component reaches values lower than the critical thickness required for supporting the operating stresses, it results in ductile failure of the component. If undetected, the degraded components can suddenly rupture, releasing high temperature steam or water. FAC has caused a large number of failures in piping and equipments in all types of fossil, industrial steam, and nuclear power plants and it is a predominant mode of failure of pipelines in the secondary circuit and has also affected carbon steel pipelines in the primary circuit of light water reactors.

In the operating conditions of nuclear power plants and fossil plants where carbon steel components are exposed to high temperature and high pressure de-oxygenated water or wet steam, protective magnetite film formation takes place on the internal surfaces. FAC occurs when the magnetite film dissolves into the flowing process stream and the magnetite film becomes thin and less protective. Even though this magnetite film is present, the rate of dissolution of oxide and the carbon steel underneath is enhanced by the flowing environment. FAC is a corrosion process the rate of which is enhanced by electrochemical dissolution and mass transfer by the flowing environment. FAC is thus, an extension of the generalized carbon steel corrosion process in stagnant water.

FAC is classified as single phase FAC and two phase FAC based on the phase of the environment. Single phase FAC occurs in liquid phase and two-phase FAC occurs in wet steam. These two forms of FAC can be distinguished on the basis of appearances of the affected surface. The signature pattern of single phase FAC is orange peel structure whereas that of two-phase FAC is tiger stripes as shown in figure 2.3 [Kain et al., unpublished report].

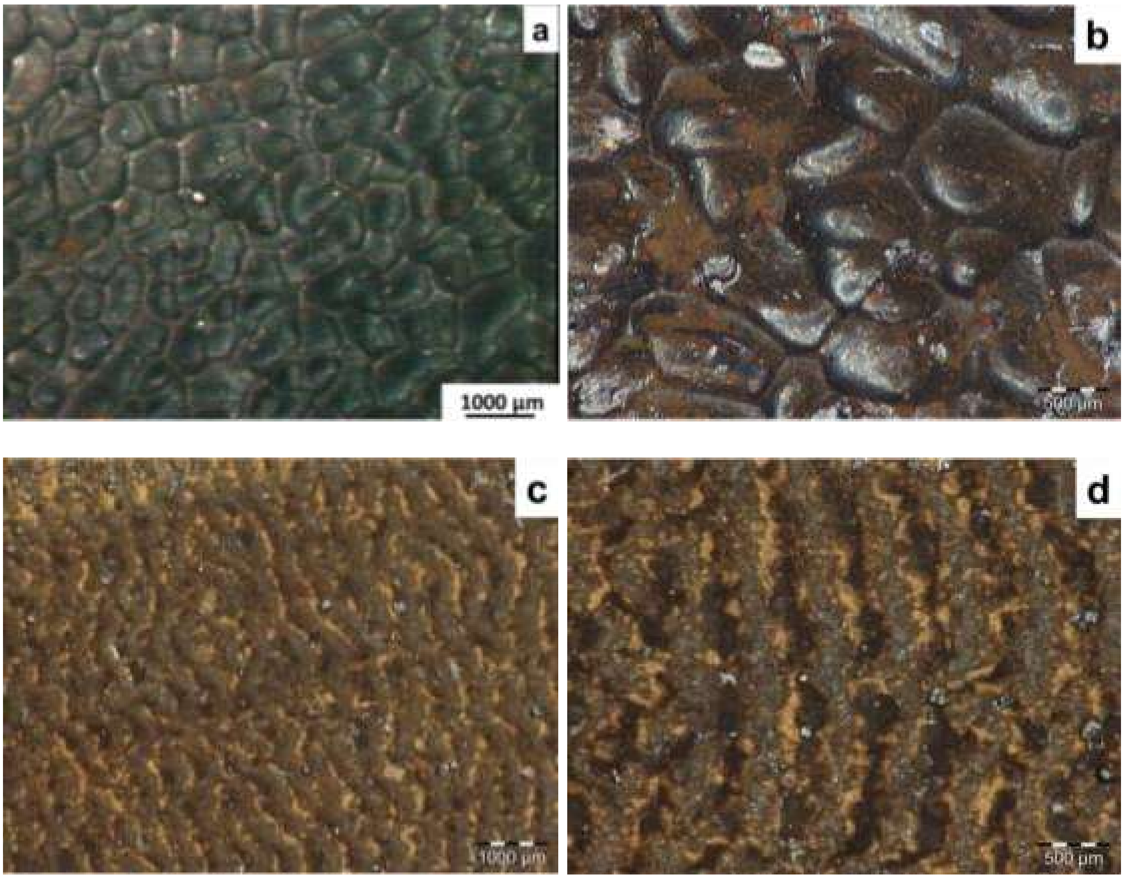

Figure 2.3 Stereomicroscopic images showing the signature pattern (a-b) scallops, single phase FAC and (c-d) tiger stripes, two-phase FAC [Kain et al., unpublished report].

2.4.1 Mechanism of FAC

Figure 2.4 [Kain, 2014] schematically illustrates the mechanism of FAC. Following are the reaction steps involved in the process of FAC.

2.4.1.1. Generation of ionic species of iron at the oxide-water interface:

Iron oxidizes (Eq. 2.1) at oxide-water interface to give ferrous ions (Fe^{2+}) and the Fe^{2+} diffuses through the oxide film. Magnetite film also reductively dissolves (Eq. 2.2 and 2.3) to give dissolved iron species at the oxide-water interface. Thermodynamic equilibrium is achieved at oxide-water interface and concentration of iron species is saturated. This layer is called saturated layer.

$$Fe = Fe^{2+} + 2e^{-} \tag{2.1}$$

$$2H_2O + 2e^{-} = 2OH^{-} + H_2 \tag{2.2}$$

$$Fe^{2+} + nOH^{-} = Fe(OH)^{(2-n)} \tag{2.3}$$

2.4.1.2. Transportation of Ferrous ions into the fluid stream through the boundary layer

The concentration of dissolved species in the saturated layer is significantly higher than that in the bulk solution. Hence, the soluble species diffuse from saturated layer to bulk solution through a diffusion layer as shown in Figure 2.4.

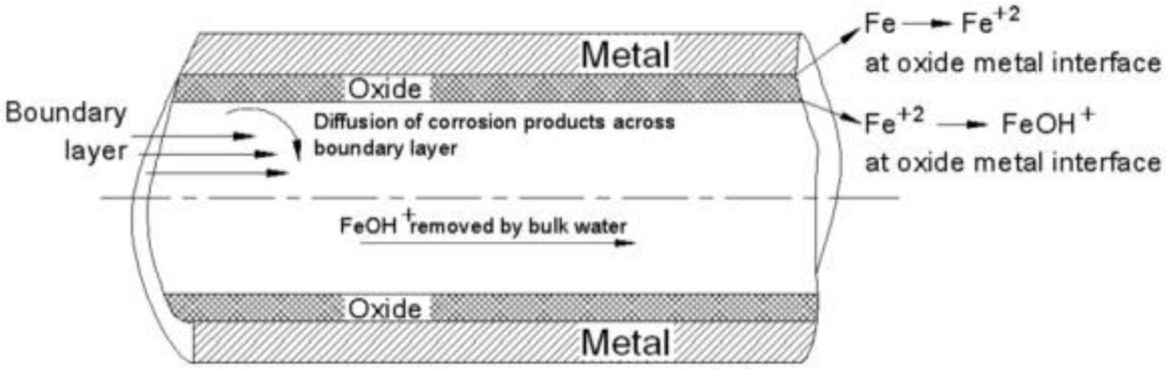

Figure 2.4 Schematic representation of the mechanism of flow accelerated corrosion (FAC) [Kain 2014].

Considering the mass transfer coefficient of the soluble species (M) as K_M, and $C_{S,M}$ and $C_{\infty,M}$ as the concentration of M in the saturated layer and the bulk solution, respectively, FAC rate can be represented in a simplified form using equation 2.4 [Kain 2014].

$$\text{FAC rate} = K_M \cdot (C_{S,M} - C_{\infty,M}) \qquad (2.4)$$

The FAC rate depends on mass transfer coefficient and solubility of the soluble species. Once the dissolved ionic species reach the bulk solution from saturated layer through diffusion layer, the value of $C_{\infty,M}$ increases and attains the value of $C_{S,M}$, thereby reducing further dissolution (in stagnant condition). If the environment is in flowing condition, it provides fresh solution to come in contact with magnetite/carbon steel. The value of $C_{S,M} - C_{\infty,M}$ remains high in case of flowing environments and FAC takes place. Flow also decreases the diffusion layer thickness and facilitates faster diffusion of dissolved ions [Kain 2014]. Therefore, FAC is mainly governed by the flow velocity/turbulence affecting the boundary layer present inside of the pipeline/component and also by the bulk solubility limit of the dissolving ions at the operating parameters.

2.4.2 Parameters Affecting FAC

As explained in the mechanism of flow accelerated corrosion, FAC depends on mass transport and solubility of the dissolved ions species [Betova et al., 2010]. The mass transport and the solubility of the dissolved species are affected by following parameters and hence these parameters affect FAC.

a. Hydrodynamics

b. Temperature

c. Dissolved oxygen

d. pH of the environment

e. chemicals used for pH

f. Materials composition

a. Hydrodynamics

Hydrodynamic factors such as flow velocity, type of flow (laminar or turbulent), geometry and surface roughness have an influence on FAC. Event of occurrence of FAC in straight pipe section is very less. FAC mostly occurs at the locations of flow disturbance such as elbows, tight bends, downstream of the valve or orifice [Poulson, 1999, Jevec et al., 2003]. At the location of flow disturbance the flow becomes turbulent and as a result the local velocity increases several fold. The turbulent flow also decreases the diffusion layer thickness [Betova et al., 2010]. Hence this local increase in velocity and decrease in diffusion layer thickness significantly increases the mass transport from the saturated layer at oxide water interface to the bulk of environment and hence increases FAC rate.

b. Temperature

The temperature effect on FAC rate is actually not direct but the "bell" shaped dependence of FAC rate on the temperature is due to two counteractive processes. The concentration of dissolved ions or solubility of the ions decreases with increase in temperature [Tremaine et al., 1980]. Thus at lower temperature the solubility is higher i.e. it can accommodate more corrosion product (dissolved ions). Hence the removal of dissolved ions from the materials is higher at lower temperature. But at the same time, flow viscosity and dissolved ions diffusivity which affect the mass transfer decreases with decrease in temperature. This implies that Cm is the highest at a low temperature and Km is the highest at a higher temperature. Because of these two competing processes we get a 'bell' shaped curve as shown in figure 2.5 [Remy F.N. et al., 1992]. The maxima in FAC is taken at 170 C (figure 2.5).

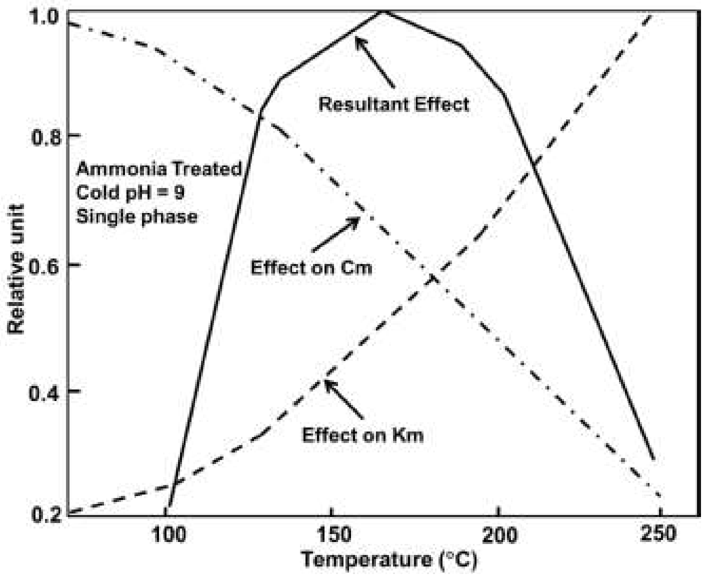

Figure 2.5 Calculated effect of temperature on relative FAC rate [Remy F.N. et al., 1992]

c. Effect of dissolved oxygen

Dissolved oxygen plays an important role on the composition of oxide film formed on carbon steel in process water at high temperature and pressure. In presence of dissolved oxygen, there is formation of ferric oxide hydrate (FeOOH) or hematite (Fe_2O_3) [Dooley et al., 2000] which goes inside the pores of magnetite. Ferric oxide layer functions as a boundary barrier for the inward diffusion of oxygen to the base material and Fe^{2+} ion transport from the steel surface through the magnetite layer. The presence of FeOOH and Fe_2O_3 also reduces the overall solubility of the oxide layer, because FeOOH and Fe_2O_3 have lower solubility [Dooley et al., 2000] than Fe_3O_4. The rate of conversion of Fe_3O_4 to FeOOH or Fe_2O_3 depends on the degree of oxidizing conditions.

d. Effect of pH

The pH of the environment affects FAC rate by changing the solubility of the dissolved ions in the environment. The dissolution of magnetite involves a reduction reaction and is therefore dependent on stable E-pH regimes. The pH value at temperature has an influence on the solubility. The E-pH diagram of iron water system at 150 °C is given in figure 2.6.

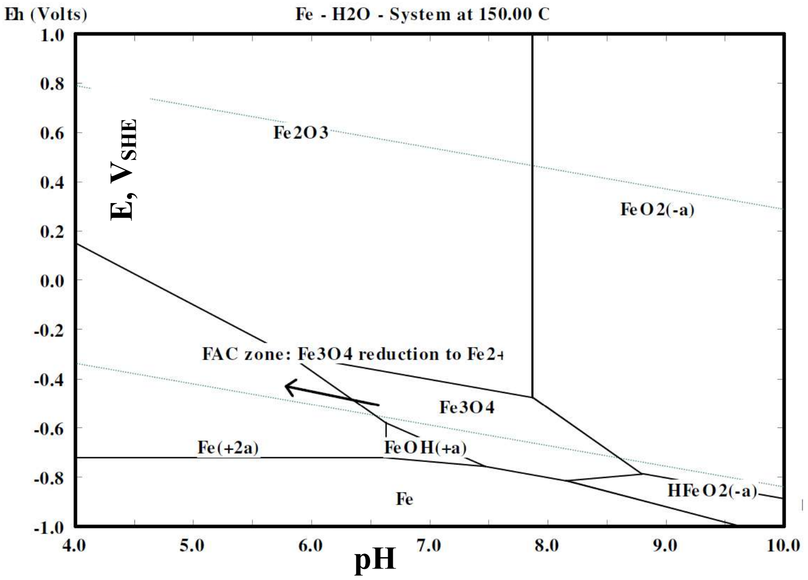

Figure 2.6 The E-pH diagram of Fe-water system at 150 °C and the area of FAC, where magnetite reduction to ferrous ions occurs [Betova et al.,2010].

The pH value affects FAC rate by changing the solubility of magnetite in the environment. The effect of pH on the solubility is also dependent of temperature. At acidic pH (3.0-4.0) where solubility is very high, there is not much effect of temperature [Tremaine et al., 1980]. At alkaline pH values of ~11.5, solubility of magnetite increases with temperature (figure 2.7). There is an inversion of solubility at 300 °C at a pH above 9.8 and this explains enhanced FAC in PHT circuit of PHWRs for feeder pipelines [Kain, 2014].

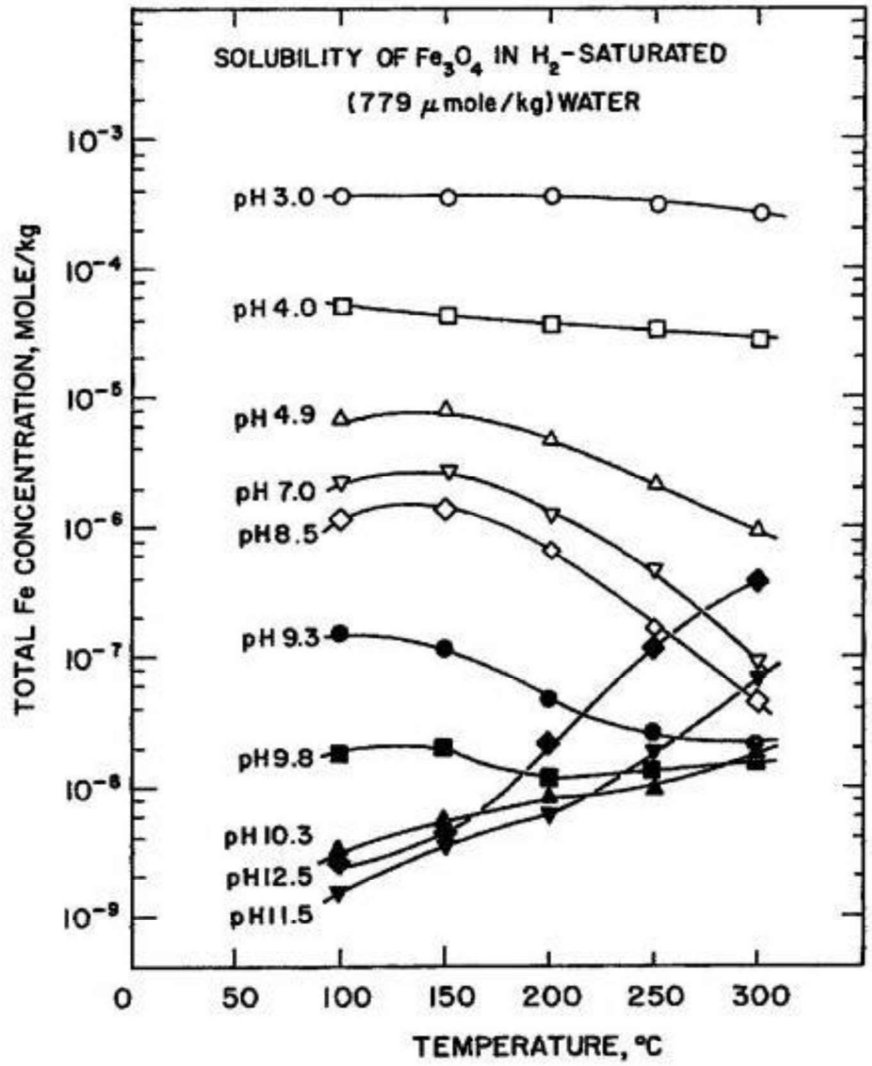

Figure 2.7: Effect of temperature on the solubility of magnetite at different pH values [Tremaine et al., 1980].

e. Effect of chemical addition

The dissolution of magnetite is a reduction reaction and oxidation-reduction potential is an important parameter for FAC. Any chemical used in the environment that is reducing in nature will facilitate the reduction of magnetite and as a result FAC rate will increase [Dooley 2008, Machiels et al., 2005, Jevec et al., 2003]. However, pH of the solution (at high operating temperature) after chemical addition is the main determining factor.

f. Material composition

Addition of alloying elements like Cr and Cu significantly influences FAC rate of carbon steel [Cubicciotti 1988]. Alloying Cr modifies the type of surface oxide film formed. In plain carbon steel, magnetite (Fe_3O_4) film is formed during operation at high temperature and low dissolved oxygen environment. Alloying carbon steel with small amount of Cr is known to promote formation of iron chromite ($FeCr_2O_4$ i.e. $FeO.Cr_2O_3$) during HTHP oxidation. The solubility of $FeCr_2O_4$ is known to be significantly (~ 1000 times) less than that of magnetite [Cubicciotti 1988]. Thus due to formation of less soluble iron chromite, FAC rate decreases. Also due to lower solubility of $FeCr_2O_4$, increase in the time of exposure results in the enrichment of Cr in the oxide. This further decreases FAC rate.

Effect of Cr on FAC rate is considered to be time-dependent [Chexal 1998]. According to theoretical model of Bouchacourt, FAC rate is predicted to decrease with Cr, the decrease becoming more pronounced over time (figure 2.8). This is supposedly due to:

- Reduction of oxide porosity progressively with as chromium concentration increases.
- Reduction of oxide solubility as the oxide is enriched with chromium.
- Increase of oxide thickness over time.

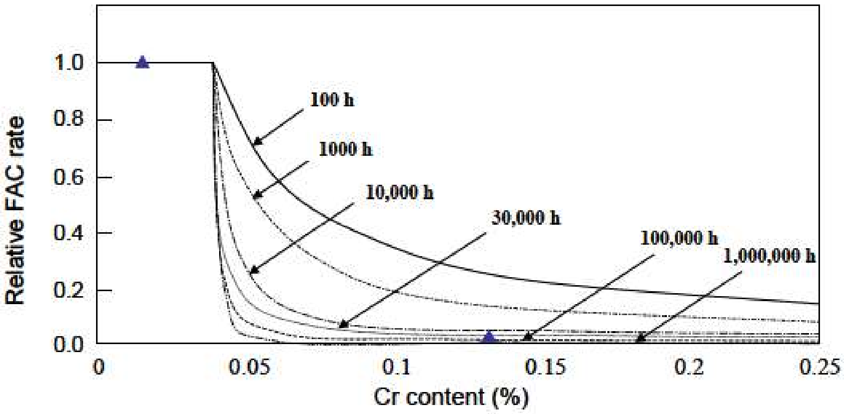

Figure 2.8 Bouchacourt model where effect of chromium content and time dependency of FAC rate are described [Chexal, 1998].

Alloying with Cu also decreases FAC rate. However, the way Cu addition influences FAC rate is different. There is no formation of Fe-Cu oxide in the nuclear power plants (NPPs) water environment. In the operating conditions, iron is oxidized to form magnetite which then dissolves into flowing water; while metallic Cu remains on the surface of the carbon steel, keeps building up with time and acts as physical barrier that impedes the passage of iron to the oxide or environment.

Hence these factors (temperature, DO, pH, materials composition, hydrodynamics etc.) affect FAC by affecting solubility of the dissolved ions and their mass transport. The nature of the oxide film formed on the surface plays an important role in FAC.

2.5 Oxidation of carbon steel in aqueous environment

Oxidation/Corrosion of carbon steel has been studied extensively in high temperature electrolytes [Robertson et al., 1989, 1991, Subramanian et al., 2014, Kiran Kumar et al., 2010, Bojinov et.al, 2009, Sinha et al., 2015]. In high temperature, high pressure, low dissolved oxygen aqueous medium, adherent protective magnetite (Fe_3O_4) film forms on the surface [Robertson et al., 1989, 1991, Subramanian et al., 2014, Kiran Kumar et al., 2010, Bojinov et.al 2009, Sinha et al.,., 2015]. Mechanism of oxide film formation is very well established in literature [Robertson et al., 1989, 1991]. Oxide film forms by two processes (a) by growth process in which base metal directly reacts with environment at high temperature and pressure and forms magnetite film at metal-oxide interface, (b) by precipitation in which the iron ions dissolved in the bulk solution precipitate back on the oxide outer surface. This renders a duplex morphology to the magnetite film formed containing compact inner layer having a very fine crystalline structure and an outer layer layer consisting of coarse crystallites [Robertson et al.,1989, 1991, Subramanian et al., 2014, Kiran Kumar et al., 2010]. Depending upon the redox potential there may be formation of hematite also [Dooley et al., 2000].

2.5.1 Oxides of iron.

Iron can form different type of oxide. These oxide are tabulated in table 2.3

Table 2.3: List of different iron oxides

Name of oxide	Formulae	Remarks
wustite	FeO	face centered cubic
magnetite	Fe_3O_4	inverse spinel structure
hematite	α-Fe_2O_3	hcp array of oxide ions with Fe^{3+} occupying octahedral sites
maghemite	γ-Fe_2O_3	inverse spinel structure

The α-Fe_2O_3 possesses a corundum structure i.e. hcp array of oxide ions with Fe^{3+} occupying octahedral sites [Cotton et al., 1976, Robertson 1989, 1991]. Wustite (FeO), magnetite (Fe_3O_4) and γ-Fe_2O_3 are structurally closely related having a closed packed cubic sub lattice of oxide ions (O^{2-}) [Robertson 1989, 1991, Gerischer, 1989, Davenport et al., 1995]. Wustite (FeO) have face centered cubic structure of NaCl type [Kofstad 1988]**.** The Fe_3O_4 and γ-Fe_2O_3 possess inverse spinel structure. Magnetite has an inverse spinel structure with eight ferric ions at tetrahedral sites and eight ferric and eight ferrous ions at octahedral sites [Gerischer 1989, Davenport et al., 1995]. The unit cell of the magnetite has formula $(Fe_8^{3+})_t[Fe_8^{3+}Fe_8^{2+]}_oO32$ [Zhuo et al.,., 2001, Cornell et al.,., 1996, Verwey et al.,., 1947, Dobson et al.,., 1970]. In γ-Fe_2O_3, 24 cation sites in the unit cell are occupied randomly by 21 1/3 ferric (Fe^{3+}) ions [Gerischer 1989, Davenport et al., 1995]. Crystal structures of different oxides like wustite, magnetite and hematite are given figure 2.9 [Parkinson et al., 2016].

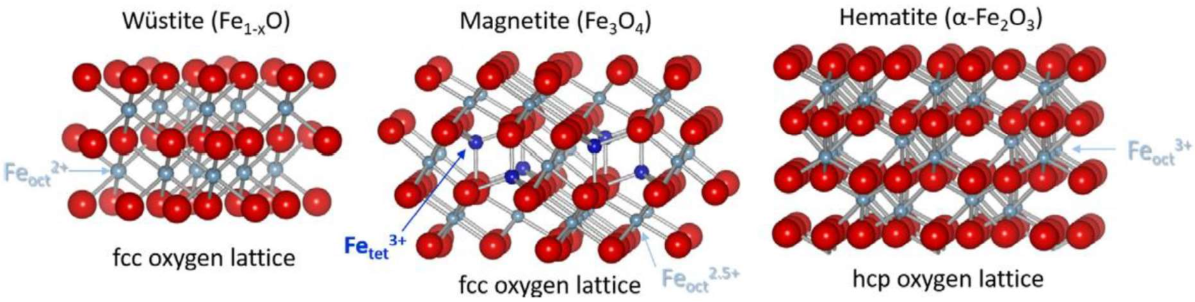

Figure 2.9: Crystal structure of iron oxides [Parkinson et al.,2016]

2.5.2 Formation of oxide film on carbon steel surface

As described in 2.5.2, in high temperature and low dissolved oxygen concentration formation of magnetite film involve two processes *viz.* growth and precipitation. In growth process, the reaction between iron and water takes place at high temperature and pressure and results in the formation of magnetite as per equation 2.5 [Robertson**,** 1989].

$$Fe + H_2O = Fe_3O_4 + H_2 \qquad (2.5)$$

In precipitation process, the oxidized iron ion (Fe^{2+}) reacts with hydroxide ions of the aqueous environment and forms ferrous hydroxide as per equations 2.6 and 2.7. As the concentration of soluble iron species becomes high and exceeds the solubility limit, the dissolved iron species gets precipitated back as magnetite on the outer surface of the magnetite layer. This reaction is called Schikorr reaction, equation 2.8 [Robertson 1989, Frayne 2002, Rihan et al., 2006].

$$Fe = Fe^{2+} + 2e \qquad (2.6)$$

$$Fe^{2+} + 2OH^- = Fe(OH)_2 \qquad (2.7)$$

$$Fe(OH)_2 = Fe_3O_4 + H_2 + H_2O \qquad (2.8)$$

When there is high dissolved oxygen in the environment the magnetite (Fe_3O_4) converts into hematite (Fe_2O_3) as per equation 2.9 [Dooley et al., 2000]

$$2Fe_3O_4 + \frac{1}{2}O_2 = 3Fe_2O_3 + H_2 \qquad (2.9)$$

Under most reducing condition, wustite (FeO) would form.

2.5.3 Defects in the oxide

All the oxides, even bulk synthetic oxides, are never perfect at temperatures above absolute zero but contain imperfection or defects in their structure. The defects found in the oxide lattice can be classified as point defects, line defects or plane defects [Kofstad 1988, Rudden et al., 1984]. Points defects can either be vacancies (cations or anions) or interstitials (cations or anions). The point defects can also be classified as stoichiometric or non-stoichiometric. Formation of cation and anion vacancy pair does not change the stoichiometric composition [Kofstad 1988]. This is called Schottky reaction. Frenkel defects are due to displacement of cation or anion to the interstitial position but do not change the stoichiometry of the oxide [Kofstad 1988]. Figure 2.10 (a)-(c) is the schematic representation of metal oxide crystal without imperfection, having Schottky defects and Frenkel defects, respectively.

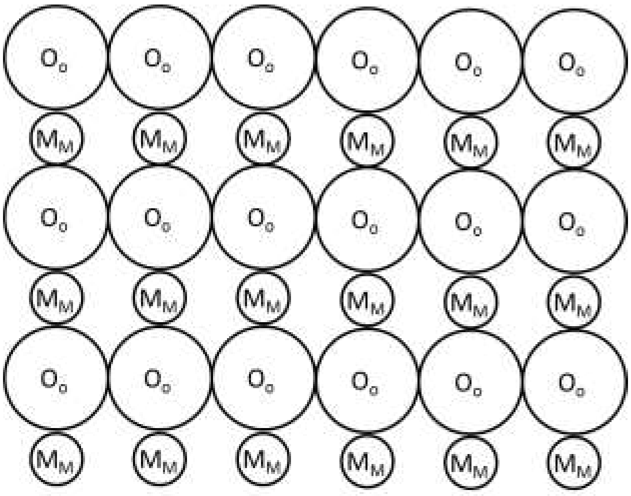

Figure 2.10 (a) Schematic Metal oxide without any imperfection

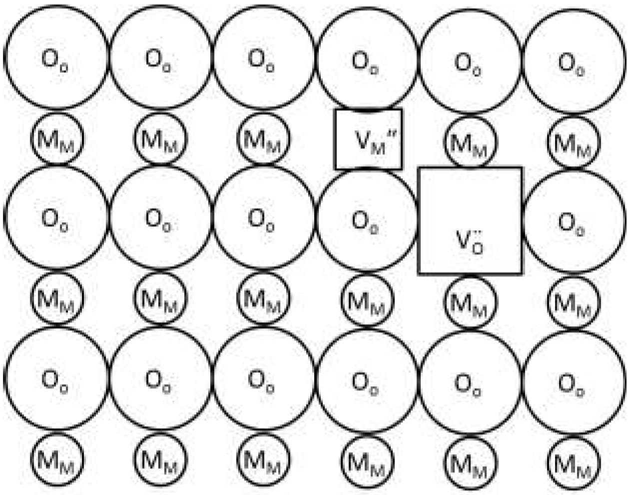

Figure 2.10 (b) Schematic Metal oxide having Schottky defect.

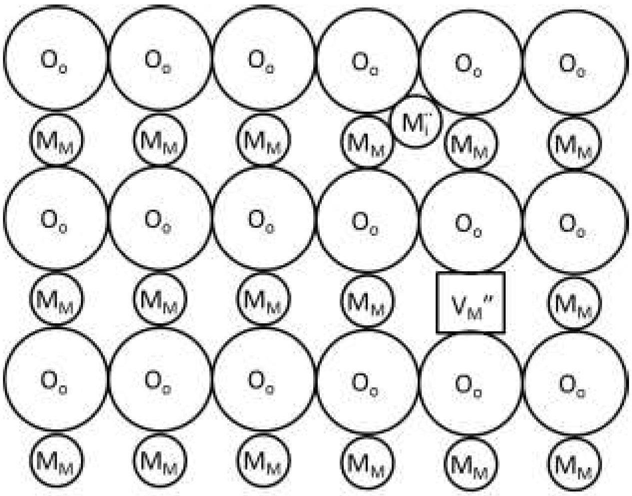

Figure 2.10 (c) Schematic Metal oxide having Frenkel defects

Point defect model (PDM) postulated that passive film are bi-layer structures [**Macdonald 1999, 2011, 2012**] comprising of highly defective barrier layer that grows into metal and an outer layer that forms via precipitation process. PDM further postulated that point defects in the barrier layer are cation vacancies, oxygen vacancies, and cation interstitials. Cation vacancies are electron acceptors resulting in p-type oxide, whereas oxygen vacancies and metal interstitials are electron donors resulting in n-type oxide.

DD Macdonald [**Macdonald 1999, 2011, 2012**] described the defect structure of barrier film. The defects structure of barrier layer was explained on the basis of defect generation and annihilation reaction occurring at metal-oxide and metal-solution interface as given in figure 2.11.

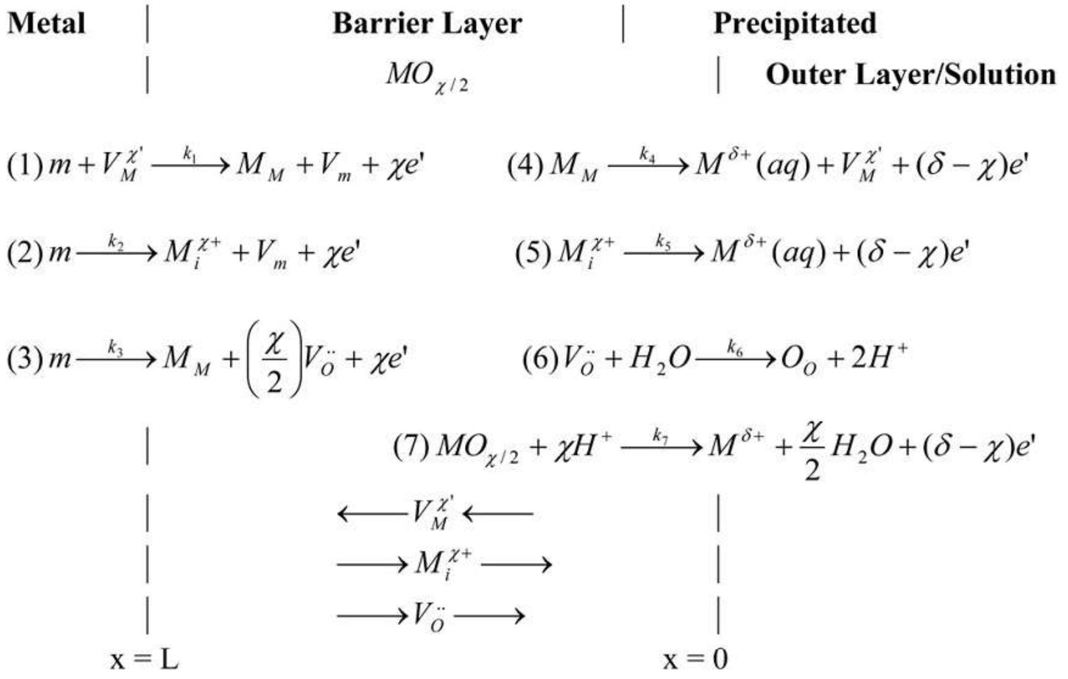

Figure 2.11 Schematics of the reactions occurring at the metal-oxide and oxide-solution interface according to point defect model [Macdonald et al., 1999, 2011, 2012**]**.

Table 2.4: Representing the different species, their position and effective charge.

Symbol	Type	Layer	Position	Charge
m	Metal atom	Metal	Metal	0
M_M	metal	Oxide	Metal	0
v_m	Vacancy	Metal	Metal	0
$M_i^{\chi+}$	Cation interstitial	Oxide	interstitial	χ+(>0)
V_O	anion vacancy	Oxide	Oxygen	+2
$M^{\Gamma+}$	ions	Solution	Solution	Γ+(>0)
O_O	Oxygen atom	Oxide	Oxygen	0

As shown in Figure 2.11, reaction 1 is a lattice conservative process where metal atom goes to cation lattice (M_M) leaving a vacancy v_m in the metal. In reaction 2, cation interstitial is produced in the oxide film by the transfer of metal atom. In reaction 3, metal atom from its lattice is transferred to the metal lattice of oxide and a corresponding oxygen ion vacancy (V_O) is created in the oxide film. At oxide solution interface, metal from lattice position (M_M) is dissolved in the environment as ($M^{\Gamma+}$) and transferred in to the solution (reaction 4) and as a result cation vacancy is created. Further, metal from interstitial also dissolves in the solution as $M^{\Gamma+}$ (reaction 5). Water at the oxide solution interface injects oxygen in to the oxide film, resulting in the consumption of oxygen ion vacancy in the oxide film as per reaction 6. Oxide film at the oxide-solution interface also dissolves in the process giving rise $M^{\Gamma+}$ ions.

The points defects present in the oxide film affect the mass transport across the oxide film. More the defect density in the oxide, less protective it is in nature.

2.6 Characterization of oxide film

The oxide films have been developed by researchers [Subramanian et al., 2014, Kiran Kumar et al., 2010, Bojinov et al., 2009, Sinha et al., 2015] on the carbon steel surface in high temperature and high pressure water either by exposure in static autoclaves or autoclaves attached to recirculation loops. The oxide layers thus developed were characterized for phase composition by XRD, Raman spectroscopy and X-ray photo spectroscopy [Subramanian et al., 2014, Kiran Kumar et al., 2010, Bojinov et al., 2009, Sinha et al., 2015]. They have demonstrated that oxide film formed is magnetite in low DO conditions.

Many researchers established the kinetics of oxidation/corrosion by weight measurement as a function of time of exposure of the material to the process fluid [Sinha et al., 2015, Mabuchi et al., 1991]. The weight measurement provides the total weight of oxide film/oxide film thickness and the total corrosion rate during exposure in high temperature and pressure environment. Sinha et al., [2015] have established effect of starting microstructure of the alloy on oxidation kinetics in simulated PHT environment. They observed that during initial exposure, the oxidation rates are sensitive to microstructural differences. However after growth of oxide film the oxidation kinetics becomes independent of microstructure.

Electrochemical impedance spectroscopy (EIS) followed by Mott-Schottky analysis has been extensively used as a technique for determination of semiconducting properties of the oxide film on metals and alloys and also for the determination of the defect densities in the oxide film [Kiran Kumar et al., 2010, Wielant et al., 2007, Guo et al., 2006, Zeng et al., 2004, Luo et al., 2012, Antunes et al., 2012, Sicupira et al., 2017]. In Mott-Schottky analysis in these studies, electrochemical impedance measurement was performed in borate buffer solution at varying potential and capacitance is measured at each potential. The relationship between capacitance and applied potential is given by Mott-Schottky equation (Eqn. 2.10). Reciprocal of the square of capacitance was plotted against the applied potential. From the slope of this plot defect density in the oxides formed at different temperatures and in different pH values was calculated using Mott-Schottky relationship (Eqn. 2.10).

$$\frac{1}{C^2} = \frac{2}{\varepsilon\varepsilon_0 q N A^2}\left(E - E_{FB} - \frac{KT}{q}\right) \qquad \textbf{(2.10)}$$

Where ε is the dielectric constant of the specimen (15.6 for magnetite), ε_o the vacuum permittivity (8.85×10^{-14} F. cm^{-1}), q the charge, N the defect density, q the electronic charge (1.602×10^{-19} C), A is surface area (cm^2) of the specimen, E_{FB} the flat band potential (V), K the Boltzmann constant ($cm^2 g s^{-2} K^{-1}$) and T the absolute temperature.

Slope of the plot gives the defect density as well as type of point defect; negative slope indicating p-type, while positive slope indicates n type semiconductor.

Subramanian et al. [2014] studied the effect of Cr addition in the alloy and level of dissolved oxygen in the environment on the defect density in the oxide film formed. They established that with increase in Cr content defect density in the oxide film has decreased (figure 2.12) and hence the oxide becomes more protective. They also showed that with increase in DO content, defect density in oxide film of carbon steel becomes less than that in Cr containing steel. They have attributed the observation to the formation of hematite. Addition of oxygen in water results in the formation of a hematite layer at the barrier layer/solution interface. Once this layer is formed, its defect structure/ dissolution rate dominates the corrosion behavior of the underlying metal. The dissolution rate of hematite is several orders of magnitude lower than that of magnetite.

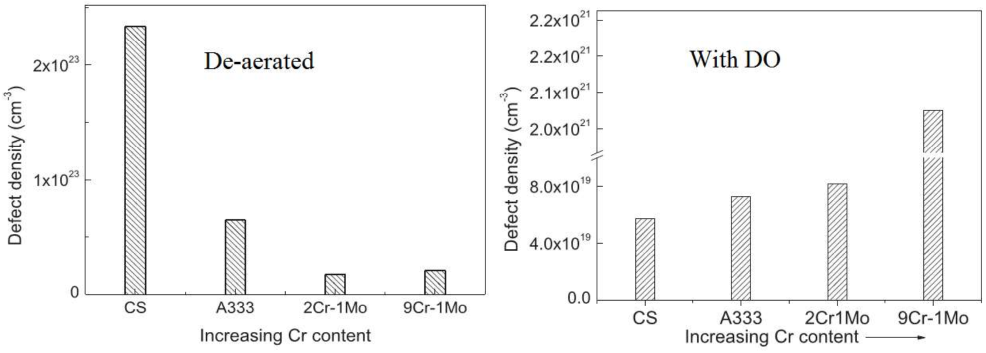

Figure 2.12 Variation of defect density with Cr alloying and DO oxygen [Subramanian et al., 2014]

This effect of phase change at the barrier layer/solution interface is different from the role played by oxygen at low temperature in increasing the defect density of barrier films on stainless steel. Thus, oxygen addition essentially shifts the location of rate control from the metal/barrier layer interface to the barrier layer/solution interface at the temperature of interest by in situ generation of an inhibitive coating. The decrease in defect densities in the oxide layer formed on carbon steel 106 Gr-B and A333 shows the beneficial effect of Cr content and DO addition.

Defect density in the barrier layer plays important role in the corrosion of structural materials. Higher the defect density, less protective will be the oxide film and vice-versa.

2.7 Solubility of the magnetite

Solubility is a thermodynamic parameter. It is the maximum amount of dissolution product that can be accommodated in the environment under given process parameters like temperature, pH, DO and redox potential. It can be said that the environment gets saturated with dissolved ionic species at and above the solubility limit.

Dissolution of magnetite at oxide-water interface involves the reduction of the ferric ions to ferrous ion and hence this is called reductive dissolution and is a function of partial pressure of hydrogen. Researchers [Tremaine et al., 1980, Sweeton et al., 1970] have measured the solubility of magnetite (Fe_3O_4) at various temperature, pH and hydrogen pressure and shown in figure 2.13. They used NaOH, KOH and HCl to maintain pH.

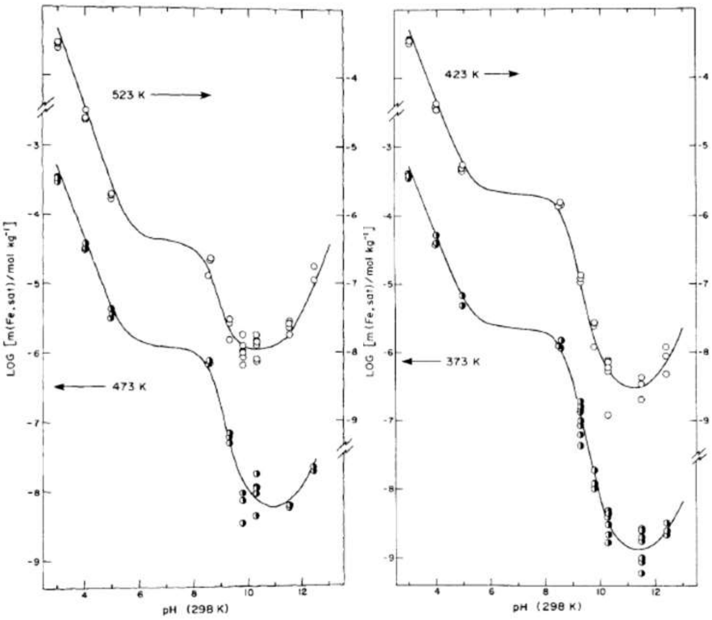

Figure 2.13 Solubility of Fe_3O_4 at 523, 473, 423 and 373 °K and 779 mol/kg H_2 [Tremaine et al., 1980].

Dissolution of magnetite and formation of dissolved ferrous or ferric species is described by eqs. 2.11 and 2.12. [Tremaine et al., 1980]

$$\frac{1}{3}Fe_3O_4 + (2-b)H^+ + \frac{1}{3}H_2 \leftrightarrow Fe(OH)_b^{(2-b)} + (\frac{4}{3}-b)H_2O \qquad (2.11)$$

$$\frac{1}{3}Fe_3O_4 + (3-b)H^+ \leftrightarrow Fe(OH)_b^{(3-b)} + \frac{1}{6}H_2 + (\frac{4}{3}-b)H_2O \qquad (2.12)$$

Here $Fe(OH)_b^{2-b}$ and $Fe(OH)_b^{3-b}$ are the hydrolyzed species of ferrous and ferric iron. The equilibrium of the aqueous species is described by Eq. 2.13.

$$Fe(OH)_b^{(2-b)} + H_2O \leftrightarrow Fe(OH)_{b+1}^{3-(b+1)} + \frac{1}{2}H_2 \qquad (2.13)$$

Polynuclear hydrolyzed species are unstable at the high temperatures and low ionic strengths. The proportion of Fe in the ferric state is negligible at pH values less than 9 [Sweeton et al., 1970]. Tremaine et al., measured the oxidation state of iron compounds at pH 9.3 (298 °K) and temperature of 373 °K with different H_2 molalities [Tremaine et al., 1980]. At H_2 concentration of 779 µmol/kg and pH 9.3 (298 °K) significant proportion of Fe was in ferric form according to the experimental data and thermodynamic calculations. Higher temperature and pH increased the proportion of the ferric iron. On the other hand, higher H_2 concentration increased the proportion of the ferrous iron.

The solubility of magnetite decreases when temperature increases except in highly alkaline solutions (figure 2.14) [Tremaine et al., 1980]. The change of solubility with temperature affects FAC rate and also the rate of magnetite deposition. In highly alkaline solutions at high temperatures magnetite solubility increases with increase in temperature. According to data of Tremaine et al., positive solubility-temperature gradient occurs at pH (298 °K) ≥ 9.4 at temperature of 573 °K and at pH (298 °K) ≥ 9.9 at temperature of 423 °K [Tremaine et al., 1980].

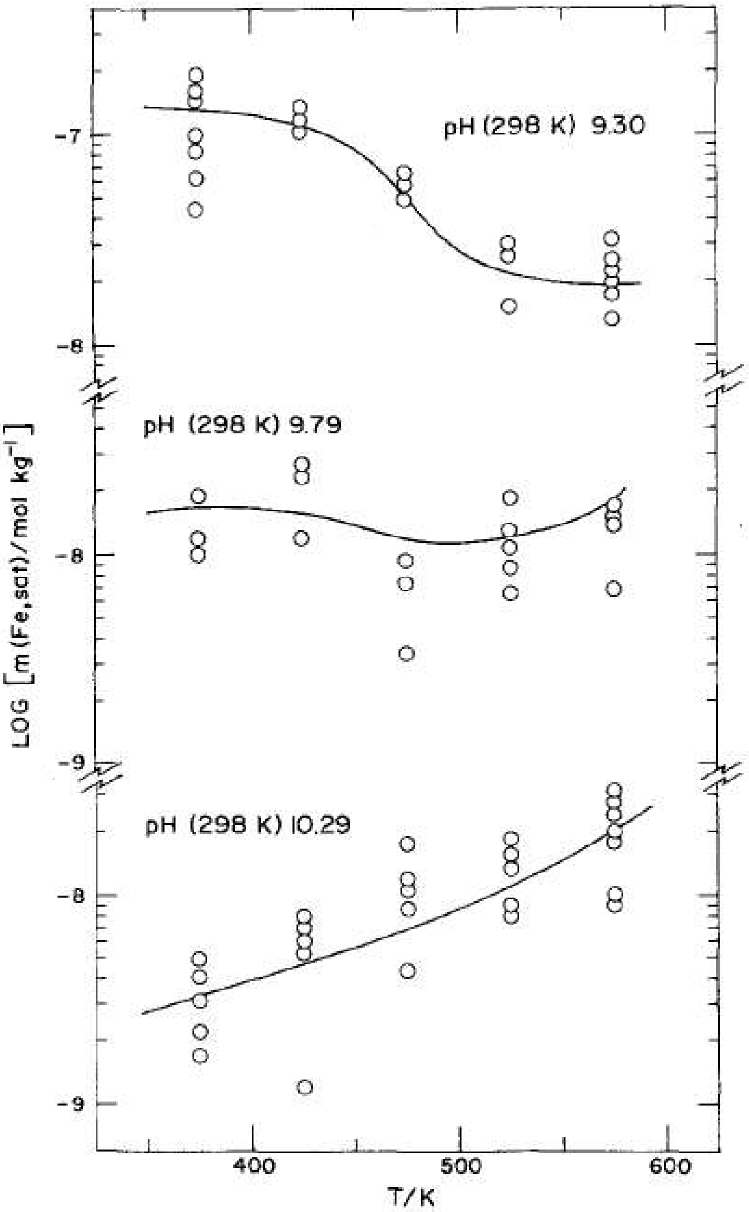

Figure 2.14 The temperature dependence of magnetite solubility at 779 µmol/kg H_2 and at different pH values [Tremaine et al., 1980].

The next sub section will explain different synthesis techniques used for magnetite synthesis; as it is essential to have well characterized powder with known parameters for solubility studies.

2.8 Synthesis techniques for magnetite powder

Synthesis of magnetite has been done using different routes viz. colloidal method, micro emulsion, sol–gel, freeze-drying, laser pyrolysis, vaporization condensation and partially reduced precipitation routes [Gribanov et al., 1990, Zhuo et al., 2001, Zhu et al., 1999, Park et al., 2005, Thapa et al., 2004, Liang et al., 2010]. However, a main challenge of these numerous and novel techniques lies in their capacity to obtain a narrow range of particle size together with the desired compositional, structural and crystalline uniformity [Martínez-Mera et al., 2007].

Co-precipitation is a common method for producing nano particles of magnetite [Park et al., 2005, Martínez-Mera et al., 2007, Mamania et al., 2016, Petcharoen et al., 2012, Khoshnevisan et al., 2016]. For the solubility study, magnetite powder needs to be confined in a high temperature and pressure autoclave using filters on the inlet and outlet sides. Hence nano particles are not suitable for such a study. Only a few researchers have synthesised powder of approximately 100 micrometer size [Sweeton et al., 1970 and Tremaine et al., 1980] using iron powders. However, synthesis of coarse (105 – 125 μm size) magnetite powder by co-precipitation is not reported in literature. The present thesis focuses on a novel synthesis route for high purity coarse magnetite powder that is used for solubility study.

2.9 Summary of literature review

FAC is a process in which corrosion/dissolution rate of the oxide film formed on the carbon steel is enhanced by flowing environment through electrochemical action. The parameters like temperature, pH, DO, redox potential, material composition and hydrodynamics affect FAC rate by affecting either the solubility or mass transfer or both. The temperature and pH may affect the nature of oxide film. The effect of pH and temperature on the nature of oxide film is not reported in literature. Effect of DO on nature of oxide film has also not been reported very systematically. FAC predominantly occurs in the location of elbow, Tee, bents, expanders etc. and have been attributed to turbulent flow leading to increased mass transport. These regions undergo cold working during fabrication. Nature of oxide film formed in the cold worked location has not been established in literature.

Solubility of magnetite film depends on pH and redox potential. The pH variation with temperature depends on the chemical used to adjust the pH owing to differences in dissociation constants. Solubility of magnetite using Ethanol amine (ETA) has not been established in literature.

Based on the available literature on the effect of several material and environmental parameters on the nature of oxide film and its dissolution behaviour, the objectives of the present thesis were formulated. The broad objective of this thesis is a systematic study of all these parameters, namely, temperature, pH, DO and cold working of carbon steel on oxide film formation and nature of oxide. Aim is also to synthesize and establish the solubility behaviour of magnetite in simulated secondary circuit environment which uses ETA. An attempt is made to put the findings in perspective in terms of their implication to FAC behaviour of carbon steel components.

Chapter 3

EFFECT OF COLD WORKING ON OXIDATION BEHAVIOUR OF CARBON STEEL AND NATURE OF OXIDE FORMED

3.1 Introduction

Carbon steel is extensively used as a structural material for majority of components in the secondary circuit of pressurized heavy water reactors (PHWRs). Feed water system of Indian PHWRs is made of carbon steel ASTM A 106 Gr B [Kain et al., 2008, Kain et al., 2011]. A major mode of degradation of these secondary circuit components/pipelines carrying high velocity water/steam is flow accelerated corrosion (FAC) which causes thinning. The secondary circuit components are exposed to temperatures upto 200 °C, the process fluid being alkaline water (pH adjusted by ethanolamine (ETA) or ammonia). It is known that the mechanism of FAC is electrochemical dissolution and the protective magnetite film formed on the internal surfaces of carbon steel pipelines/components dissolves at a faster rate in a high velocity fluid environment, resulting in an increased rate of wall thinning [Ahmed et al., **2010,** Guimaraes et al., **2003,** Poulson, **1999,** Dooley **et. al. 2000**]. FAC is a major mode of degradation in carbon steel piping used in fossil, industrial steam and nuclear power plants [Kain et al., 2008, Kain et al., 2011, Kain 2014, Moon **et al.,** 2005, Betova **et. al.** 2010].

The parameters that affect FAC are environmental, material and hydrodynamic [Sweeton et. al., 1970, Tapping, 2008]. Environmental parameters include water chemistry parameters such as pH, dissolved oxygen (DO) etc. and temperature of the water. Material parameters include alloying elements in the carbon steel such as chromium, molybdenum and copper. While hydrodynamic parameters affects FAC rate as it determines whether the flow is turbulent or laminar and determines the velocity of process fluid. Water chemistry parameter, especially pH, affects FAC rate by altering the solubility of the oxide film formed on the internal surfaces of components/pipelines [Betova et al., 2010, Sweeton et al., 1970]. DO in water affect the oxide solubility by not only changing the redox potential of the environment but also by altering the type of oxide formed, which has a different solubility. Presence of DO converts the magnetite to hematite or ferric oxide hydrate that has a very low solubility compared to that of the magnetite [Dooley et al. **2000**]. Temperature of the environment also affects FAC rate by affecting the solubility of magnetite [Betova et. al., 2010, Sweeton et al., 1970]. Alloying carbon steel such as ASTM A 106 Gr B, with a small amount of Cr (0.3 %) has been reported to lead to over 50% enhancement in life of the components in the primary heat transport circuit of PHWRs [Tapping 2008]. Alloying with chromium helps to produce iron chromite on the surfaces that has a lower solubility [Cubicciotti **1988**]. Alloying with copper also reduces FAC rate by a different mechanism [Cubicciotti **1988**, Trevin **2012**]. Hydrodynamic parameter of the environment is the key parameter that affects FAC rate and its role in affecting FAC has been extensively studied [Betova et al., 2010, Matsumura, 2015, Zhu et al., 2013, Smith et al., 2001, Shoji et al., 2006, Singh et al., 2012]. It is reported that flow turbulence increases the local flow velocity of the environment significantly and this results in a high mass transport from oxide-environment interface, thus increasing the FAC rate significantly [Betova et al., 2010]. It is reported that failure due to FAC is predominant at the location of elbows, bents, reducer etc. where there is a change in flow velocity/direction, leading to a disturbed/turbulent flow [Kain et al., 2008, Betova et al., 2010, Matsumura **2015, Zhu et al., 2013,** Smith **et al., 2001,** Shoji **et al., 2006,** Singh **et al., 2012**].

Materials at elbows, bents, reducer etc. are in cold worked condition induced during fabrication and these are also the locations of high FAC susceptibility. Cold working is expected to affect the nature of surface oxide formed which has a strong influence on FAC susceptibility. The aim of the present study is to establish the effect of cold working on the oxidation kinetics of the carbon steel in high temperature and pressure aqueous environment and to characterize the semiconducting property oxide formed (by impedance spectroscopy and Mott-Schottky analysis) and correlate it with FAC susceptibility. Oxidation/corrosion kinetics of carbon steel by weight measurement as a function of time of exposure of the material to the process fluid has been reported earlier [Sinha et al., 2015, Mabuchi et. al., 1991]. The Mott-Schottky method is also extensively used for the determination of semiconducting property of the oxide film on metals and alloys and also for the determination of the defect density in the oxide film [Kumar et al., 2010, Wielant et al., 2007, Guo et al., 2006, Zeng et al., 2004, Luo et al., 2012, Antunes et al., 2012, Sicupira et al., 2017]. There is no reported literature on the effect of cold working on the nature of oxide formed and its influence on FAC rate in carbon steel.

3.2 Experimental

3.2.1 Material and cold rolling

Carbon steel of grade ASTM A 106 grade B was used in this study.The material used was in the form of a sheet of 5 mm thickness. The chemical composition was analysed by spark optical emission spectroscopy and is given in Table-2.1. Cold rolling of this as-received (AR) sheet was done to obtain thickness reduction of 5%, 10%, 20% and 30%.

3.2.2 Microstructure

Specimens of size 15 mm x 10 mm were cut from the as-received and different cold rolled samples and were ground on successively fine emery papers from 80 to 600 grit. Final polishing was done using 1 μm diamond paste. Microstructure of these specimens was obtained by swab etching the samples with nital (ethanol + nitric acid) solution. Different compositions of the nital solution (2% - 5%) were tried and finally the optimized concentration was 2% nital solution for the cold worked sample. The developed microstructures were examined under an optical microscope and images were recorded.

3.2.3 Microhardness Measurement

Samples polished till 1 μm diamond paste was used for hardness measurements. Microhardness was measured using Vickers scale, with the applied force of 300 gf and a dwell time of 15 seconds. Surface hardness was measured at five different locations for each sample and the average value is reported. Hardness of as-received and cold rolled samples was also measured across the cross-section to determine the uniformity of strain hardening across the thickness. The gap between the indents was 0.1 mm near the surface and in the mid-thickness gap between the indents was 0.2-0.5 mm.

3.2.4 Oxidation in Autoclave

Coupons of approximate size 15 mm x 10 mm were cut from the as received and cold rolled sheet and ground on successively finer emery papers up to 600 grit. Dimensions of each coupon were accurately measured using a vernier to calculate the surface area of the samples. All the coupons were cleaned ultrasonically in acetone and air dried. The coupons were then weighed up to 1 μg accuracy (W_1) to record the initial weight.

Coupons were hung from a stand and placed in an autoclave. Demineralised water with pH adjusted to 10-10.2 using lithium hydroxide was added to the autoclave and autoclave lid was closed and heating started. High purity argon gas was purged up to 70 °C and this temperature was held for 1 h with continuous purging of argon gas. Venting was done at 150 °C and then the temperature increased to 270 °C. The samples were exposed in the autoclave in this environment at 270 °C for different durations from 4 h up to 240 h. Argon purging and venting at 150 °C was done to ensure removal of oxygen (DO < 45 ppb) [ASTM G2 / G2M **2011**]. Temperature and pH in the static autoclave can be maintained as per actual plant conditions. Temperature and corresponding pressure can be simulated in a static autoclave. In static autoclave flow conditions are not maintained. Capacity of the autoclave used was 1.5 L. and there was negligible change in the pH value after the experiment.

Selected number of coupons was intermittently withdrawn from the autoclave after predetermined duration of exposure and the exposure was continued for the remaining coupons at the same temperature. The coupons removed were washed with acetone and weighed (W_2). Few exposed coupons were descaled (removal of oxide layer) using Clark's solution (2% antimony trioxide and 5% stannous chloride in 100 ml concentrated hydrochloric acid (37-38%)). After descaling, the samples were again weighed (W_3). The weight loss, total iron dissolved and thickness of the magnetite layer formed were calculated from equations (3.1)-(3.3).

$$\Delta W_{(oxide)} = W_2 - W_3 \qquad (3.1)$$

$$\Delta Fe_{(total)} = Fe_{(oxide)} + Fe_{(solution)} = (W_1 - W_3) \qquad (3.2)$$

$$t_{oxide} = \Delta W_{(oxide)}/\rho_{Fe3O4} \text{ x } 10\hat{}4 \qquad (3.3)$$

Where W_1 is initial weight of the samples (g/cm^2), W_2 is weight after exposure (g/cm^2), W_3 is weight after descaling (g/cm^2), $\Delta W_{(oxide)}$ is weight loss after descaling i.e. weight of oxide (g/cm^2), $\Delta Fe_{(total)}$ is the total iron oxidised (g/cm^2), t_{oxide} is thickness of oxide film (μm), ρ_{Fe3O4} is density of magnetite (5.15 g/cc), $Fe_{(oxide)}$ is weight of iron in the oxide film (g/cm^2), $Fe_{(solution)}$ is weight of dissolved Fe ions (g/cm^2) during exposure in autoclave. t_{oxide} is thickness of oxide in μm.

In calculation of the weight different of W_2 and W_3, weight correction was incorprated by measuring the weight loss of blank (fresh carbon steel without oxide) samples during descaling with Clarke's solution.

3.2.5 Oxide film characterization

All the coupons after exposure in autoclave were examined by scanning electron microscopy (SEM) to establish surface oxide morphology. Micro laser Raman spectroscopy (MLRS) and X-ray diffraction (XRD) were used to study the nature of the oxide film formed on samples. In MLRS, measurements were carried out using green visible light of wavelength 514 nm and laser power of 18 mW in air at room temperature. XRD was done on the autoclave exposed coupons using $Cu_{K\alpha}$ x-ray (1.5406 Å). XRD was carried out at a scan rate of 0.02 °/s with 2θ range 25° to 90°.

3.2.6 Electrochemical Characterization

Potentiodynamic polarization was done at the scan rate 30 mV/min to determine the potential range at which the magnetite is stable in the borate buffer solution of pH 9.2 at room temperature. This was done using the standard three electrode system wherein the oxidized coupon was made the working electrode, platinum as counter electrode and saturated calomel electrode (SCE) was used as the reference electrode. All potentials reported in this study are with respect to SCE (V_{SCE}). Deaeration of the borate buffer solution was done by bubbling argon gas for 30 minutes before start of the experiment and also continued during the experiment.

Mott-Schottky analysis was done by determining the capacitance at different potential. For this purpose electrochemical impedance measurement was done in the potential range -300 mV_{SCE} to 1000 mV_{SCE} at a step potential of 100 mV in borate buffer solution of pH 9.2 and capacitance was determined at 1000 Hz [Wielant et al., 2007, Guo et al., 2006, Zeng et al., 2004, Luo et al., 2012, Antunes et al., 2012, Sicupira et al., 2017]. Reciprocal of the square of capacitance was plotted against applied potential. From the slope of this plot defect density (/cc) in the oxides of each cold worked sample was calculated using Mott-Schottky relationship (equation 3.4) [Wielant et al., 2007, Guo et al., 2006, Zeng et al., 2004, Luo et al., 2012, Antunes et al., 2012, Sicupira et al., 2017].

$$\frac{1}{C^2} = \frac{1}{C_H{}^2} + \frac{2}{\varepsilon\varepsilon_0 qNA^2}(E - E_{FB} - \frac{KT}{q}) \qquad (3.4)$$

Where ε is the dielectric constant of the sample (15.6 for magnetite) [Simoes et al., 1990], ε_o the vacuum permittivity (8.85×10^{-14}), q the charge, N the defect density, q the electronic charge (1.602×10^{19} C), A is surface area of the specimen (cm^2), E_{FB} the flat band potential, K the Boltzmann constant, T the absolute temperature.

3.3 Results and Discussion

3.3.1 Material and Microstructure

The chemical composition of the carbon steel as analyzed is given in Table 2.1 confirming the material used in the study is carbon steel ASTM A106 Grade B [ASTM A106 **2015**].

Table 3.1: Chemical composition of carbon steel sheet used in the study

Elements	C	Mn	P	V	Ni	Mo	S	Si	Cr	Cu	Fe
Wt %	0.115	0.33	0.017	0.09	0.021	0.005	0.019	0.11	0.043	0.040	Bal.

Microstructure of the samples after etching with 2% nital solution is shown in figure 3.1 which clearly shows the typical ferrite-pearlite structure of the AR sample (figure 3.1(a)). With increasing level of cold working from 5-30%, the ferrite-pearlite structure was not distinctly visible, indicating fragmentation of the structure with increasing level of cold rolling (Figure 3.1(b-e)). The surface of the 30% cold worked sample became black without revealing the microstructure, for the same extent of etching. This may be attributed to high levels of uniform strain in the material which reacts with the etchant uniformly and does not reveal the microstructure.

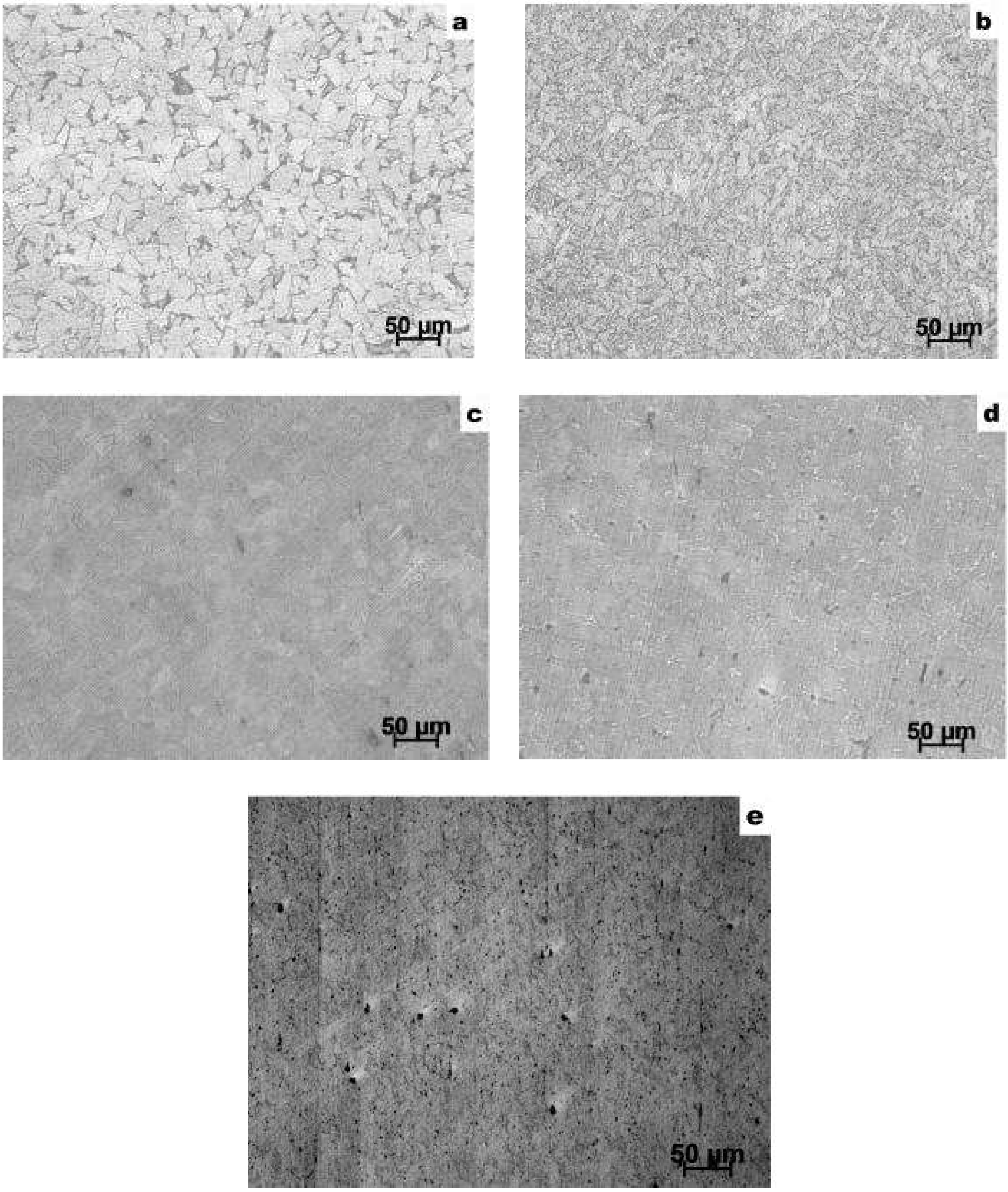

Figure 3.1 Micro structure of carbon steel sample in (a) as-received, (b) 5%, (c) 10%, (d) 20% and (e) 30 % cold rolled conditions

3.3.2 Hardness Measurement

Figure 3.2 shows micro hardness of the different cold worked carbon steel samples as measured on the surface. As carbon content of the steel is low (0.115%) (Table 2.1), micro hardness value of as-received carbon steel was low i.e. 126 HV [Sinha et al., 2015]. Microhardness increased with increasing extent of cold working which may be attributed to the increase in strain hardening due to an increase in the dislocation density due to cold working. It is clear from figure 3.2(a) that the extent of hardness increase is much more with the initial levels of cold rolling (5%, 10%) and with increased levels of cold rolling (20%, 30%) the extent of hardness increase is lesser. This is attributed to the saturation of the strain hardening capacity of the material. The hardness profile across the thickness of AR and cold rolled samples remained almost constant throughout the thickness and varied within a narrow range of ± 10 HV, indicating uniform strain hardening across the thickness as can be seen in figure 3.2(b).

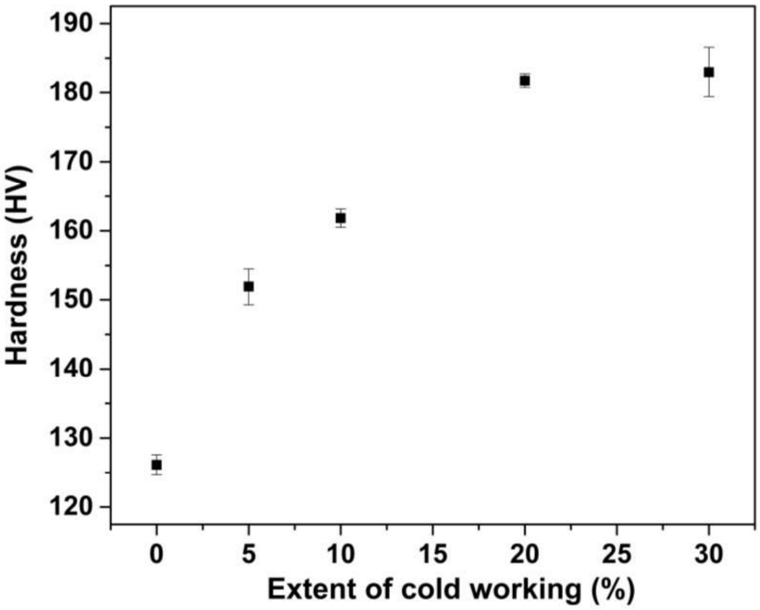

Figure 3.2(a) Variation of hardness with extent of cold rolling.

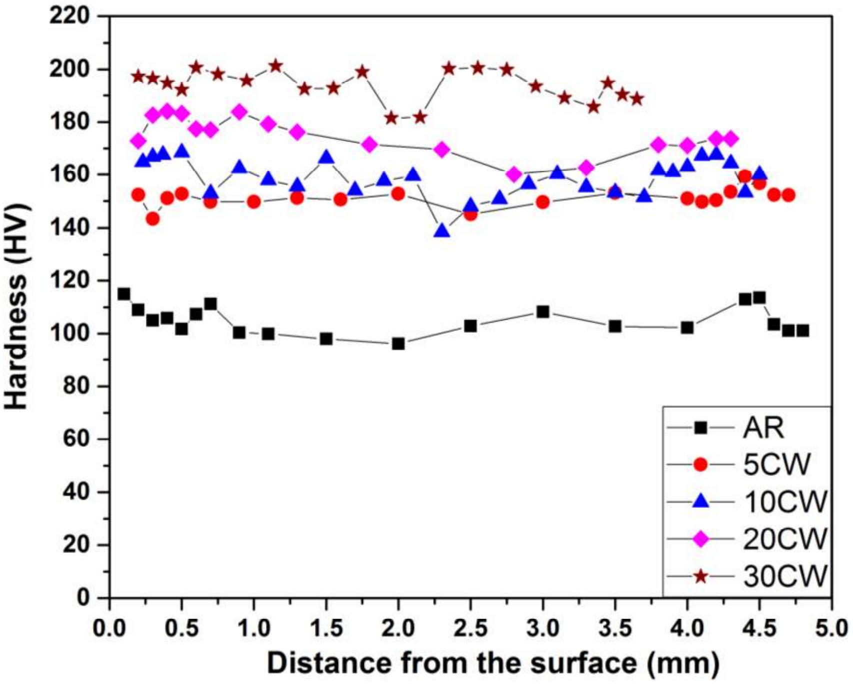

Figure 3.2(b) Hardness profile of cold rolled sample across its thickness.

3.3.3 Oxidation behaviour

During the oxidation of carbon steel in high temperature water two processes occurs simultaneously: a) formation of oxide film on the surface of carbon steel by the reaction of metal and environment by growth and precipitation mechanism [Robertson 1989, Frayne 2002, Rihan et al., 2006, Schwertmann et al., 2000, Fujiwaraa et al., 2011] leading to weight gain of the sample and b) dissolution of the metal/oxide in the environment resulting in weight loss. The mechanism of this high temperature corrosion process is well established [Robertson 1989, Frayne 2002, Rihan et al., 2006]. Thus, two competing processes are occurring simultaneously and the extent to which each process occurs will determine the weight gain or loss of the coupons.

Measurement of weight of samples at different stages (W_1, W_2 and W_3) gives the oxidation behaviour and the relative extent of occurrence of these two competing processes, which gives mechanistic insight into the evolution of oxide during autoclave exposure. The difference in weight W_2 and W_1 gives the resultant weight change due to the occurrence above two competing processes (simultaneous oxide formation and dissolution along with metal dissolution). The difference in weight W_2 and W_3 ($\Delta W_{(oxide)}$) gives the weight of oxide film remaining on the surface after exposure. The difference in weight W_1 and W_3 ($\Delta Fe_{(total)}$) gives the total loss of metal due to oxidation and dissolution, which is the sum of the iron ions (ferrous and ferric) in oxide film and that dissolved in the water during autoclave exposure. Thickness of the oxide film (t_{oxide}) was calculated from the weight of oxide and density of the magnetite (equation 3.3). It was assumed that the density of the oxide film formed on different cold worked sample remains the same.

The weight of oxide remaining on the surface ($\Delta W_{(oxide)}$), the total loss of metal due to oxidation and dissolution ($\Delta Fe_{(total)}$) was normalised by the exposed surface area of the coupons. Figures 3.3(a-c) shows the variation in (a) area normalised weight of oxide ($\Delta W_{(oxide)}$), (b) area normalised total corrosion rate and (c) thickness of the oxide film (t_{oxide}) formed on the carbon steel with different extent of exposure in autoclave. The oxide formation rate (Figure 3.3(a)) was found to increase with extent of cold working. This may be attributed to the increase in the surface energy due to increase in dislocation density by cold working. In all the cases the oxidation kinetics decreased with time, following the parabolic rate law. This is because the formation of oxide film is a diffusion controlled process.

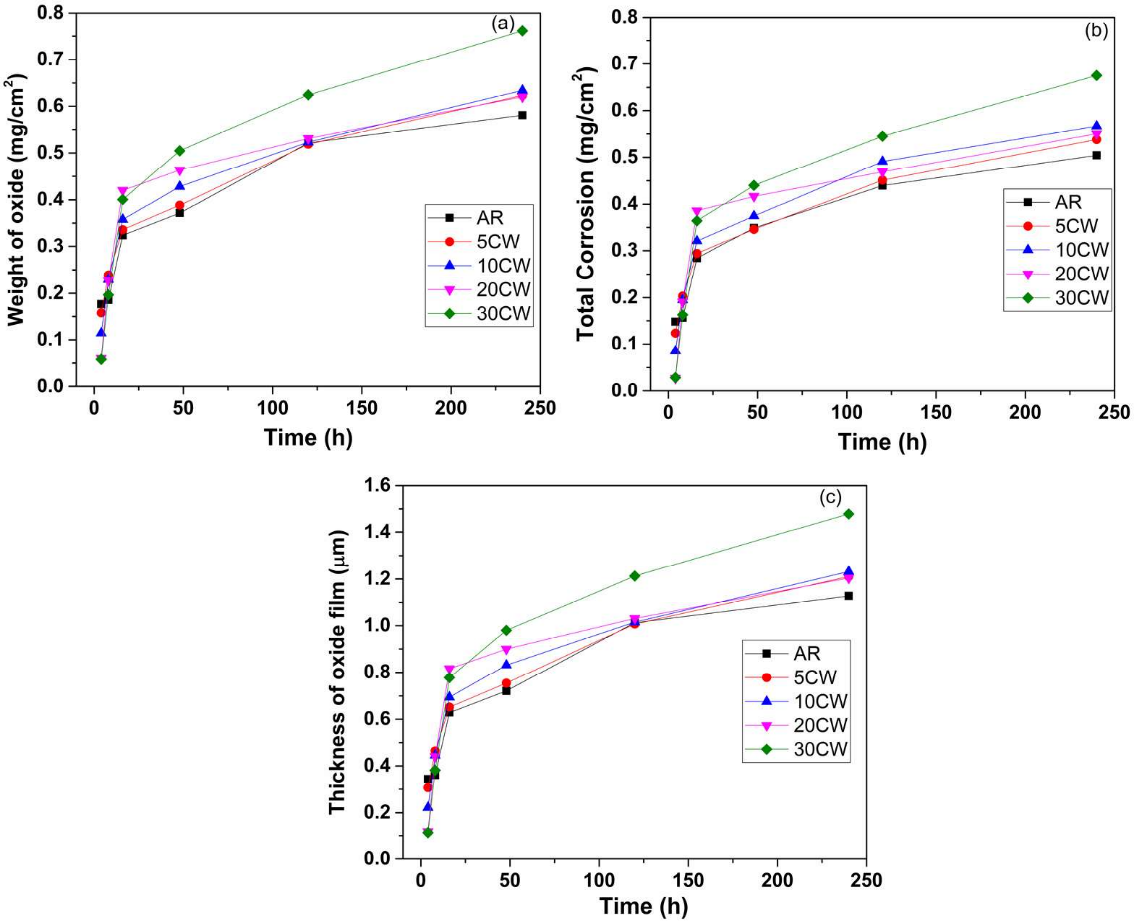

Figure 3.3 Variation of (a) weight of oxide film, (b)total corrosion rate and (c) film thickness with time of exposure in lithiated (10-10.2 pH) water at 270 °C.

3.3.4 Oxide film characterization

Figure 3.4 shows the SEM image of the different cold worked carbon steel sample exposed in lithiated water (pH 10-10.2) in autoclave at 270 °C for 120 h. SEM image clearly showed that the oxide film uniformly covered the entire surface. Surface morphology of the oxide film showed formation of duplex type of oxide consisting of a compact inner layer having a fine crystalline structure and an outer layer having a coarse crystalline structure which is in agreement with earlier reported literature [Robertson **1989,** Frayne 2002, Rihan **et al., 2006,** Schwertmann **et al.,** 2000]. The inner layer directly formed on the carbon steel surface by the oxidation of iron and reduction of hydrogen ion [Robertson **1989**] from the environment (eq. 3.5).

$$Fe + H_2O = Fe_3O_4 + H_2 \tag{3.5}$$

Outer layer of magnetite forms by the precipitation reaction. The oxidized iron ion in the environment (Fe^{2+}) reacts with hydroxide ions of the environment and form ferrous hydroxide according to eq. 3.6 and 3.7. When the concentration of soluble iron species becomes very high and exceeds the solubility limit in the environment, it gets precipitated as magnetite on the surface of the coupons and forms the outer layer of the oxide film. This reaction (eq. 3.8) is known as the Schikorr reaction [Robertson **1989,** Frayne 2002, Rihan **et al., 2006**].

$$Fe = Fe^{2+} + 2e \tag{3.6}$$

$$Fe^{2+} + 2OH^- = Fe(OH)_2 \tag{3.7}$$

$$Fe(OH)_2 = Fe_3O_4 + H_2 + H_2O \tag{3.8}$$

The oxide formed on all the cold worked sample show similar duplex morphology indicting that cold working does not affect the morphology of the oxide film.

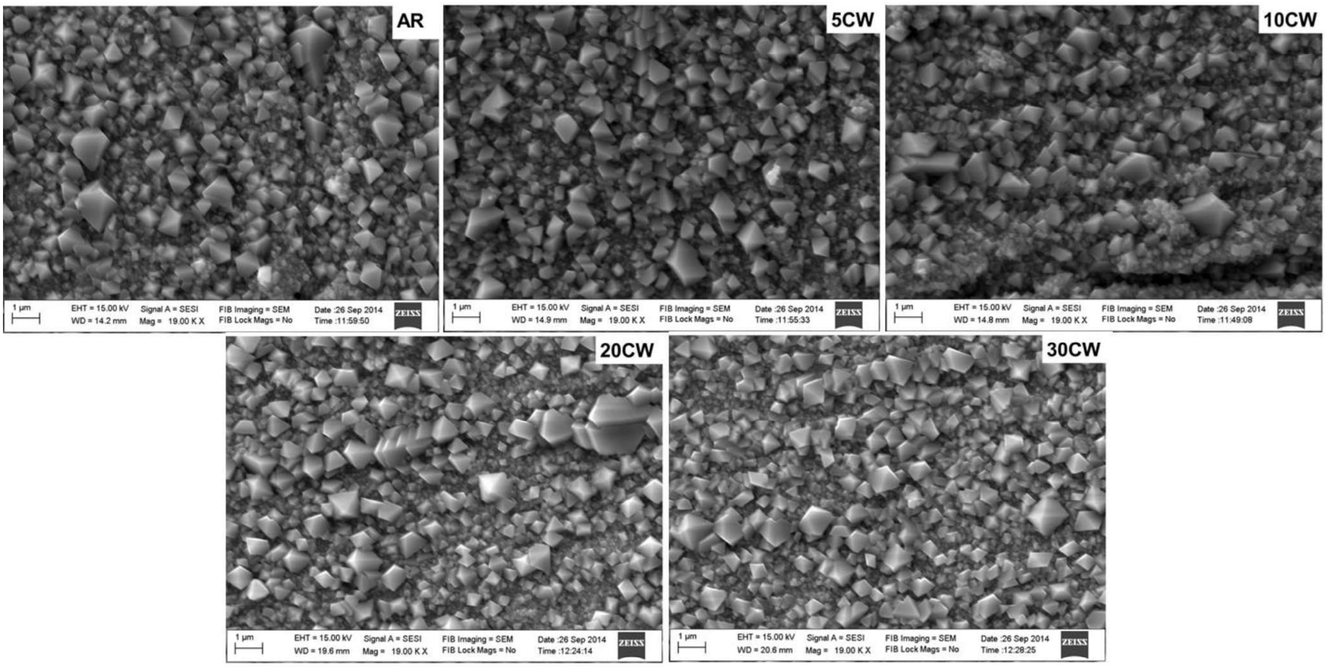

Figure 3.4 SEM images of the carbon steel sample exposed in autoclave for 5 days for (a) as-received, (b) 5% cold rolled, (c) 10% cold rolled, (d) 20% cold rolled and (e) 30% cold rolled conditions.

SEM images also showed the crystal size of the outer layer is similar in AR sample and cold rolled samples. Formation of this outermost layer takes place via the deposition (crystallization) at the surface of the dissolved iron ions (in the solution) according to equation 2.8 [Sweeton 1970, Robertson **1989,** Frayne 2002, Rihan **et al., 2006**]. Crystallization of the dissolved species onto the surface of the samples depends on the solubility of magnetite in the environment. When the local concentration of the dissolved species increases beyond the solubility limit, it gets precipitated as magnetite crystals (Schikorr reaction). Tremaine et al., (1980) have reported that the solubility of magnetite depends upon environmental parameters such as temperature, pH and hydrogen partial pressure and the type of iron species changes with change in the environmental parameters. At lower temperature and lower pH (<9.3), ferrous species is predominant in the environment and as temperature and pH increased, ferric species are predominant. The precipitation of these species results in to formation of outer magnetite film. The extent of precipitation also depends on the chemical used for the pH adjustment of the water [Olmedo **et al., 2015**] by affecting the solubility. Since the environmental parameters such as temperature, pressure, pH and DO remained same for the AR and cold rolled samples, the magnetite crystal would remain the same. This is the reason that similar type of oxide morphology was obtained for as-received as well as cold worked samples.

The XRD of oxides grown on the different cold worked carbon steel coupons after exposure in autoclave for five days were carried out to assess the phases present in the oxide. Figure 3.5 shows types of oxide formed on the carbon steel coupons exposed in autoclave for five days, as detected in XRD. Peaks observed at 2θ of 44.69°, 65.04° and 82.31° corresponds to base material (α-Fe) [Islam et al., **2015**]. The XRD peak at 2θ of 30.13° (*hkl* 220), 35.54°(*hkl311)*, 43.17°(*hkl 400)*, 57.06°(*hkl 511) and* 62.63° (*hkl 440)* observed in the oxide film formed on different cold worked samples corresponds to magnetite (JCPDS, No. 19-0629). MLRS also confirmed (Figure 3.6) that no other peaks except magnetite and base material were seen confirming formation of only magnetite phase during the exposure in autoclave. Other phases of iron oxide like hematite, goethite etc. were not detected in both XRD and MLRS. Presence of peaks due to base material (α-iron) in XRD indicates that the oxide film is very thin. This result is in agreement with the thickness determined by the weight change method. The thickness of the oxide film after five days exposure was calculated to be 1.0-1.2 μm. Figure 3.6 shows the MLRS spectra of the oxide formed on different cold work carbon steel. It was observed that irrespective of the extent of cold working, magnetite having Raman shift of 662 – 668 cm^{-1} and 538-543 cm^{-1} [Shebanova **et al., 2003,** de Faria **et al., 1997,** Mendili **et al., 2014**] was formed in all the experimental conditions.

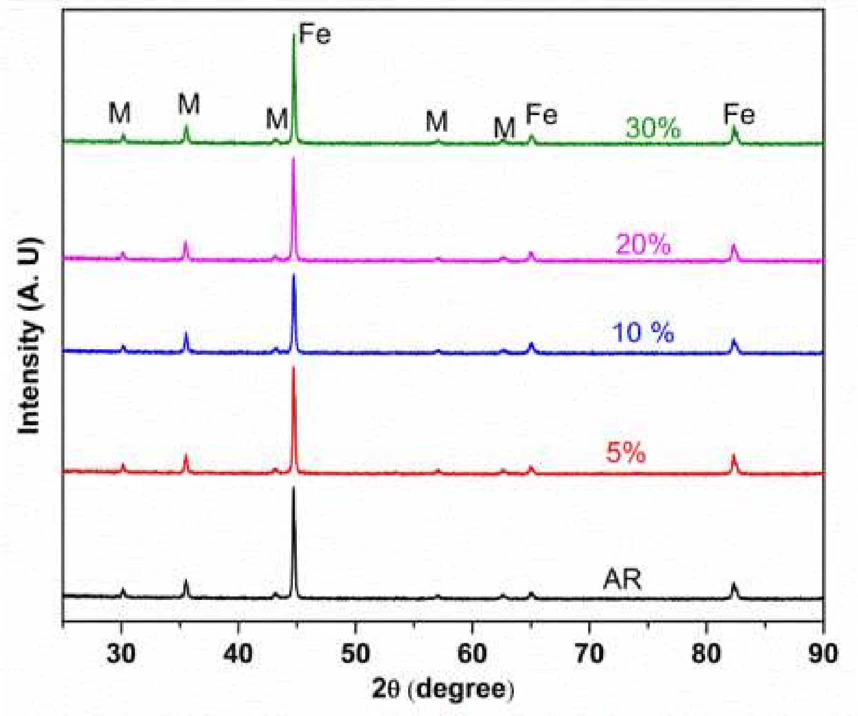

Figure 3.5 XRD of different cold worked sample exposed in autoclave for 5 days.

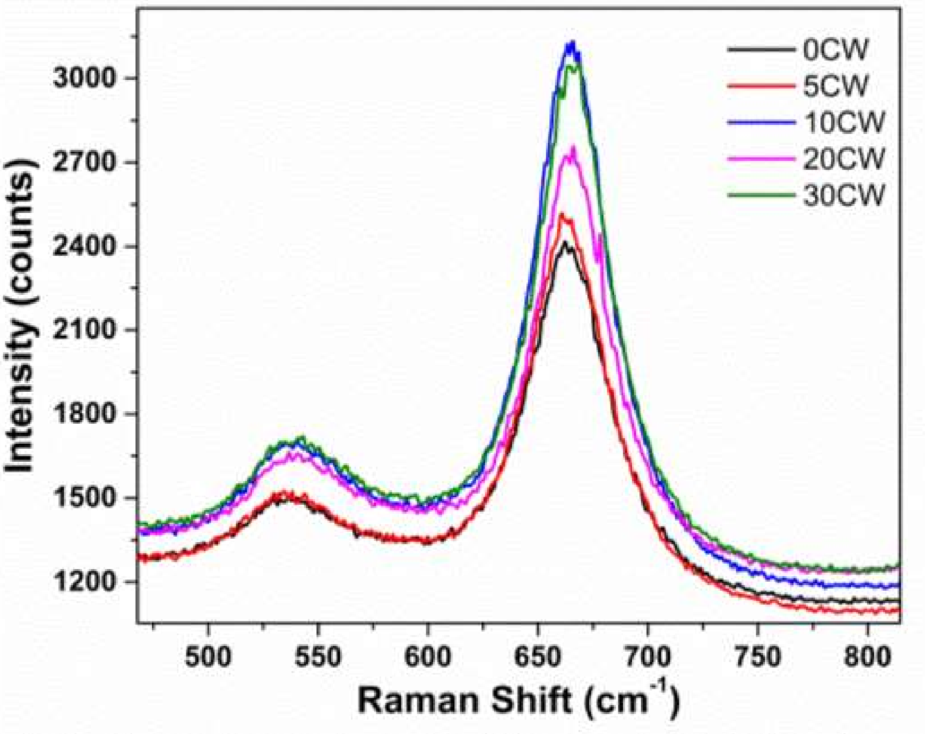

Figure 3.6 Raman spectrum of the of the different cold worked sample exposed in autoclave for 5 days.

3.3.5 Electrochemical Analysis

Figure 3.7 shows the potentiodynamic polarization curve of oxidized sample in borate buffer solution (pH 9.2). This is to ascertain the stability (passive zone) of the magnetite in the potential range from -300 mV_{SCE} to 850 mV_{SCE}. Passive current density in this potential was measured to vary in the range 0.22 to 0.95 μA cm^{-2}.

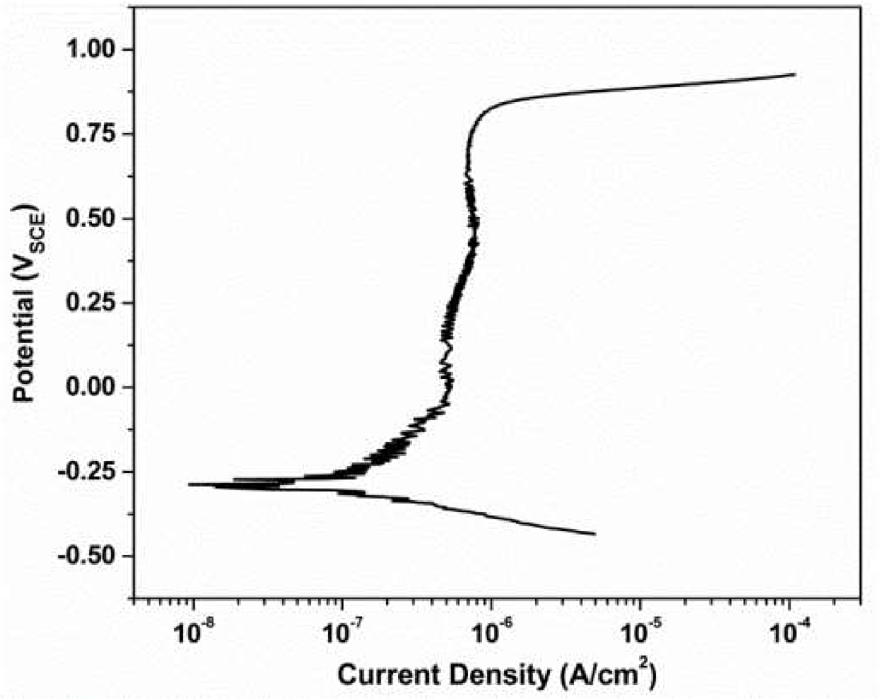

Figure 3.7 Potentiodynamic polarization curve of AR 120 h oxidized carbon steel samples showing the stability region of magnetite film in borate buffer solution.

Magnetite film formed on the coupons due to exposure to high temperature water is semiconducting in nature. The metal loss through the magnetite i.e. total corrosion rate depends on the concentration of point defects present in the magnetite film [Zhang **et al., 1998,** Macdonald 1999, Fujimoto **et al., 2007,** Bojinov **et al., 2000**]. Points defects present in the oxide film facilitate the diffusion of ions through the film. Mott-Schottky analysis was used for determination of defect density in the oxide film [Kumar **et al., 2010,** Wielant **et al., 2007,** Guo **et al., 2006,** Zeng **et al., 2004,** Luo **et al., 2012,** Antunes **et al., 2012,** Sicupira **et**

al., 2017]. In this process, the electrochemical system consists of two capacitance in series i.e. depletion layer capacitance C_{SC} and Helmholtz layer capacitance $C_{H.}$ The capacitance value of Helmholtz layers (C_H) is always very high as compared to depletion layer capacitance $C_{SC.}$ As they are in series, total capacitance value will be predominantly due to depletion layer capacitance C_{SC}.

Mott-Schottky analysis was done to measure the capacitance of each cold worked sample exposed for 120 h to calculate the defect density. In this analysis, the capacitance was measured as a function of applied potential. Figure 3.8 shows the Mott-Schottky plot of the different cold worked specimen oxidised for 120 h in autoclave. The type of defect present in the oxide can be determined from the nature of the slope. A positive slope indicates the oxide is an n-type semiconductor while a negative slope indicates the oxide to be p-type semiconductor. Mott-Schottky plot of all the cold worked specimen showed two positive slope indicating magnetite films on the carbon steel is a n-type semiconductor. The reason for the presence of a second positive slope has been attributed to the change in donor type and/or donor density with potential or by the presence of second donor level in the band gap [Luo **et al., 2012**]. The defect density was calculated on the basis of both the slope using the equation 2.4. Average value of the defect density in the oxide film of different cold worked samples is shown in Figure 3.9 and the values reported earlier are also included for comparison.

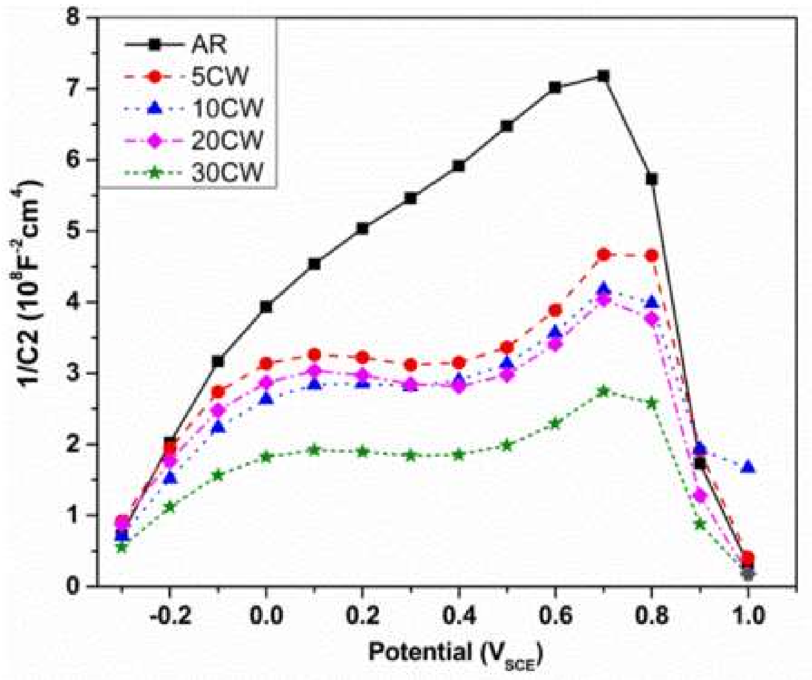

Figure 3.8 Mott-Schottky plot of different cold worked sample exposed in autoclave for 120 h.

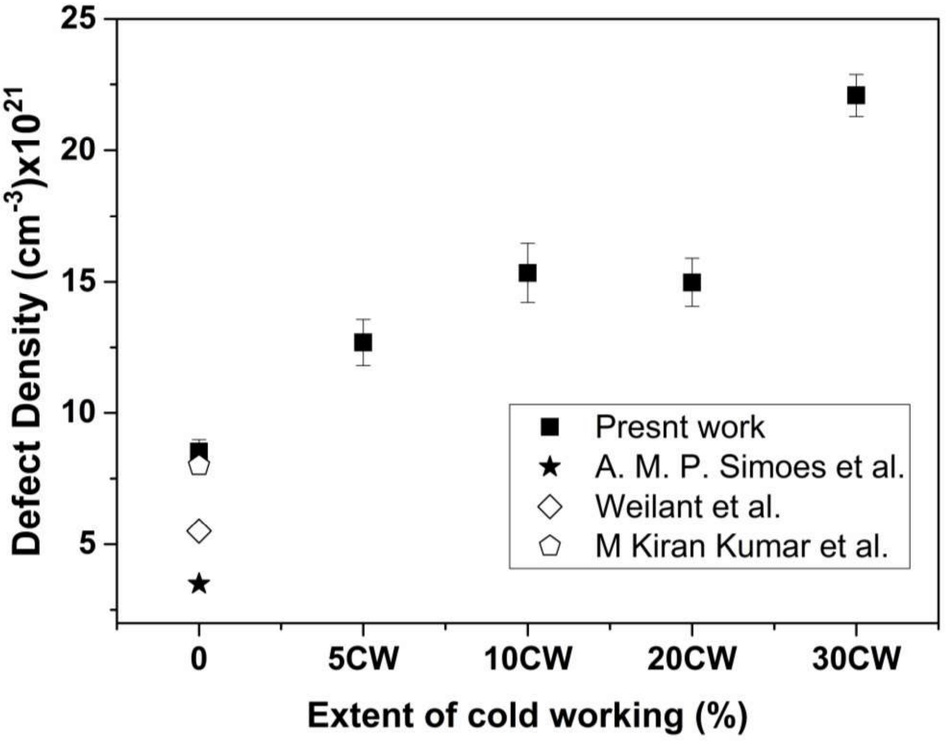

Figure 3.9 Variation of the defect density in the oxide film formed in deferent cold worked sample exposed in an autoclave for 120 h calculated by Mott-Schottky analysis.

Defect density in the magnetite film has been reported earlier to be in the range of $3x10^{21}$-$8x10^{21}$ cm^{-3} [**Kumar et al., 2010, Wielant et al., 2007, Simoes et al., 1990**] which is comparable to the defect density values measured in the present study for the oxide formed on AR specimens. In the oxide of cold worked samples, the defect density was found to increase and the maximum value measured was $2.2x10^{22}$ cm^{-3}.

According to point defect model [**Chao et al., 1981, Moon et al., 1998**], the passive film formed on metals/alloys contains a number of point defects such as cations at interstitial positions and cation and oxygen vacancies. Interstitial cations and oxygen ions vacancies act as a donor leading to the formation of n-type oxide while and cation vacancies acts as acceptor leading to the formation of p-type oxide. In the cold worked carbon steel samples there is an increase in the dislocation density and a consequent increase in the surface energy. Due to increase in surface energy during oxidation the generation of cation at metal-oxide interface would be rapid. Due to rapid formation of cations during oxidation, it will not get sufficient time to go to lattice position in the oxide and will be present as interstitials favouring formation of n-type oxide. Hence there is increased rate of oxide film formation with extent of cold working.

The faster rate of oxide formation resulted in an increased rate of oxidation (Figure 3) and also in the increased disordered structure and hence higher defect density. Higher defect density leads to the faster diffusion of the iron ions from the metal oxide interface to oxide water interface and thereby increasing in the total corrosion rate which matches with the total corrosion rate as shown in Figure 3(b).

3.3.6 Implication of the results towards FAC susceptibility

The results obtained in the present study indicate that cold working of carbon steel does not alter the type of oxide formed (magnetite) as compared to that of AR material. Also the size of the crystallites formed on the outermost layer also remained the same irrespective of the level of cold working of the material. However, defect density of the oxide formed increased with level of cold working. This increased defect density therefore finally resulted in increased level of oxidation as a function of increased level of cold working of the carbon steel, as shown in Figure 3.

Since FAC is electrochemical dissolution of the oxide film into the environment (through the boundary layer, and is also dictated by the solubility limit of the dissolving ions in the bulk solution), one may expect an increasing trend of dissolution with increased levels of cold work due to the increased defect density in the oxide. However, the extent of the contribution of the increased defect density in affecting solubility has to be shown by further systematic studies. However, it was not the intent of the present study to establish FAC behaviour of the carbon steel having oxides with different defect density. The authors hope the present study would lead to further studies on this aspect.

3.4 Highlights

A sheet of 5 mm thickness of A 106 Gr B was cold rolled to obtain 5-30% reduction in thickness and the these specimen were exposed to lithiated water (pH 10-10.2) at 270°C in an autoclave for different durations up to 240 h. From the experimental results following highlights were made.

1. The total oxidation/corrosion rate ($Fe_{(oxide)} + Fe_{(solution)}$) increased with the extent of cold working.
2. At 270 °C, the defect density of magnetite formed on carbon steel increased with increasing level of cold working of the material. This increased defect density was the reason for increased oxidation of the carbon steel with increased level of cold working (hence increased thickness of the magnetite film on higher cold worked samples).

3. XRD and Raman spectra showed the formation of magnetite film on all the samples i.e. AR and cold rolled. The composition of the film did not change with the cold working. No other oxides of iron were formed.
4. SEM images of the AR and cold worked samples showed the morphology of precipitated (outermost) layer. The morphology and size of the crystals remained the same for all the samples (AR and cold worked) as it depends mainly on environmental factors rather than the cold worked condition of the material.

Chapter 4

EFFECT OF pH AND TEMPERATURE ON OXIDATION BEHAVIOUR AND NATURE OF OXIDE

4.1 Introduction

Carbon steel is extensively used as structural material for majority of the components in the secondary circuit of pressurized heavy water reactors (PHWRs). Feed water system of Indian PHWRs is made of carbon steel ASTM A 106 Gr B [Kain **et al.,** 2008, Kain **et al.,** 2011]. The major mode of degradation of these secondary circuit components/pipelines is flow accelerated corrosion (FAC). Flow accelerated corrosion causes thinning of carbon steel components/pipelines carrying high velocity water/steam. The secondary circuit components are exposed to temperatures upto 200 °C and the process fluid is de-aerated alkaline water (pH adjusted by ethanolamine (ETA) or ammonia). It is known that the mechanism of FAC is electrochemical dissolution of the protective magnetite film (formed on the internal surfaces of carbon steel pipelines/components) at a faster rate in a high velocity environment [Ahmed 2010, Guimaraes 2003, Poulson 1999, Dooley et al., 2000]. FAC has caused a large numbers of failures in piping used in all types of fossil, industrial steam and nuclear power plants [Kain **et al.,** 2008, Kain **et al.,** 2011, Dooley et al., 2000, Moon et al., 2005, Kain 2014].

The parameters that affect FAC are environmental, material and hydrodynamic [Kain 2014, Betova et al., 2010]. Environmental parameters include water chemistry e.g. pH, dissolved oxygen (DO) and temperature of the process fluid. Water chemistry, especially pH affects FAC rate by altering the solubility of the oxide film formed on the internal surfaces of components/pipelines [Betova 2010, Sweeton1970]. Dissolved oxygen (DO) present in the process fluid also affects the solubility by changing the redox potential of the environment but its effect is more pronounced on the type of oxide formed on the base material. Presence of DO converts magnetite (Fe_3O_4) to hematite (Fe_2O_3) or γ-FeOOH [Dooley et al., 2000] that has a very low solubility in the process fluid compared to that of the magnetite [Dooley et al., 2000]. Temperature of the environment also affects FAC rate by affecting the solubility of the corrosion product of magnetite [Betova et al., 2010, Sweeton et al., 1970, Tremaine et al., 1980].

Many researchers have shown the effect of temperature and pH on the solubility of magnetite using magnetite powder [Betova et al., 2010, Sweeton et al., 1970, Tremaine et al., 1980]. There are also studies in literature on the formation of oxide film and its characterization [Sinha et al., 2015, Kumar et al., 2010]. However, there is no systematic study available in literature that shows the effect of temperature and pH on the formation of magnetite film and nature of the oxide film. The characteristics of the magnetite film formed at different temperatures and in different pH conditions may be different. If so, the nature of the magnetite film formed may affect its dissolution kinetics, hence its FAC behavior. Therefore, the aim of the present work is to show the effect of temperature and pH on the oxide film formation kinetics and how these parameters affect the nature of the oxide film.

Many researchers established the kinetics of oxidation/corrosion by weight measurement as a function of time of exposure of the material to the process fluid [Sinha et al., 2015, Mabuchi et al., 1991]. The weight measurement provides the total weight of oxide film/oxide film thickness and the total corrosion rate during exposure in high temperature and pressure environment. The Mott-Schottky method is also extensively used for determination of semiconducting property of the oxide film on metals and alloys and also for the determination of the defect density of the oxide film [Kumar et al., 2010, Mabuchi et al., 1991, Wielant et al., 2007]. The detailed characterization of the oxides formed on carbon steel has been done in this study using the weight gain measurements as well as Mott-Schottky analysis to arrive at the defect density in the oxides formed.

4.2. Experimental

4.2.1 Material and Microstructure

Carbon steel ASTM A 106 grade B was used in this study. The material used was in the form of a sheet of 5 mm thickness. The chemical composition was analysed by spark optical emission spectroscopy and is given in Table-3.1. Specimens of size 15 mm x 10 mm were cut from the sheet and were ground on successively finer emery papers up to 600 grit. Final polishing was done using 1 µm diamond paste. Microstructure of these specimens was obtained by swab etching of the specimens with 2% nital (ethanol + nitric acid) solution and examination under an optical microscope.

4.2.2 Oxidation in Autoclave

The specimen from carbon steel sheet were cut (size ~ 20 mm x 10 mm) and ground on successively finer emery papers up to 600 grit. Dimensions of each specimen were accurately measured using a vernier caliper to calculate the surface area of the specimens. All the specimens were cleaned ultrasonically and weight was measured up to 1 µg accuracy and designated as W_1.

These specimens were fixed on a stand and placed in an autoclave. Oxide film was developed in the following two conditions:

- **a.** To study the effect of temperature, six temperatures viz. 150 °C, 180 °C, 210 °C, 240 °C, 270 °C and 300 °C were selected. Specimens were exposed in an autoclave in DM water for 7 days at the selected temperature.
- **b.** To study the effect of pH of the environment, two pH values were selected viz. DM water (neutral pH) and pH_{RT} 9.5. The pH was maintained using ethanol amine (ETA). Specimens were exposed in an autoclave for different time intervals for up to 20 days at 150 °C.

Temperature and pH in the static autoclave can be maintained as per actual plant conditions. Temperature and corresponding pressure can be simulated in a static autoclave. In static autoclave flow conditions are not maintained. Capacity of the autoclave used was 1.5 L. and there was negligible change in the pH value after the experiment.

The oxide film was grown in a completely de-aerated condition. For this purpose, high purity Ar gas was purged till the temperatures of 70 °C was attained and this temperature was held for 1 h maintaining continuous purging of Ar gas. The Ar purging was stopped at 70 °C and then temperature raised to 150 °C. The venting was done at 150 °C as per ASTM G2M [2011] and then the temperature was raised to the final temperature. The corresponding pressure at 150 °C, 180 °C, 210 °C, 240 °C, 270 °C and 300 °C were ~3.7, 9.0, 18.0, 32.5, 54.0 and 84.5 bar respectively. This process ensured the DO as low as possible (<45 ppb) [ASTM G2M 2011]. After exposure for the intended duration at the selected temperature, the specimens were withdrawn, washed with acetone and weighed (W_2). Some exposed specimens were descaled using Clark's solution (2% antimony trioxide and 5% stannous chloride in 100 ml conc. hydrochloric acid (37-38%)). After descaling, the specimens were weighed (W_3). The weight loss, total iron dissolved and thickness of the magnetite layer formed were calculated from equations (4.1)-(4.3). For calculation of W_2 four specimens were used and for W_3 three specimen. Calculations were done using average values.

$\Delta W_{(oxide)} = W_2 - W_3$ (4.1)

$\Delta Fe_{(total)} = Fe_{(oxide)} + Fe_{(solution)} = (W_1 - W_3)$ (4.2)

$t_{oxide} = \Delta W_{(oxide)} / \rho_{Fe3O4}$ (4.3)

Where W_1 is initial weight of the specimens, W_2 is weight after exposure at selected temperature, W_3 is weight after descaling, $\Delta W_{(oxide)}$ is weight loss after descaling i.e. weight of oxide, $\Delta Fe_{(total)}$ is the total iron oxidised, t_{oxide} is thickness of oxide film, ρ_{Fe3O4} is density of magnetite (5.15 g/cc), $Fe_{(oxide)}$ is weight of iron in the oxide film, $Fe_{(solution)}$ is weight of dissolved Fe ions during exposure in autoclave.

In calculation of the weight different of W_2 and W_3, weight correction was incorporated by measuring the weight loss of the blank (fresh carbon steel specimen without any oxide) specimen during descaling with Clarke's solution.

4.2.3 Oxide film characterization

All the specimens subjected to autoclave exposure were examined by scanning electron microscopy (SEM) to establish surface morphology. Micro laser Raman spectroscopy and X-ray diffraction (XRD) were used to study the nature of the oxide film formed on the specimens. In Raman spectroscopy, measurements were done using green visible light of wavelength 514 nm and laser power of 18 mW in air at room temperature. X-ray diffraction study was done on the autoclaved specimen using Cu $K\alpha$ (1.5406 Å). XRD was carried out at a scan rate of 0.02 °/s with 2θ range 25 to 90°.

4.2.4 Electrochemical characterization of the oxide film

All the electrochemical experiments were done in a borate buffer solution of pH 9.2 (0.075 M $Na_2B_4O_7$, $10H_2O$ + 0.05 MH_3BO_3) at room temperature. Electrochemical polarization was done to determine the potential range at which the oxide film is stable. This was done using the standard three electrode system wherein the oxidized specimen was made the working electrode, platinum as counter electrode and saturated calomel electrode (SCE) was used as the reference electrode. All potentials reported in this study are with respect to saturated calomel electrode. De-aeration of the borate buffer solution was done by bubbling Ar gas 30 minutes before the start of the experiment and the gas was also bubbled during the experiment.

Electrochemical impedance analysis followed- by Mott-Schottky analysis was done by determining the capacitance at different potentials. For this purpose electrochemical impedance measurement was done in the potential range -300 mV_{SCE} to 1000 mV_{SCE} at a step potential of 100 mV in the borate buffer solution and capacitance was determined at 1 kHz [Mabuchi et al., 1991, Guo et al., 2006, Zeng et al., 2004, Luo et al., 2012, Jinlong et al., 2014, Zhu et al., 2016]. At the frequency ~1 kHz, The capacitance values were nearly frequency independent [Mabuchi et al., 1991]. The relationship between capacitance and applied potential is given by Mott-Schottky equation (eqn. 4.4) [Mabuchi et al., 1991, Guo et al., 2006, Zeng et al., 2004, Luo et al., 2012, Jinlong et al., 2014, Zhu et al., 2016, Gomes et al., 1996, Simoes et al., 1990]. Reciprocal of the square of capacitance was plotted against the applied potential. From the slope of this plot defect density in the oxides formed at different temperatures and in different pH values was calculated using Mott-Schottky relationship (Eqn. 4.4).

$$\frac{1}{C^2} = \frac{2}{\varepsilon\varepsilon_o qNA^2}\left(E - E_{FB} - \frac{KT}{q}\right) \qquad (4.4)$$

Where ε is the dielectric constant of the specimen (15.6 for magnetite) [Jinlong et al., 2014], ε_o the vacuum permittivity (8.85×10^{-14} F. cm^{-1}), q the charge, N the defect density, q the electronic charge (1.602×10^{-19} C), A is surface area (cm^2) of the specimen, E_{FB} the flat band potential (V), K the Boltzmann constant ($cm^2 g s^{-2} K^{-1}$) and T the absolute temperature.

4.3. Results and Discussion

4.3.1 Materials and Microstructure

The chemical composition of the carbon steel is shown in Table 4.1 confirming the material used in the study is carbon steel ASTM A106 Grade B [ASTM A106 2015].

Table 4.1: Chemical composition of carbon steel sheet used in the study

Elements	C	Mn	P	V	Ni	Mo	S	Si	Cr	Cu	Fe

Weight%	0.115	0.33	0.017	0.09	0.021	0.005	0.019	0.11	0.043	0.040	Bal
ASTM A106 Gr-B	0.3*	0.29-1.06	0.035*	0.08#	0.4*	0.15*	0.035*	0.1#	0.4*	0.4*	Bal

* Maximum, #minimum

The microstructure of the materials after etching with 2% nital solution is shown in figure 4.1. Figure 4.1 clearly shows the ferrite-pearlite structure of the as – received (AR) specimen. As the carbon content is towards lower side, the pearlite content in the microstructure is very less.

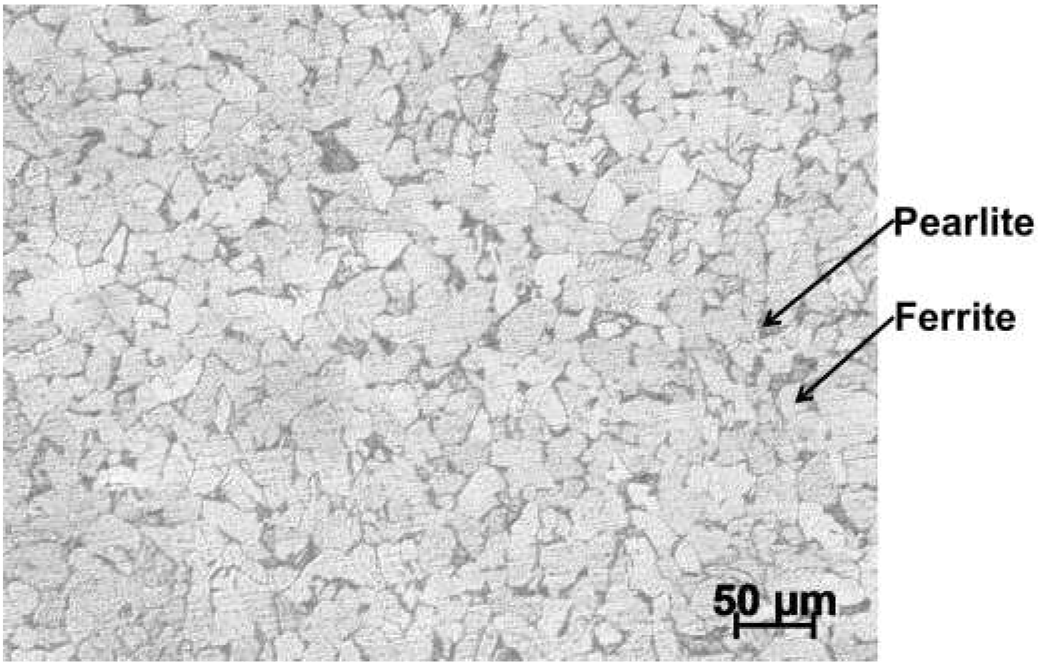

Figure 4.1 Microstructure of carbon steel specimen showing ferrite-pearlite and confirming microstructure of a low carbon steel.

4.3.2 Oxidation behaviour

Analysis of the weight of specimens measured at different stages provides the oxidation behaviour of the carbon steel. During the oxidation process of carbon steel, two processes take place simultaneously: a) formation of oxide film on the surface of carbon steel by the reaction of metal and environment by growth and precipitation mechanism [Robertson 1989, Frayne 2002, Rihan et al., 2006, Schwertmann et al., 2000, Fujiwaraa et al., 2011]. This process results in the weight gain of the specimen. b) Dissolution of the carbon steel in the environment. This results in weight loss of the specimen in high temperature corrosion process. The mechanism of this high temperature corrosion process is very well established [Robertson 1989, Frayne 2002, Rihan et al., 2006, Schwertmann et al., 2000, Fujiwaraa et al., 2011]. The difference in weight W_2 and W_1 gives the resultant of the above mentioned two processes. The difference in weight W_2 and W_3 give the weight of the oxide film formed on the surface of the specimen and that in W_1 and W_3 gives the total corrosion/oxidation of the specimen i.e. the sum of the iron ions (ferrous and ferric) in the oxide film and that dissolved in the water during autoclave exposure. Thickness of the oxide film was calculated from the weight of oxide and density of the magnetite (5.15 g/cc). It was assumed that the density of the oxide film formed at different temperature and in different pH conditions remains the same i.e. 5.15 g/cc.

4.3.2.1 Effect of temperature

Figure 4.2 shows the resultant weight change after the exposure of specimen for 7 days in an autoclave at different temperatures. It can clearly be seen that up to the exposure temperature of 240 °C, there is weight loss of the specimen and on exposures at temperatures above 240 °C, weight gain was observed. This behaviour can be explained on the basis of the mechanism of oxide formation. During the oxide film formation, the base material oxidises producing ions (ferric/ferrous) and these ions may either dissolve in the environment or form oxide on the surface. Along with base materials, a part of the oxide formed may also dissolve in the environment. The dissolution processes results in weight loss whereas oxide formation results in weight gain. Therefore, there is a competition between these two processes. At temperatures lower than 240 °C, where oxide solubility is high [Sweeton et al., 1970, Fujiwaraa et al., 2011, Styrikovich et al., 1971], there is an overall weight loss whereas at temperatures higher than 240 °C, where oxide solubility is low, weight gain was observed. This is the reason why during the hot conditioning the temperature is kept above 240 °C although there is alkaline pH (10-10.2) by addition of lithium hydroxide [Kumar et al., 2010].

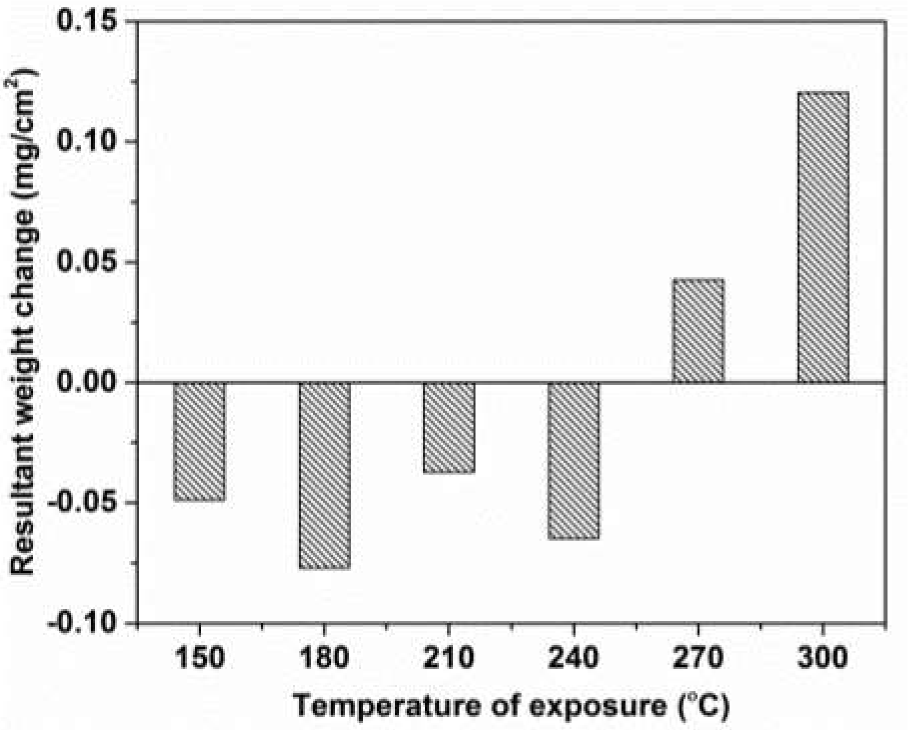

Figure 4.2 Effect of temperature on weight change of the carbon steel exposed at different temperatures for 7 days.

Figure 4.3 is the weight of the oxide film formed on the surface of carbon steel exposed for 7 days at different temperatures. There was an increase in the weight of the oxide film (W_2-W_3) with increase in exposure temperature, but this increase is gradual up to the exposure temperature of 240 °C and after that the increase is sharp. This is also attributed to lower solubility of oxide at higher temperature [Sweeton et al., 1970, Fujiwaraa et al., 2011, Styrikovich et al., 1971] that leads to more oxide formation by precipitation and hence a sharp increase in weight of the oxide. The weight of the oxide was converted to thickness of the oxide using density as per equation (4.3). Variation in thickness of the oxide showed a similar profile as shown in figure 4.3

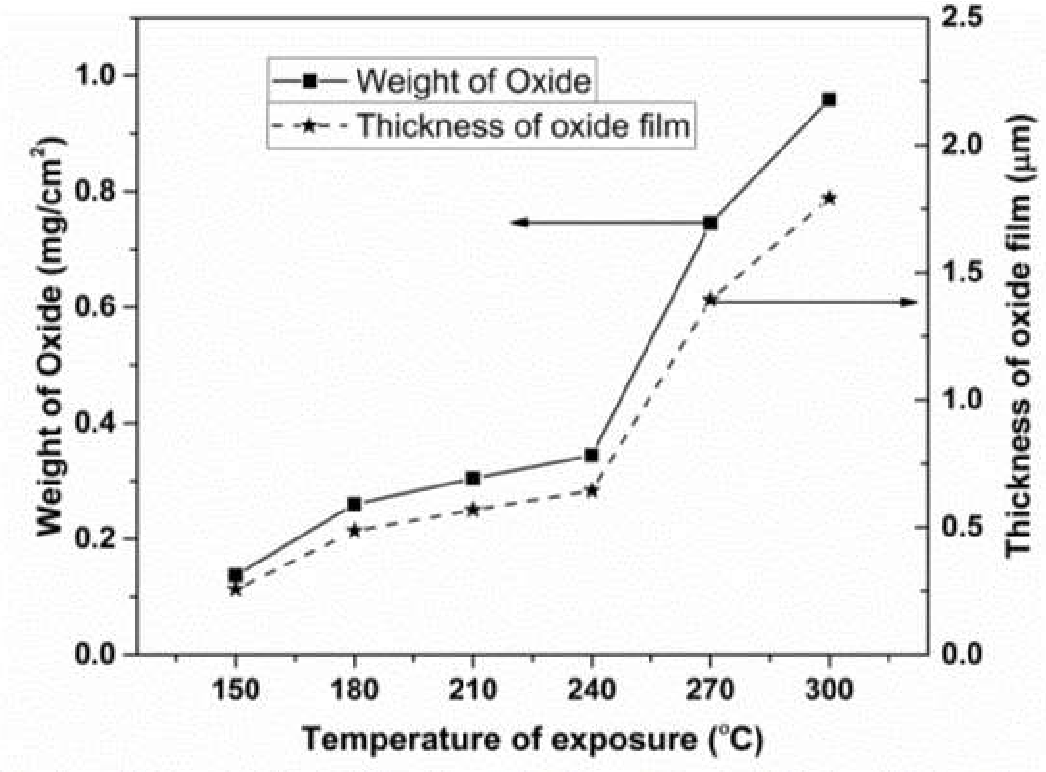

Figure 4.3 Variation in (a) weight of oxide and (b) thickness of oxide film with temperature of exposure (exposure duration 7 days).

The total corrosion/oxidation of base metal was calculated from the weight difference of W_1 and W_3. This gives the total weight of iron in the oxide, $Fe_{(oxide)}$ and the weight of the dissolved iron, $Fe_{(solution)}$. The total oxidation along with weight of oxide is plotted against temperature of exposure and is shown in figure 4.4. It is very clearly seen that the total oxidation is higher as compared to the weight of oxide upto exposure temperatures of 240 °C and above the exposure temperature of 240 °C, the total oxidation became lower than the weight of oxide. This implies that the oxidised species tends to have more dissolution than formation of oxide below 240 °C and vice versa. This result is in line with the reasultant weight change, shown in figure 4.2.

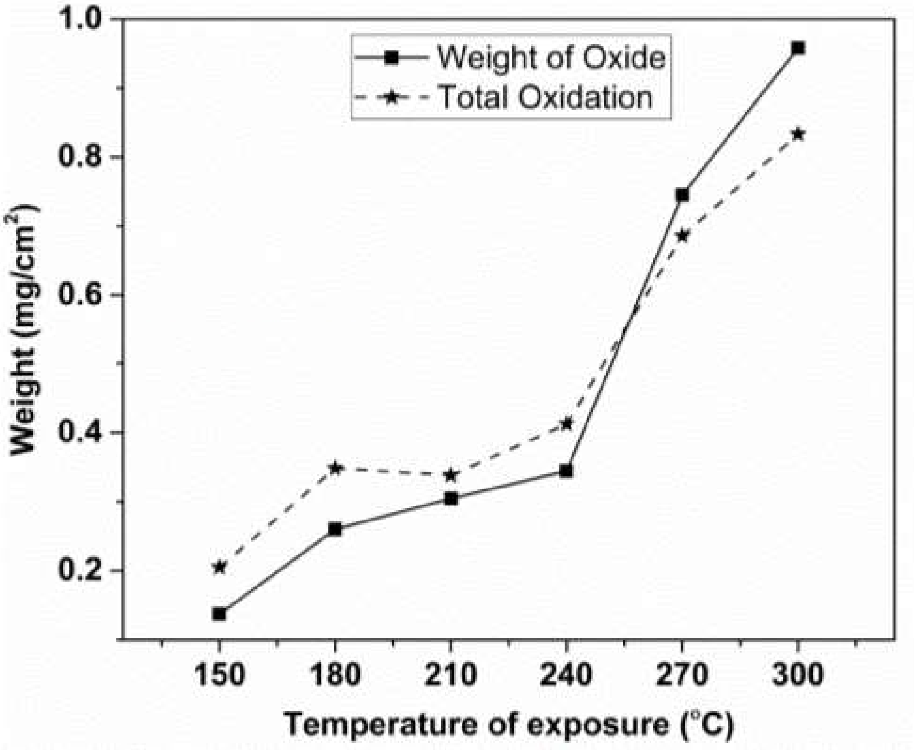

Figure 4.4 Effect of temperature on weight of oxide and total oxidation

The total dissolved iron ($Fe_{(solution)}$) during the formation of oxide was calculated as per equation 4.5.

$$Fe_{(solution)} = \text{Total corrosion} - W_{(oxide)} \times 0.7236 \qquad (4.5)$$

Figure 4.5(a) shows the variation of $Fe_{(solution)}$ with exposure temperaure. It was clearly seen that the dissolved iron ($Fe_{(solution)}$) increased up to the exosure temperature of 240 °C and above exposure temperature of 240 °C, the dissolved iron ($Fe_{(solution)}$) was less. This implies that most of the iron dissolving from the base material above the exposure temperature of temprature 240 °C goes into formation of the magnetite film and a very small fraction of that dissolves out into the process fluid as ionic iron. Iron in oxide is caculated on the basis of iron content in magnetite (Fe_3O_4) i.e. 72.36%. The ratio of iron dissolved to iron in oxide is plotted against the exposure temperaure and is shown in figure 4.5(b). Figure 4.5(b) shows that the ratio of iron dissolved in solution to the iron remained in the oxide decreased with increase in exposure temperaure. Although the total oxidation rate increased with temperature as shown in figure 4.4, the ratio of $Fe_{(solution)}$ to $Fe_{(oxide)}$ decreased from 55% at 150 °C to just 10% at 300 °C. This implies that the incorporation of oxidised iron in the oxide increased with the exposure temperaure.

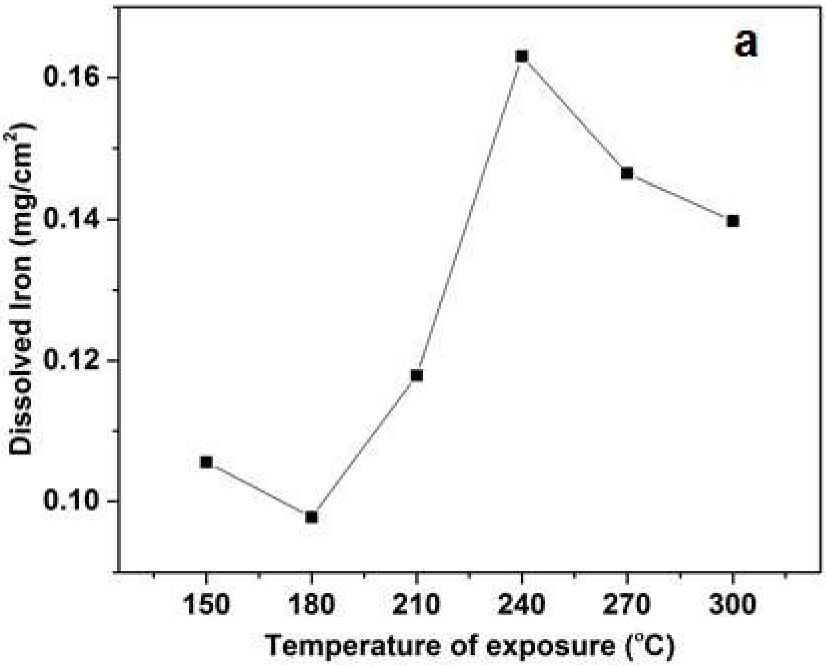

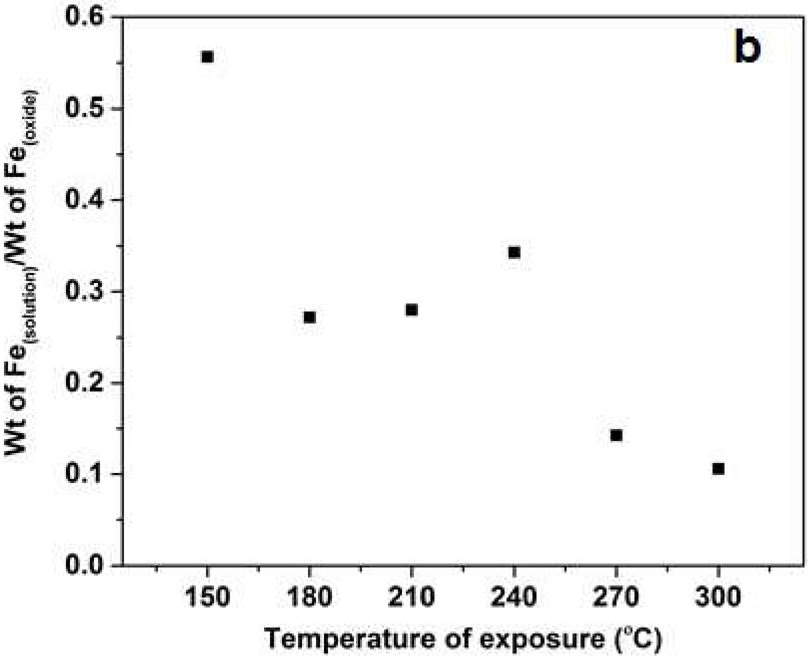

Figure 4.5 Effect of temperature on (a) dissolved iron and (b) ratio of dissolved iron to iron in oxide during exposure of specimen in the autoclave.

4.3.2.2 Effect of pH

The effect of pH on the oxidation behaviour was studied by forming oxide film on carbon steel at a fixed temperature and at different pH values. The temperature taken was 150 °C and two pH values selected were (i) neutral pH (DM water) and (ii) alkaline pH 9.5 (using ethanolamine). As explained earlier, carbon steel specimens were exposed for different durations and weight measurements were done at different stages. On the basis of weight measurements, the resultant weight after exposure, weight of the oxide, total oxidation, weight of dissolved iron during oxidation and ratio of iron dissolved to iron in the oxide were calculated and are shown in figure 4.6 (a), (b), (c), (d) and (e) respectively for both the pH values.

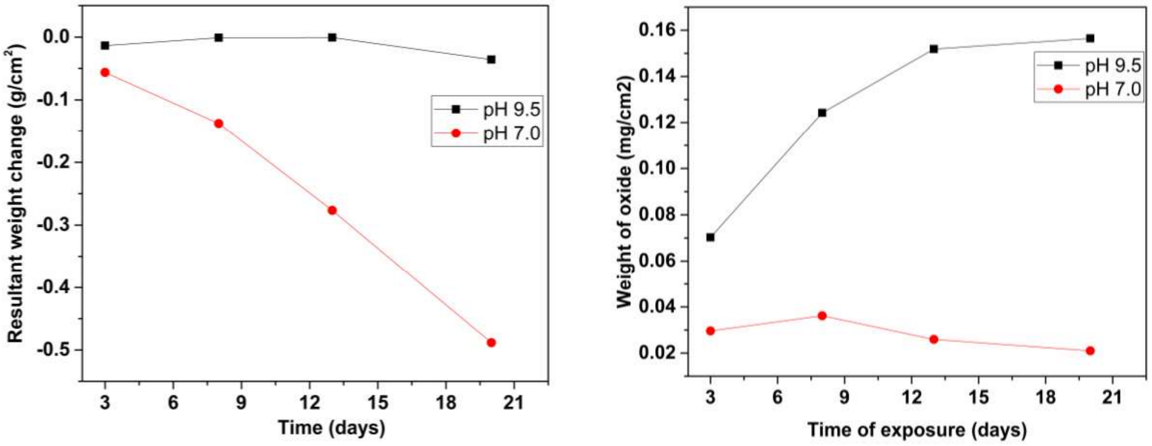

(a) (b)

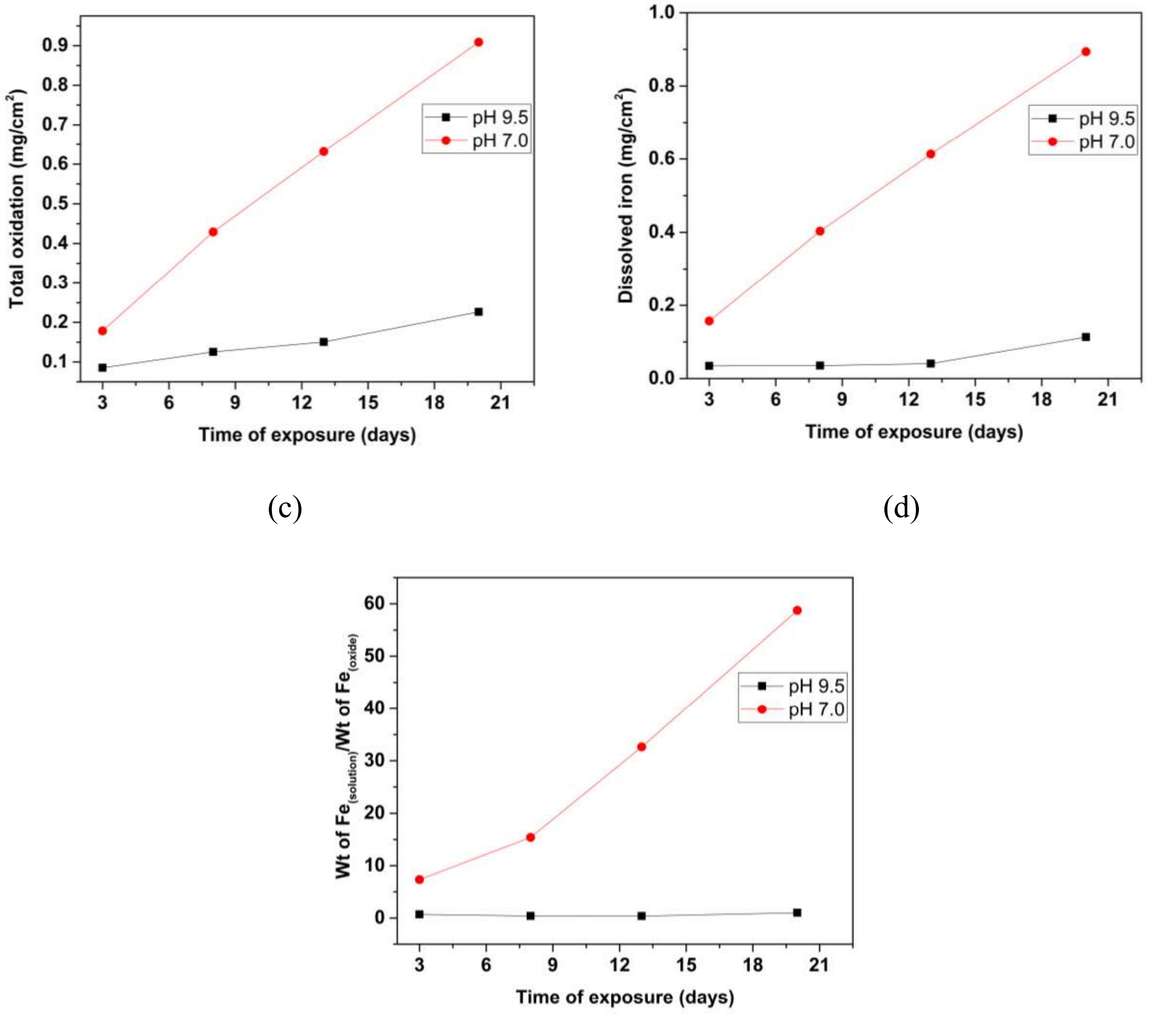

(c) (d)

(e)

Figure 4.6 Variation in (a) resultant weight (b) weight of oxide (c) total oxidation (d) dissolved iron and (e) ratio of Fe$_{(solution)}$ to Fe$_{(oxide)}$ with temperature.

As explained in section 4.2.1, the resultant (overall) weight change is the result of two processes taking place simultaneously i.e. dissolution into solution and oxide film formation. Figure 4.6(a) shows the weight loss in both the environment but the weight loss in neutral pH is much higher than that at the alkaline pH value. Figure 4.6(b) shows that the weight of oxide film formed in neutral environment is lower than that formed in alkaline pH. The weight of oxide in DM water decreased with exposure time while that increased in case of alkaline pH. This indicates that rate of dissolution of base/oxide is more than that of oxide formation in neutral pH environment. Total oxidation i.e. weight of iron in oxide and weight of iron dissolved in the environment are shown in figure 4.6(c) indicating that the total oxidation in neutral pH is more than that in alkaline pH at 150 °C. The extent of oxidation is increased with increase in exposure time. The weight of dissolved iron is shown in figure 4.6(d) and it also shows a similar behaviour. The ratio of the weight of dissolved iron to the weight of iron in the oxide is plotted and shown in figure 4.6(e). This indicates that the dissolved iron in DM water is 10.7 fold higher than that is alkaline water for the 3 days exposed specimen at 150 °C. The extent of dissolved iron increased with increase in exposure time and was 58.8 fold higher after 20 days of exposure. All the above results are attributed to the higher solubility of base/magnetite in DM water than in alkaline water.

4.3.2.3 Mechanism of oxidation

The results shown in figure 4.6 can be explained on the basis of mechanistic representation given in figure 4.7. The oxidation of iron from the carbon steel takes place by release of Fe^{+2} from the base material (step-1), as shown in figure 4.7. The Fe^{+2} ions are also generated by the reductive dissolution of magnetite (step-2). The iron ions (Fe^{2+}) may either diffuse into the bulk solution (step-3) (directly, if there is no oxide film present or by diffusion through the oxide film) or may form oxide on the surface of carbon steel.

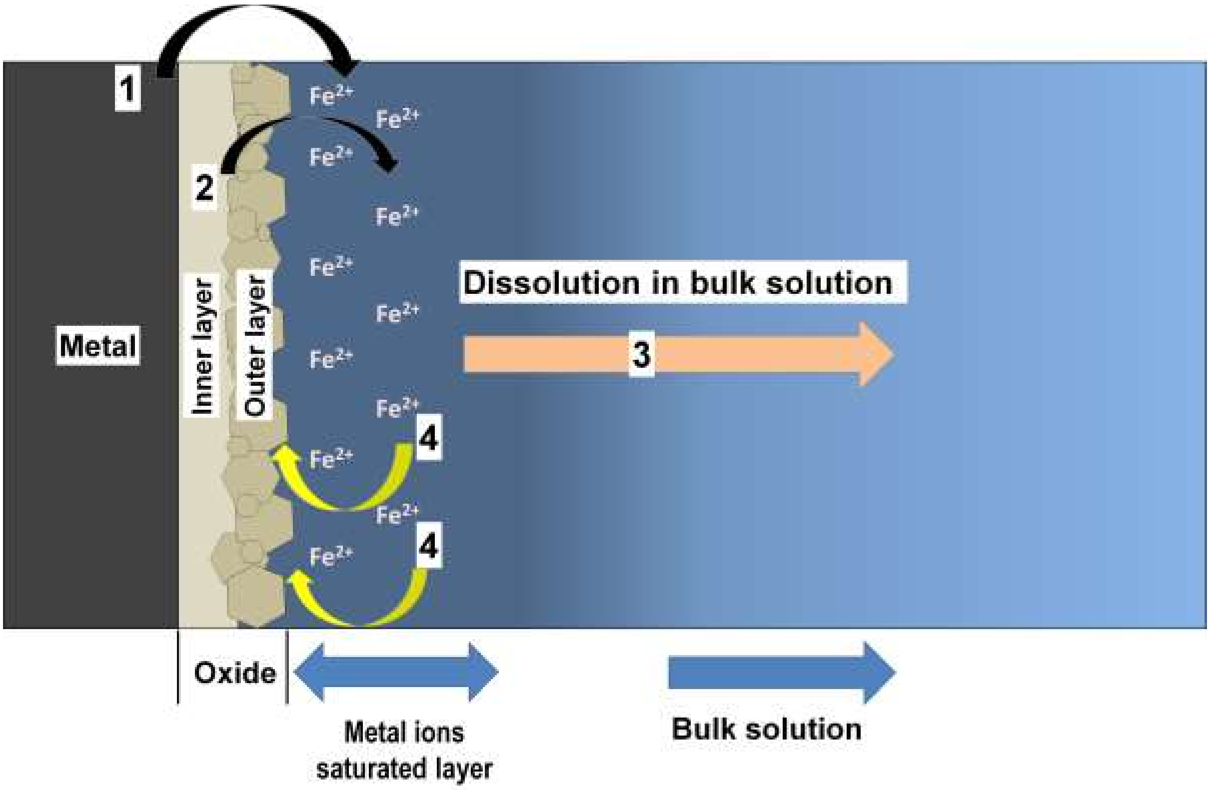

Figure 4.7 Schematic of oxide formation and dissolution process.

A fraction of the dissolved Fe^{+2} may precipitate back onto the outer surface of the oxide (step-4) after the solubility of Fe^{+2} is exceeded in immediate vicinity of the oxide film. Solubility is the maximum amount of the dissolved ions that can be accommodated in the particular water chemistry and temperature. More the solubility of the environment more diffusion of oxidised iron species from the surface to the bulk environment will take place and remain dissolved in the bulk solution. If the solubility is less, the reverse process i.e. precipitation will be a dominant process and oxide film formation by precipitation will take place.

4.3.3 XRD Characterization

The X-ray diffraction (XRD) studies of the oxides grown on the carbon steel specimens after exposure in an autoclave at different temperatures for seven days were carried out to establish the phases present in the oxide. Figure 4.8 shows the X-ray diffractogram (using Cu Ka incident radiation, 1.5406 Å) of the carbon steel exposed in an autoclave for seven days. Peaks are observed at 2θ of 44.75°, 65.04° and 82.31° corresponding to base material i.e. α-Fe (BCC crystal) [Islam et al., 2015]. The XRD peak at 2θ of 30.19° (hkl 220), 35.54° (hkl 311), 43.25° (hkl 400), 53.55° (hlk 422) 57.06° (hkl 511) and 62.63° (hkl 440) observed in the oxide film formed on specimens at different temperature correspond to magnetite (Fe_3O_4) (JCPDS, No. 19-0629). However, It can very clearly be seen from figure 4.8(a) that only the peaks, at 2θ of 35.54° (hkl 311) and 43.25° (hkl 400), with very less intensity of magnetite are observed (formed at 150 C). As the temperature of exposure was increased to 180 °C, the intensity of the peaks at 35.54° (hkl 311) and 43.25° (hkl 400), increased with the emergence of new peaks at 30.19° (hkl 220) and 62.63° (hkl 440) as seen in figure 4.8(b). Similarly, as we moved towards higher exposure temperatures viz. 210 °C, 240 °C, 270 °C and 300 °C, the intensity of the peaks due to magnetite increased with emergence of new peaks (figure 4.8 (c), (d), (e) and (f) respectively). This is attributed to increased magnetite film thickness with increase in the formation temperature. This result is in line with the thickness calculated by weight measurement (figure 4.3(b)).

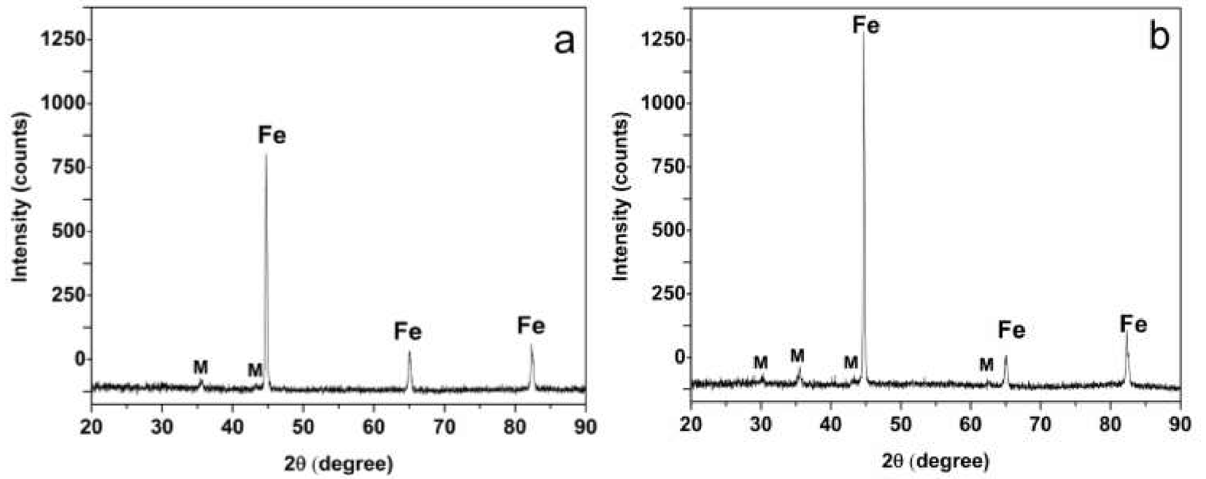

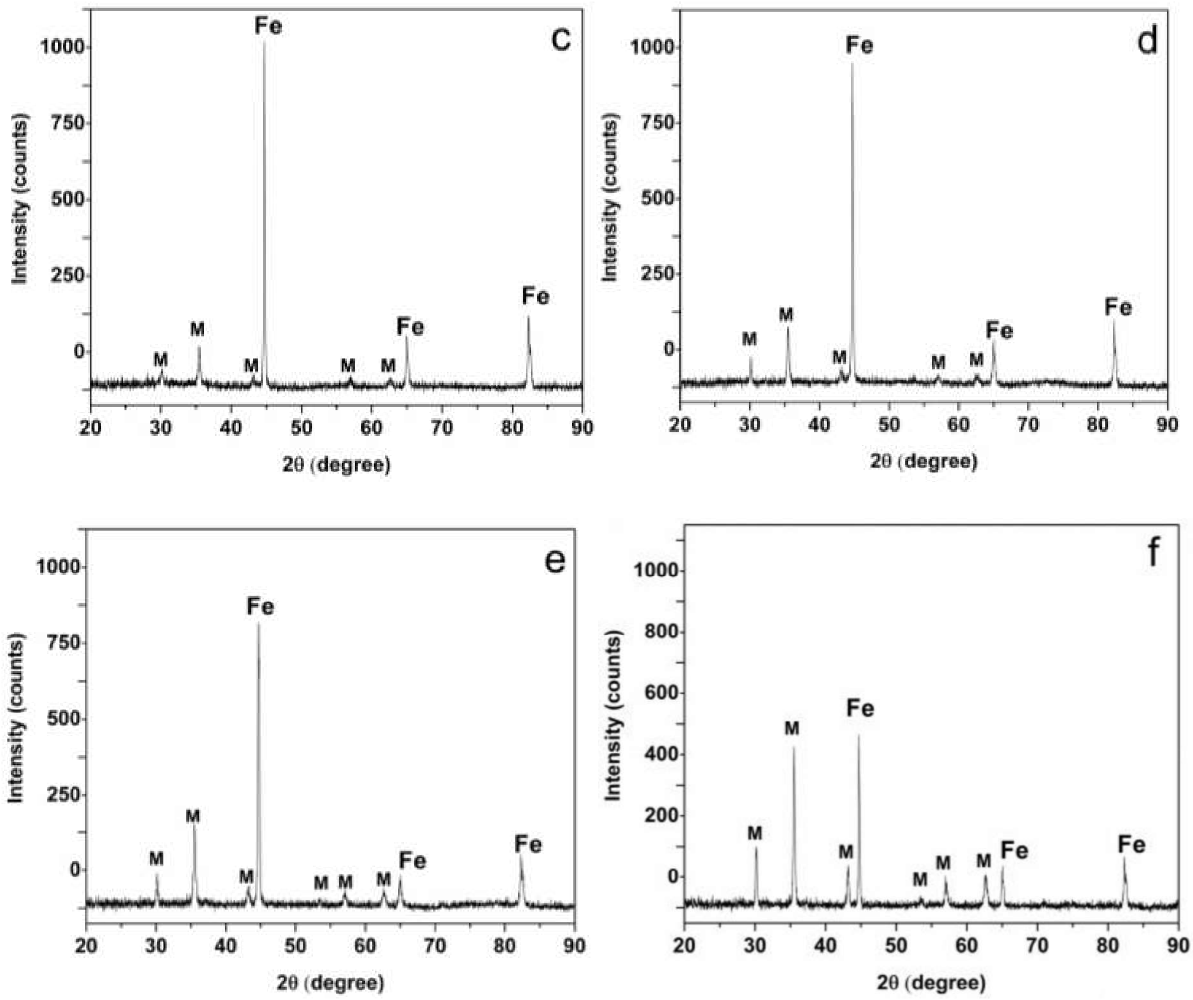

Figure 4.**8** XRD of the carbon steel exposed in DM water in autoclave at (a) 150 °C, (b) 180 °C, (c) 210 °C, (d) 240 °C, (e) 270 °C and (f) 300 °C for 7 days showing increase in number and intensity of magnetite peaks with increase in exposure temperature.

It can clearly be seen from the figure 4.8 that no other peak except that for magnetite and base material were observed. So, only magnetite phase of the iron oxide formed during the exposure in autoclave at temperatures from 150 °C to 300 °C, and other phases of iron oxide like hematite, goethite etc. did not form. The peaks due to base materials in the XRD indicate that the oxide film formed is very thin. The thickness of the oxide film in seven days exposure at 150 °C to 300 °C is 0.25-1.79 µm. Hence magnetite is formed at all the exposure temperatures.

The nature of oxide film formed at different temperatures on carbon steel was also studied by micro laser Raman spectroscopy. Figure 4.9 shows the Raman spectra of the oxide formed at different exposure temperature on carbon steel. It was observed that irrespective of temperature of formation, magnetite having Raman shift of 662 – 682 cm^{-1}, 538-548 cm^{-1} and 320-340 cm^{-1} was formed and these peaks correspond to phonon bands A_{1g}, T_{2g} and E_g respectively of magnetite [Shebanova et al., 2003, de Faria et al., 1997, Mendili et al., 2014]. Hence, XRD and Raman analysis both confirmed the formation of pure magnetite film on the surface of carbon steel.

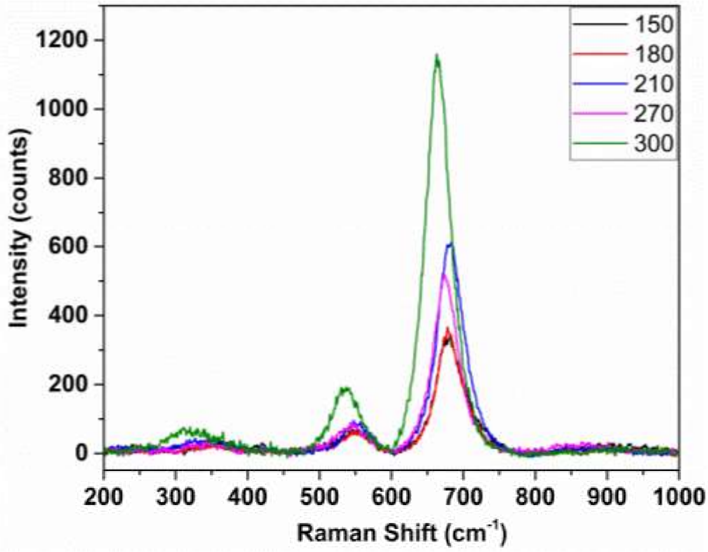

Figure **4.9** Raman spectra of the carbon steel exposed in DM water in autoclave at different temperatures for 7 days.

Figures 4.10 shows the SEM images of the carbon steel specimen exposed in DM water at different exposure temperatures (150-300 °C) in autoclave for 7 days. The SEM images in figure 4.10 clearly show that the oxide film formed covered the entire surfaces uniformly. Many researchers have demonstrated that magnetite film on carbon steel has a duplex morphology [Sinha et al., 2015, Bojinov et al., 2009]. The Inner layer is compact and has a fine crystalline structure. The outer layer has a coarse crystalline structure. The inner layer forms by the growth process, by the reaction of iron and water [Robertson 1989, Frayne

2002, Rihan et al., 2006]. The outer layer forms by precipitation from the bulk solution [Robertson 1989, Frayne 2002, Rihan et al., 2006]. The reaction mechanism for the formation of inner layer and outer layer is very well known [Robertson 1989, Frayne 2002, Rihan et al., 2006, Schwertmann et al., 2000]. This inner layer directly formed on the carbon steel surface by the oxidation of iron and reduction of hydrogen ion [Frayne, 2002] from the environment as per eq. 4.6.

$$Fe + H_2O = Fe_3O_4 + H_2 \quad (4.6)$$

The outer layer of magnetite forms by the precipitation reaction. The oxidised iron ion (Fe^{2+}) reacts (eq.4.7) with hydroxide ions of the aqueous environment and form ferrous hydroxide as per eq. 4.8. As the concentration of soluble iron species becomes high and it exceeds the solubility limit and the dissolved iron species gets precipitated back as magnetite on the outer surface of the magnetite layer. This reaction is called as Schikorr reaction, equation 4.9 [Robertson 1989, Frayne 2002, Rihan et al., 2006].

$$Fe = Fe^{2+} + 2e \quad (4.7)$$

$$Fe^{2+} + 2OH^- = Fe(OH)_2 \quad (4.8)$$

$$Fe(OH)_2 = Fe_3O_4 + H_2 + H_2O \quad (4.9)$$

However, the oxide formed at 150 °C showed only a compact inner layer and no clear outer layer was seen (figure 4.10(a)). At the exposure temperature of 180 °C, some fine precipitates are observed, as can be seen in figure 10(b). At further increased temperatures of 210 °C and 240 °C, the extent of these precipitated oxides has increased, as can be seen from figures 4.10 (c) and (d). At the exposure temperatures of 270 and 300 °C, very clear duplex type of oxide are seen with octahedral precipitated magnetite crystallites. The size and amount of the precipitated crystals increased with increase in formation temperature (figure 4.10). This observation on surface morphology (of crystallites) was also related to solubility limit in the environment. As the solubility of magnetite is higher as lower temperature (<240 °C), the formation of oxide due to precipitation was very less and as we increased the temperature the solubility comes down and the formation of magnetite by precipitation process becomes preferable.

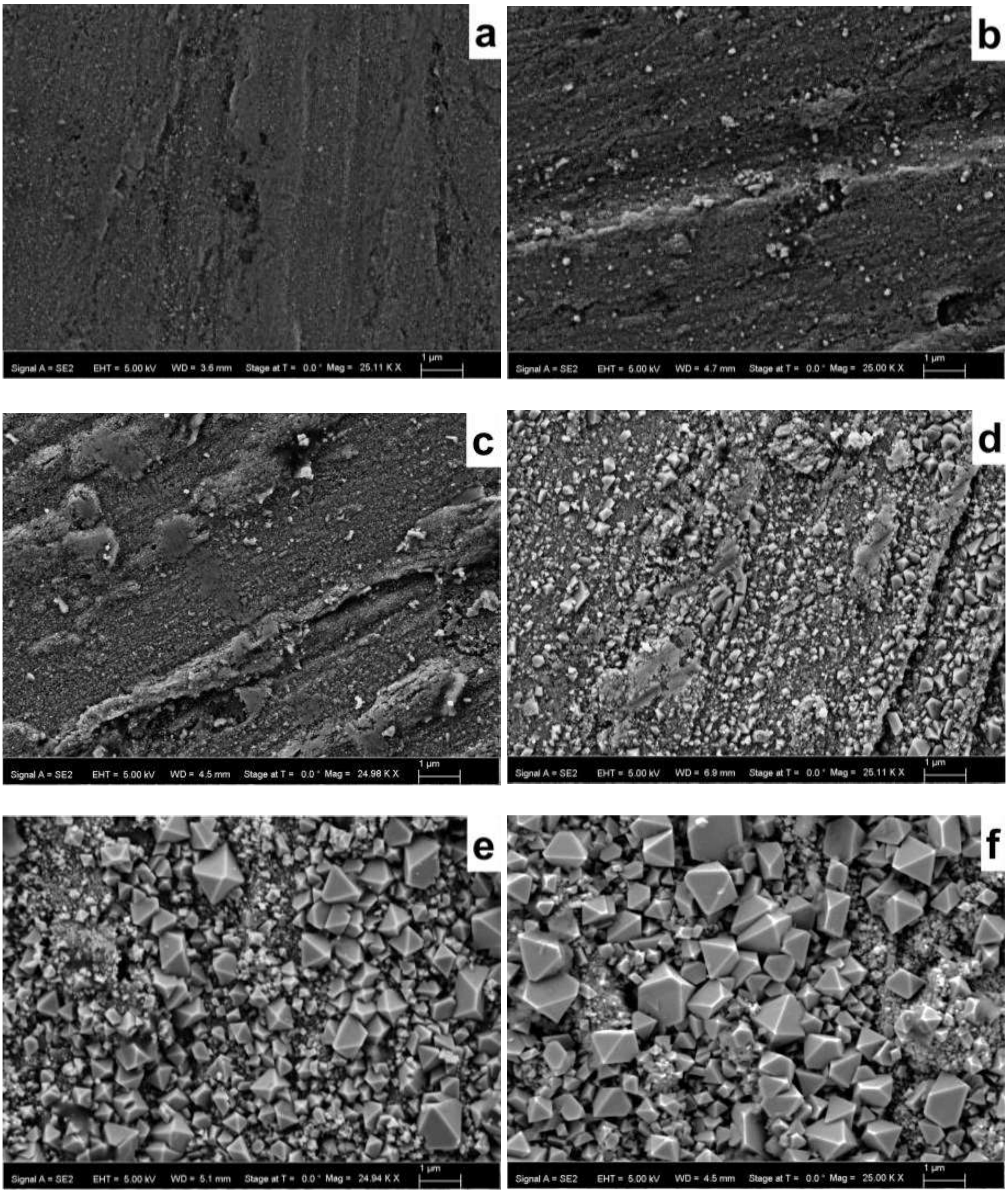

Figure 4.10 SEM of the carbon steel exposed in DM water in autoclave at (a) 150 °C, (b) 180 °C, (c) 210 °C, (d) 240 °C, (e) 270 °C and (f) 300 °C for 7 days showing increase in the extent of precipitation with increase in exposure temperature.

4.3.4 Electrochemical Analysis

4.3.4.1 Effect of temperature

The potentiodynamic polarization experiment on the specimen exposed at 300 °C for 7 days was carried out in borate buffer solution (pH 9.2) at room temperature. This was done to determine the stability (passive zone) of the magnetite in the borate buffer solution. The stable potential range was found from -230 mV_{SCE} to 900 mV_{SCE}. The passive current density in this potential was in the range of 0.4 to 1.5 $\mu A\ cm^{-2}$.

The oxide film formed on carbon steel specimens at different temperatures is shown to be magnetite (by XRD and Raman techniques, figures. 4.8 and 4.9). The magnetite film is semiconducting in nature. The metal loss through the magnetite i.e. total corrosion rate depends on the concentration of point defects present in the magnetite film [Zhang et al., 1998, Macdonald 1999, Fujimoto et al., 2007, Bojinov et al., 2000]. These point defects facilitate the diffusion of ions in the oxide film enabling dissolution/oxidation. Mott-Schottky analysis was used for determination of defect density in the oxide film [Mabuchi et al., 1991, Wielant et al., 2007, Zhu et al., 2016, Gomes et al., 1996]. In this process, the electrochemical system consists of two capacitance in series i.e. depletion layer capacitance C_{SC} and Helmholtz layer capacitance $C_{H.}$ The capacitance value of Helmholtz layers (C_H) is always very high as compared to depletion layer capacitance $C_{SC.}$ As they are in series, total capacitance value will be predominantly due to depletion layer capacitance C_{SC} [Hamadou et al., 2005]

Mott-Schottky analysis was done to measure the capacitance of the oxide film formed on carbon steel exposed at different temperatures for 7 days to calculate the defect density. The capacitance was measured as a function of applied potential. Figure 4.11 is the Mott-Schottky plot of the specimen exposed at different temperatures for 7 days. Defect density was calculated from the slope of the curve. From the sign of the slope of curve, the type of defect can be determined. Mott-Schottky plot of all the carbon steel specimen exposed at different temperatures showed two positive slopes indicating the magnetite film on the carbon steel is an n-type semiconductor [Hamadou et al., 2005]. The reason for the second positive slope has been explained by the change in donor type and/or donor density with the potential [Zhu et al., 2016, Simoes et al., 1990, Subramanian et al., 2014] or by the presence of second donor level in the band gap [Zhu et al., 2016, Simoes et al., 1990, Subramanian et al., 2014].

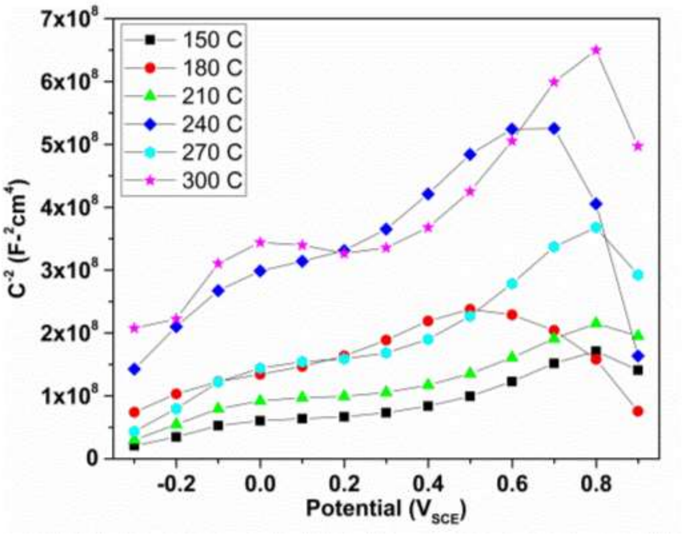

Figure 4.11 Mott-Schottky plot of specimens exposed at different temperature in autoclave for 7 days.

The defect density was calculated on the basis of first slope using Mott-Schotty relationship **(eq 4.4)**. The defect density was calculated from the slope of the linear region of Mott-Schotty curve below the potential 0 V_{SCE}. The value of defect density in the oxide film on the specimen exposed at different temperatures for 7 days is shown in figure 4.12.

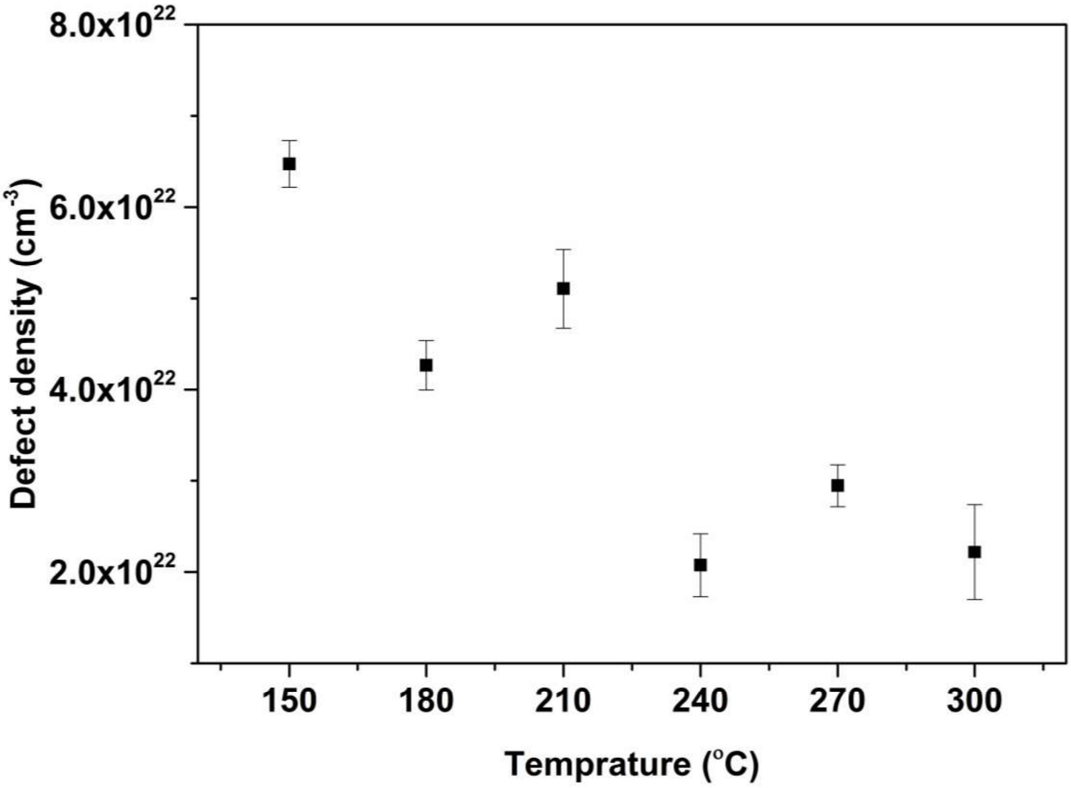

Figure 4.12 Variation of the defect density in the oxide film formed at different temperatures in DM water for 7 days calculated through Mott-Schottky analysis.

It has been shown by many researchers [Kumar et al., 2010, Wielant et al., 2007, Simoes et al., 1990] that the defect density in the magnetite film is in the range of $3\text{x}10^{21} – 8\text{x}10^{21}$ cm^{-3}. In the present study, the defect density was found to be in the range of $2\text{x}10^{22} – 6.5\text{x}10^{22}$ cm^{-3}. This level of defect density is higher than that measured by many researchers [Kumar et al., 2010, Wielant et al., 2007, Simoes et al., 1990].

However, there are other published papers reporting the value of defect density to be as high as 10^{23}/cm^3. Such high values have been attributed to the continuous processes of generation and annihilation of the vacancies at metal-oxide interface and oxide-solution interface [Subramanian et al., 2014, Guo et al., 1998, Macdonald, 2012]. In the present study, the environment is DM water (pH-7) in the temperature range 150 °C – 300 °C (figure 4.11-

4.12). In this environment (pH-7, no chemical addition) the oxide film formed continuously gets dissolved due to high solubility. Hence rate of generation and annihilation of the vacancies/interstitial at metal-oxide interface and oxide-solution interface is more. This may be the reason of higher defect density in Mott-Schottky analysis.

The defect density in the oxide formed at different temperatures was found to decrease with increase in the formation temperature (Figure 4.13). At 150 °C formation temperature, the defect density was found to be 6.5×10^{22} cm^{-3} and with subsequent increase in the formation temperature, the defect density decreased. The decrease in defect density was attributed to the formation of ordered and compact oxide at higher temperatures.

Higher defect density leads to the faster diffusion of the iron ions from the metal oxide interface to oxide water interface. This higher diffusion rate and higher solubility leads to increase in ratio of dissolved iron to iron in oxide at lower temperature (Figure 4.5(b)). At higher temperature the increased diffusion rate is facilitated by temperature but due to lower solubility it leads to formation of oxide by precipitation process.

4.3.4.2 Effect of pH

Figure 4.13 shows the Mott-Schottky plot of the carbon steel specimens exposed in two different pH environments in autoclaves for up to 20 days. The defect density in the oxide film was calculated for each specimen, exposed in two pH solution for different durations using Mott-Scotty relationship **(equation 4.4)**.

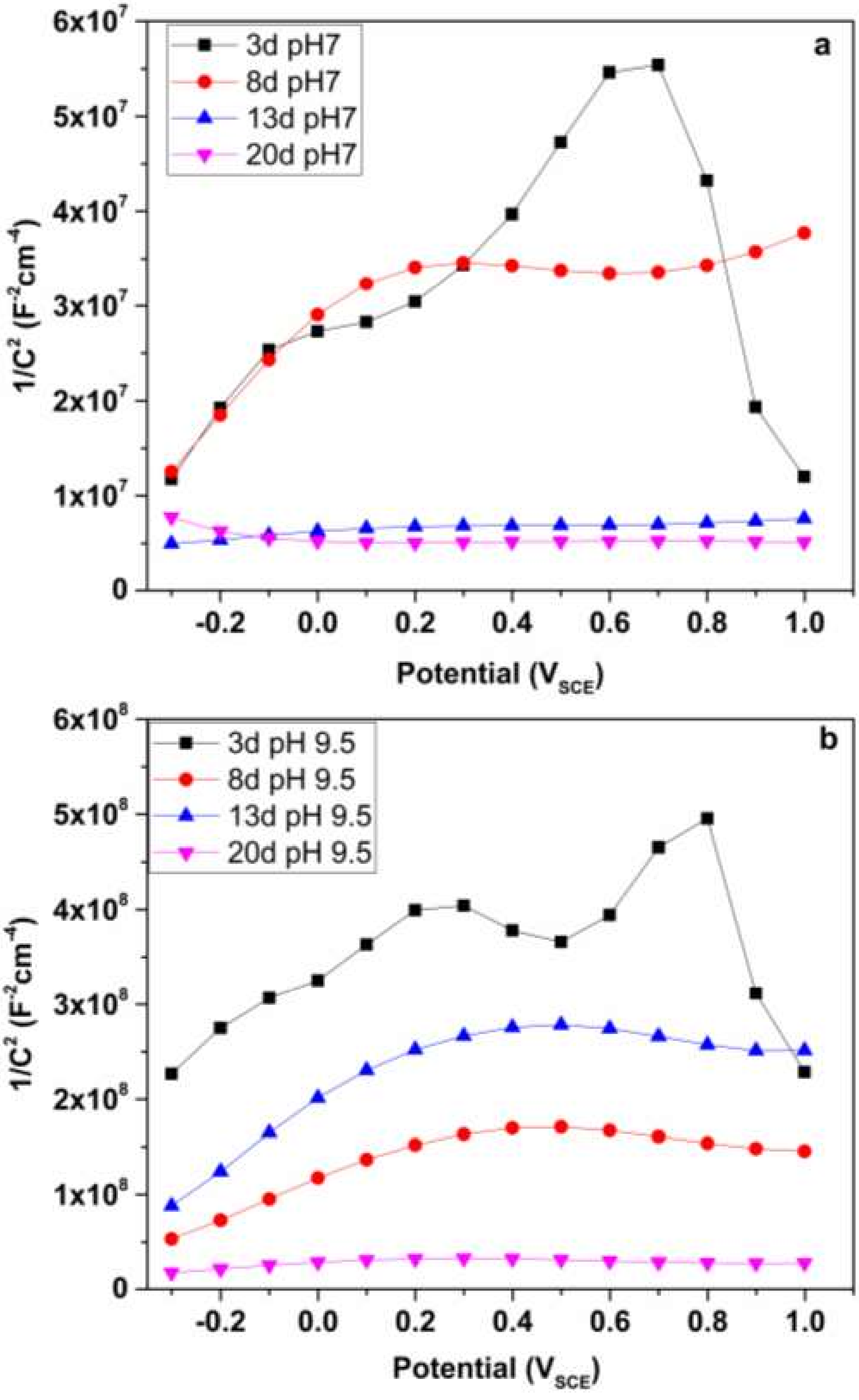

Figure 4.13 Mott-Schottky plot of carbon steel exposed in (a) neutral pH and (b) pH 9.5, environment.

Figure 4.14 shows the variation of defect density with exposure time of the specimens exposed in two pH environments at 150 °C. It can be seen that the defect density in the oxide film formed in neutral pH increased with time and that formed in pH 9.5 remained almost constant. This implies that in neutral pH solution, the corrosion protection ability of the oxide film deteriorated with time. The higher defect density facilitates faster diffusion of ions from metal oxide interface to oxide water interface. As the solubility of in neutral environment is higher, it will tend to dissolve in the bulk environment. Hence, at neutral pH both, the nature of oxide film and solubility of the environment, leads to a faster rate of corrosion. This may be the reason for faster dissolution of materials in neutral environment than in alkaline environment.

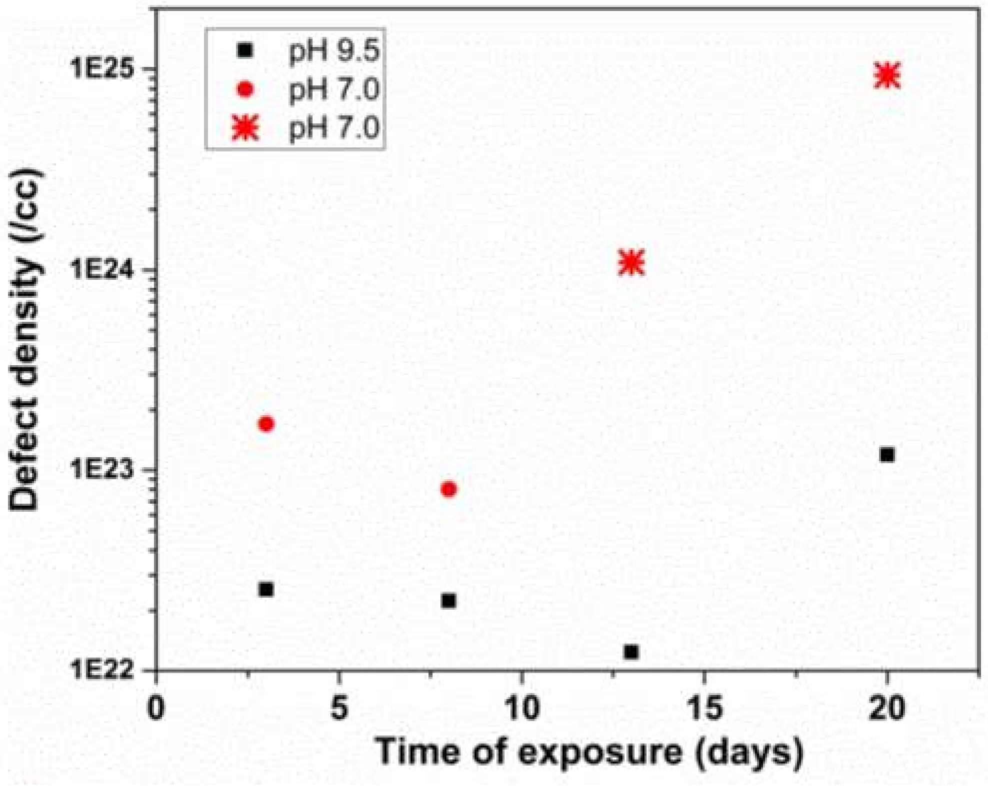

Figure 4.14 Variation of defect density with pH and time of exposure at 150 °C.

The combination of pH 7 and 150 °C is highly aggressive for carbon steel as there is a dominating effect of material dissolution. The behaviour of material dissolution is shown in figure 4.6. Since the material dissolution rate is fast under such conditions of exposure of carbon steel, it leads to increased rate of generation and annihilation of the vacancies/interstitial at metal-oxide interface and oxide-solution interface. In a scenario of fast material dissolution e.g. the combination of pH 7 and 150 °C, the rate of formation of Fe^{+2} at metal-oxide interface is very fast and also the rate of diffusion/migration of Fe^{+2} through the oxide film to the oxide/environment interface is very high. Therefore, the donor defect density (i.e. Fe^{+2} in interstitial positions in the oxide) would tend to be high in such conditions. This is what is reflected by very high defect density values after longer exposure periods in figure 4.14 (for pH7).

However, the values in the range of 10^{24}-10^{25} are very high. We have to say that such a very high value of donor density may probably reflect a more serious limitation of Mott-Schottky analysis. The oxide film in this case is very thin (~40 nm calculated from the weight of oxide). This thin film may lead to the complication in Mott-Schottky analysis due to possible contribution of electronic surface states to the measured capacitance as reported in the literature [Mantia et al., 2010].

4.4. Highlights

Oxide film was formed on carbon steel at six different temperatures up to 300 °C and two pH values at 150 °C. Weight of the specimens were measured at different stages to determine resultant weigh change, weight of oxide film, weight of dissolved iron, weight of iron in the oxide etc. XRD and Raman were carried out to identify the oxide film. SEM was done to determine the surface morphology of the oxide film. Mott-Schottky analysis was done to determine the defect density in the oxide film. Following highlights were made on the basis of result obtained.

1. In DM water, weight loss was observed up to 240 °C and above this temperature weight gain was observed and attributed to the dominant dissolution process up to the exposure temperature of 240 °C.
2. XRD and Raman showed the formation of magnetite at all the exposure temperatures.
3. Surface morphology by SEM showed no precipitated layer at 150 °C. The formation of precipitated layer increased with increase in the exposure temperature.
4. At 150 °C in DM water, the weight of oxide formed is lower than that formed in alkaline pH and this gap increased with the exposure time.
5. The ratio of $Fe_{(solution)}$ to $Fe_{(oxide)}$ in high at lower temperature and neutral pH value. Therefore, at low temperatures, there was much less precipitation of magnetite crystallites from solution.
6. Defect density in the oxide film formed at lower temperatures and neutral pH is found to be higher. The higher defect density enables more diffusion through the oxide hence a higher oxidation/dissolution rate.
7. The defect density showed an increasing trend with time of exposure at 150 °C in DM water while the defect density remained low in alkaline environment. This indicates formation of a stable magnetite film in an alkaline environment with increased time of exposure but a faster corroding magnetite film in DM water with increased time of exposure.

Chapter 5

EFFECT OF DISSOLVED OXYGEN ON THE CORROSION BEHAVIOUR OF CARBON STEEL

5.1 Introduction

Carbon steels are used in nuclear industry as components in the primary and secondary sides of a nuclear reactor. Carbon steel ASTM A 333 Grade 6 is used for the feeders and headers in the primary heat transport (PHT) system of pressurized heavy water reactors (PHWR) and ASTM A106 Grade B is used in most of the piping and components in the secondary circuit. Role of dissolved oxygen (DO) in the corrosion of carbon steel and stainless steel has been studied extensively in different medium [Beak et al., 2001, Cáceres et al., 2009a, Cáceres et al., 2009b, Li et al., 2010, Stratmann et al., 1994]. It was demonstrated that the DO plays an important role in formation and on properties of oxide film on the carbon steel [Beak et al., 2001]. Cáceres et al., [2009a, 2009b] found that the oxygen reduction reaction on iron is a mixed mass transfer and charge transfer controlled process, the cathodic current is predominantly mass-transfer controlled and steadily decreases with corrosion time at high NaCl concentrations, whereas at low NaCl concentrations, the current is predominantly charge-transfer controlled and increases with corrosion time. Li Y et al., [Li et al., 2010] demonstrated that the cathodic process on Q235 carbon steel in O_2-saturated 3.5% NaCl solution contains dissolved oxygen reduction, iron oxides reduction and hydrogen evolution, the oxygen molecule adsorption is inhibited by the adsorption of chloride ion on Q235 steel, the rate of oxygen reduction reaction will decrease with the increase of the concentration of chloride ion. However, so far, investigations are still inadequate to fully understand the relationship between oxygen and the corrosion mechanism of steel.

It was shown that in oxygenated treatment, surface is covered with a layer of ferric oxide hydrate (FeOOH) or hematite (Fe_2O_3) which also goes inside the pores of the magnetite [Dooley et al., 2000]. Ferric oxide layer functions as a boundary barrier for the inward diffusion of oxygen to the base material and Fe^{2+} ion transport from the steel surface through the magnetite layer. The presence of FeOOH and Fe_2O_3 also reduces the overall solubility of the oxide layer, because FeOOH and Fe_2O_3 have lower solubility than Fe_3O_4. The rate of conversion of Fe_3O_4 to FeOOH or Fe_2O_3 depends on the degree of oxidizing conditions.

The aim of present work is to establish the effect of dissolved oxygen in process water on the properties of oxide film by electrochemical methods. In this work the effect of dissolved oxygen on the corrosion behaviour of carbon steel in borate buffer solution (pH 9.2) as well as in reactor simulated environment (pH 9.5 ETA) at 70 °C has been established. Very little study is available regarding the corrosion of carbon steel in the above and effect of dissolved oxygen over it. The effect of DO was also established by exposing the magnetite in high DO in an autoclave at 150 °C in pH 9.3-9.5 maintained by ethanol amine.

5.2. Experimental

5.2.1 Materials and Environment

The carbon steel used in the current study was A106 grade B with the chemical composition (in wt%): C(0.115), Mn (0.33), P(0.017), Ni (0.021), S (0.019), Cr (0.043), Cu (0.040) and Fe (bal). Rectangular samples of approximately 10 x 15 cm^2 were cut from the plate and polished up to 600 grit emery paper. Milli-Q DM water was used for the preparation of solution for oxide formation and electrochemical measurements.

5.2.2 Oxide Film Formation

To study the corrosion/oxidation behavior of oxidized carbon steel, the samples of carbon steel were exposed in an autoclave for the formation of oxide film. The oxide film was formed by exposing the samples in autoclave at 270 °C for 4 days in deoxygenated water of pH 10-10.2 (LiOH).

5.2.3 Effect of dissolved oxygen on nature of oxide film

The effect of dissolved oxygen on the nature of oxide film has been studied by applying two approaches.

a. The 4 days oxidized carbon steel specimens were potentiostatically polarized at +300 mV_{SCE} for 3 h and 18 h in borate buffer solution of pH 9.2 at 70 °C.

b. The 4 days oxidized carbon steel specimens were further exposed to pH 9.5 solution maintained by ethanol amine (ETA) in two different DO levels at 150 °C for different duration up to 48 h. Two different DO levels are low DO where the environment is completely de-aerated and high DO where no de-aeration was done. Measuring DO in static autoclave is not possible as the commercially available DO sensor does not work at high temperature. However LDO corresponds to <10 ppb as purging and venting ensure complete de-aeration. In this work ASTM G 2 M recommended de-aeration practices was followed that guarantees DO << 45 ppb. HDO conditions used in these experiments may have few ppm DO. Temperature and pH in the static autoclave can be maintained as per actual plant conditions. Temperature and corresponding pressure can be simulated in a static autoclave. In static autoclave flow conditions are not maintained. Capacity of the autoclave used was 1.5 L. and there was negligible change in the pH value after the experiment.

5.2.4 Characterization of the oxide film

Oxide films formed on carbon steel in different DO level are characterized by Raman spectroscopy and XRD for the determination of phases of iron oxide. Elemental depth profile and thickness of the oxide film was determined by glow discharge optical emission spectroscopy (GDOES) and morphology of the oxide films formed on carbon steel in different DO level were characterized by SEM.

5.2.5 Electrochemical impedance spectroscopy and Mott-Schottky analysis.

Electrochemical impedance spectroscopy (EIS) of the oxidized carbon steel before and after potentiostatic polarization at +300 mV_{SCE} was carried out. This potential corresponds to stability of hematite in the E-pH diagram [Beverskog et al., 1996]. EIS was done by applying a sinusoidal frequency of potential amplitude ±10 mV in the frequency range from 10 kHz to 10 mHz in a borate buffer solution. In similar way the EIS of the oxide exposed in different DO levels (LDO and HDO) were carried out.

Mott-Schottky analysis was carried out to characterize the electronic property of the oxide film formed at different oxygen level. In Mott-Schottky analysis, the EIS was carried out over the potential range -300 mV_{SCE} to 1000 mV_{SCE}. The capacitance at each potential were measured from each EIS was plotted against the applied potential.

5.2.6 Electrochemical Noise analysis

The measurement of electrochemical noise for corrosion studies was first described by Iverson in 1968 [Iverson 1968].Electrochemical noise (ECN) analysis was carried to determine the noise resistance of the carbon steel in the LiOH (pH 9.2-9.5) at 70 °C in different DO level. The experiments were carried out as per American Society for Testing and Material (ASTM) standard [Kearns et al., 1966]. ECN was done using two identical working electrodes (carbon steel) and a reference saturated calomel electrode. Electrochemical potential noise and electrochemical current noise were measured with time.

5.3 Results and Discussion

Presence DO facilitates the formation of FeOOH or hematite by the reactions given in equation (5.1)-(5.4), which protects the base material [Dooley et al., 2000]. Hematite have higher resistance that magnetite that forms in low DO conditions. Higher dissolved oxygen favours the formation of hematite and also magnetite (Fe_3O4) is converted into hematite (Fe_2O_3) or γ-FeOOH. If magnetite is already formed on the surface, the dissolved oxygen converts the magnetite into hematite or the formation of hematite will take place in the pores of magnetite. Formation of hematite in the pore creates resistance to the diffusion of ferrous ions from metal-oxide interface to oxide-environment phase. Also the solubility of hematite is lower than that of magnetite. These two processes decreased the corrosion rate of carbon steel in high DO condition.

$$Fe^{2+} + 2OH^{-} \rightarrow Fe(OH)_2 \qquad (5.1)$$

$$2Fe(OH)_2 + \frac{1}{2}O_2 \rightarrow 2FeOOH + H_2O \qquad (5.2)$$

$$2Fe(OH)_2 + \frac{1}{2}O_2 \rightarrow Fe_2O_3 + 2H_2O \qquad (5.3)$$

$$2Fe_3O_4 + \frac{1}{2}O_2 \rightarrow 3Fe_2O_3 \qquad (5.4)$$

Oxide film formed on the carbon steel specimen in autoclave at 270 °C in pH 10.0-10.2 (LiOH) for 4 days was characterized by XRD. All the peaks correspond to the magnetite peaks and peaks corresponding to base material were also observed as shown in figure 5.1. In presence of dissolved oxygen in the environment, already existing magnetite would convert in hematite as per eq. (4.1).

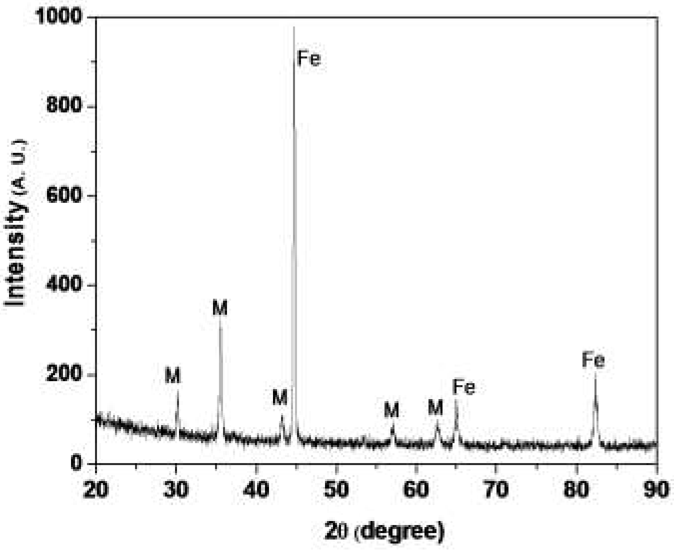

Figure 5.1 XRD of the carbon steel sample exposed in autoclave at 270 °C for 4 days indicating the formation of magnetite (M = magnetite).

The effect of oxygen was simulated by potentiostatic polarization of oxidized carbon steel at +300 mV_{SCE} at 70 °C in borate buffer solution. Figure 5.2 shows the effect of time of potentiostatic polarization of oxidized carbon steel (magnetite film) on the OCP values. It can be clearly seen that OCP value is increased with time of potentiostatic polarization. Hence the magnetite film become more passive and was attributed to the conversion of magnetite to hematite or γ-FeOOH at 300 mV_{SCE} [Beverskog et al., 1996].

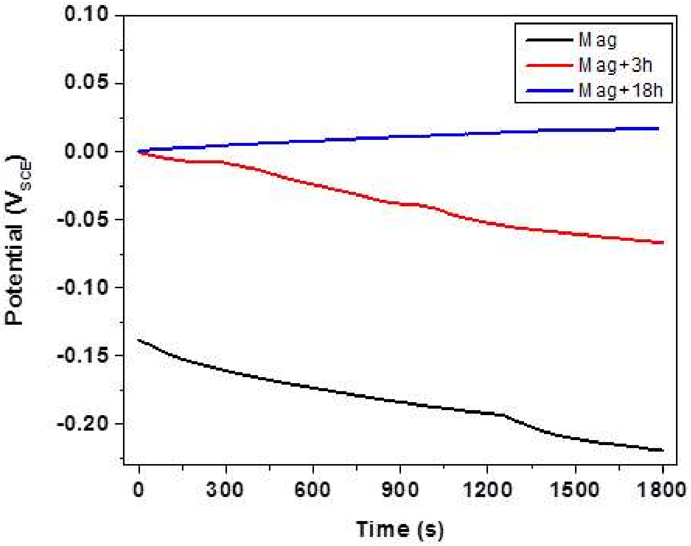

Figure 5.2 Variation of OCP of magnetite in borate buffer solution at 70 °C and after potentiostatic polarization for 3 h and 18 h.

Figures 5.3(a) and 5.3(b) are the Bode and Nyquist representation of the electrochemical impedance spectra (EIS) of magnetite film and EIS after potentiostatic polarization as well. The charge transfer resistance (impedance at lower frequency) is increased after the potentiostatic polarization for 3 h and it further increased when the potentiostatic polarization was done up to 18 h. This showed that the corrosion resistance of the film is increased after potentiostatic polarization. These results are in good agreement with the results of OCP measurements.

The defect density in the magnetite film was by Mott-Schottky method. In this, capacitance was measured at different applied potential from -300 mV$_{SCE}$ to 1000 mV$_{SCE.}$ Mott-Schottky (MS) plot of the magnetite film and magnetite film after potentiostatic polarization, done for different duration, at +300 mV$_{SCE}$ is shown in figure 5.4(a).

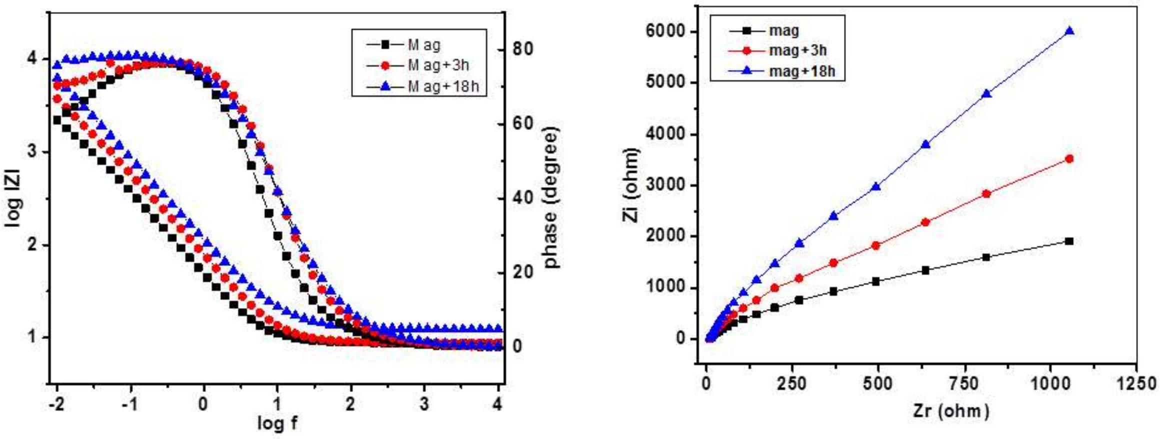

(a) **(b)**

Figure 5.3 (a) Bode and (b) Nyquist plot of EIS of magnetite and after potentiostatic polarization done for different duration.

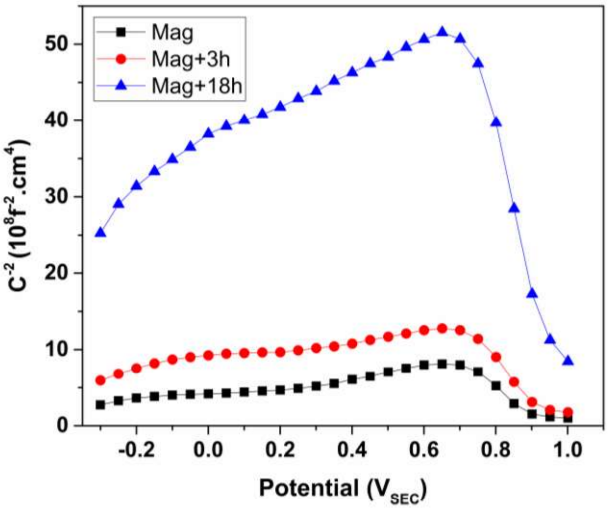

Figure 5.4 (a). Mott-Schottky plot of magnetite and magnetite after potentiostatic polarization for 3 h and 18 h

The defect density from plot (figure 5.4(a)) was calculated using the Mott-Schottky equation (eq 5.5).

$$\frac{1}{C^2} = \frac{1}{C_H{}^2} + \frac{2}{\varepsilon\varepsilon_0 q N_D A^2}(E - E_{FB} - \frac{KT}{q}) \qquad (5.5)$$

ε = dielectric constant (16 for magnetite)

ε_o = vacuum permittivity (8.85 x 10^{-14})

q = charge

N_D = defect density

A = exposed surface area

E_{FB} = flat band potential

K = Boltzmann's constant

T = temperature

C= capacitance

C_H = Helmholtz capacitance

From Mott-Schottky equation, slope of the plot $1/C^2$ vs applied potential will give the defect density. Value of defect density is inversely proportional to the slope of MS plot. Figure 5.7 (a) clearly shows that the slope of the MS plot is increased when the magnetite sample was potentiostatically polarised at +300 mV_{SCE}. This slope is further increased with duration of potentiostatic polarizations. Calculated defect densities for all the three conditions are given in figure 5.7 (b) and table-5.1.

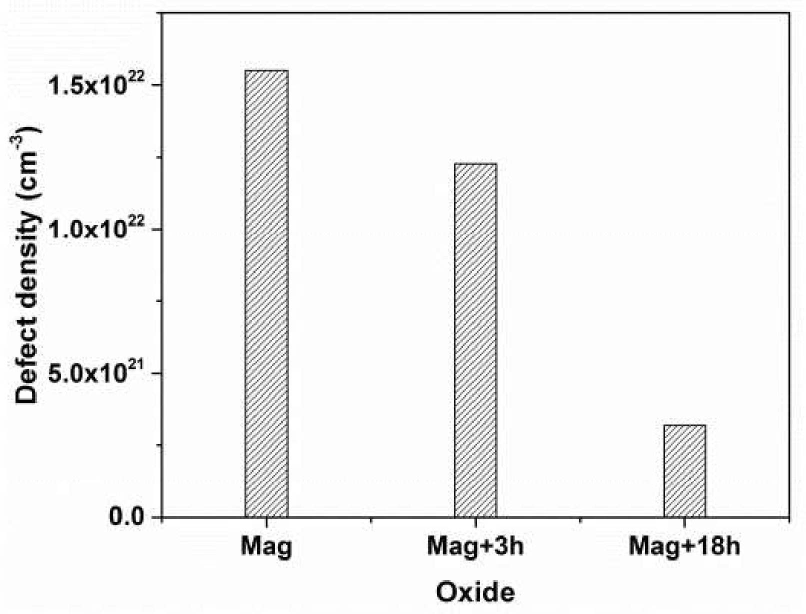

Figure 5.4 (b) Defect density of magnetite and magnetite after potentiostatic polarization for 3 h and 18 h.

Table-5.1: Calculated defect density in magnetite film and after potentiostatic polarization for 3 h and 18 h

Material Condition	Magnetite	Magnetite + 3 h	Magnetite + 18 h
Defect Density	$1.55x10^{22}$	$1.23x10^{22}$	$3.19x10^{21}$

Application of +300 mV$_{SCE}$ simulates the increased DO level. This shows that the defect density in the oxide film decreased when it was potentiostatically polarized at this potential. This may be attributed to formation of some hematite in the magnetite having less defect density. Lower defect density in the oxide film due to increased DO level would increase the corrosion resistance.

Figure 5.5 shows the SEM image of the carbon steel exposed at (a) 270 °C for 4 days and subsequently magnetite film containing specimens exposed for (b) 2 h, (c) 6 h, (d) 24 h and (e) 48 h at 150 °C in pH 9.3-9.5 solution maintained by ethanol amine in high DO environment.

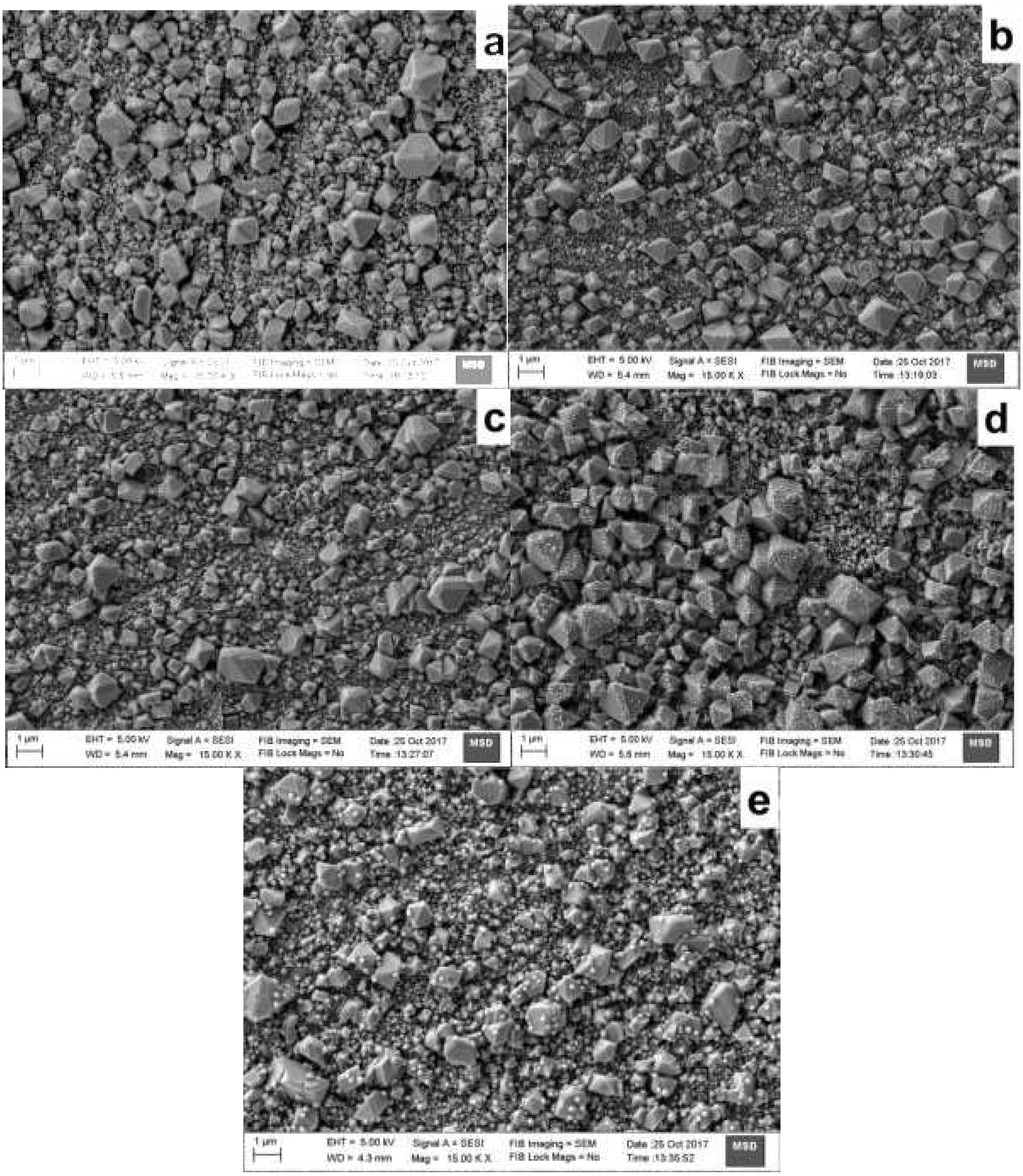

Figure 5.5 SEM image of the carbon steel exposed at (a) 270 °C for 4 days and subsequently exposed for (b) 2 h, (c) 6 h, (d) 24 h and (e) 48 h at 150 °C in pH 9.3-9.5 solution maintained by ethanol amine in high DO environment.

Figure 5.5(a) clearly shows the formation duplex layer oxide with inner layer compact fine crystallite size and outer layer coarse octahedral particles. This type of duplex layer has been explained by many researchers [Robertson **1989,** Frayne 2002, Rihan et al., **2006,** Schwertmann et al., 2000]. When this oxide was exposed in high DO environment (without de-aeration) there is no significant change in the oxide film morphology up to 6 h exposure as shown in figures 5.5(b) and 5.5(c). However, when the exposure duration was increased to 24 h there is formation some fine circular particles on the oxide and in the gaps. This oxide may be the formation of hematite (Fe_2O_3) or γ-FeOOH due to high DO [Dooley et al., 2000]. SEM images of oxide film exposed at 150 °C in completely de-aerated condition did not show any change in morphology.

To identify these fine oxide particle GI-XRD and Raman analysis was carried out. Figure 5.6 is the XRD of oxidized carbon steel at 270 °C in de-aerated environment and this oxidized sample further exposed to 150 °C for 48 h in high DO environment. In de-aerated environment all the peaks corresponds to magnetite confirming the formation of magnetite film. However when the specimens exposed in high DO environment peak at 33.16° that corresponds to hematite is also visible along with the peaks of magnetite. This confirms the formation of some hematite in the magnetite matrix. The XRD of oxide film exposed at 150 °C in completely de-aerated condition showed peaks due to magnetite only.

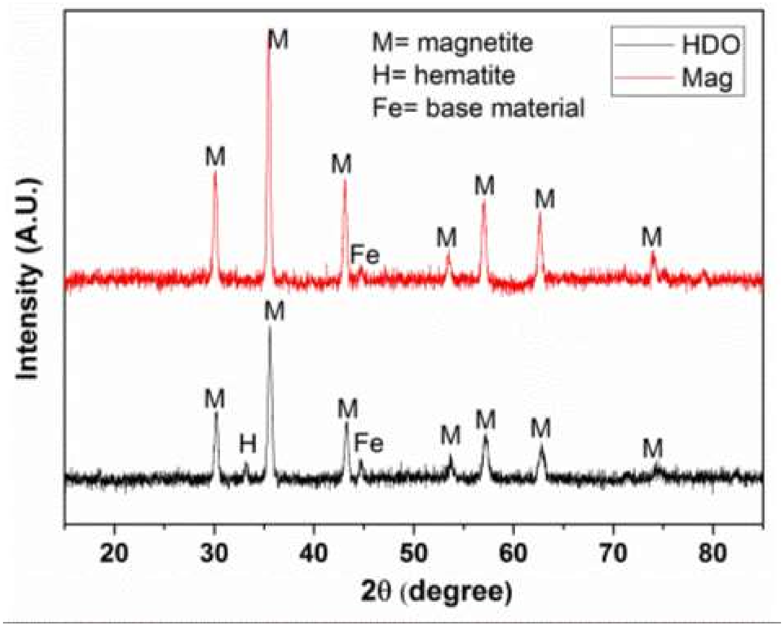

Figure 5.6 XRD image showing the formation of hematite in presence of HDO environment.

Formation of hematite is also confirmed by the micro laser Raman spectroscopy. Figure 5.7 is the Raman spectra of the oxidized carbon steel at 270 °C in de-aerated environment and this oxidized sample further exposed to 150 °C for 48 h in high DO environment. A detail of the Raman peaks and peaks observed in the literature work is given Table 5.2.

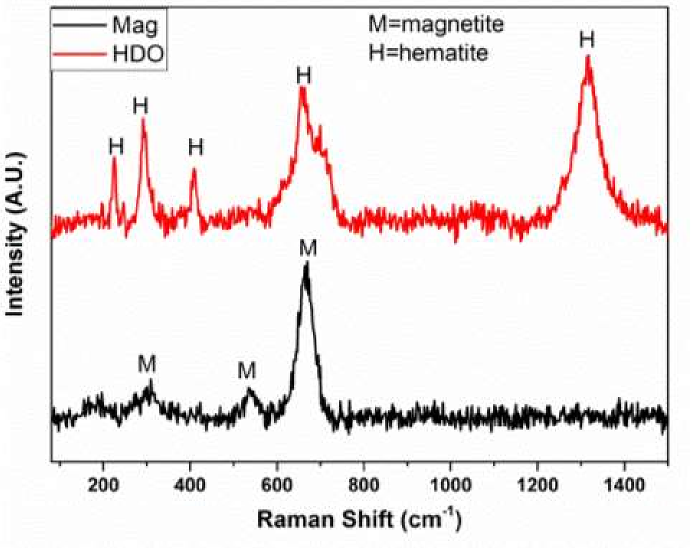

Figure 5.7 Raman spectra of the specimen showing the formation of hematite in presence of HDO environment.

Table 5.2: Overview of Raman peaks reported in different studies and in this work.

Compounds	**Raman Shift (cm^{-1})**							**Ref.**
Fe_3O_4			308			536	667	This work: specimen oxidized in de-aerated environment at 270 °C for 4 days
Fe_2O_3	225	292		409		660	1314	This work: above specimen exposed in HDO environment at 150 270 °C for 48 h
Fe_2O_3	224	294		408		657	1320	[de Faria et al., 2007]
Fe_2O_3	226.7	292.5		410.9	497.1	611.1		[de Faria et al., 1997]
Fe_3O_4	193		308			540	670	[Gasparov et al., 2000]
Fe_3O_4	226		336		490	570	706	[Graves et al., 1988]
Fe_3O_4	193		306			538	668	[Shebanova et al., 2003]
Fe_3O_4		298	319	418	470	550	676	[Dunnwald et al., 1989]

In de-aerated environment peaks at wave numbers 308, 536 and 667 cm^{-1} corresponds to magnetite confirming the formation of magnetite film. After exposure of this specimen at 150 °C in high DO for 48 h peaks at 225, 292, 409, 660 and 1314 cm^{-1} corresponding to hematite was observed. This confirms the formation of hematite in high DO condition. This result is in line with the results obtained by XRD. However, XRD showed the prominent peaks of magnetite even after the exposure in high DO environment. This is due to high penetration depth of XRD and this resulted in the depth information of oxide film whereas laser Raman spectroscopy gives only the surface information. Raman spectroscopy of oxide film exposed at 150 °C in completely de-aerated condition showed peaks due to magnetite only.

In depth elemental composition profiling was done using a glow discharge optical emission spectroscopy (GDOES) (GD Profiler, HORIBA Jobin Yvon). The circular specimen surface of diameter 2 mm of different oxidized surface was sputtered in an argon atmosphere of pressure 650 Pa by applying radio frequency 13.56 MHz at 20W power. The surface oxide formed is an iron oxide, the spectral line used for the depth profile is only for oxygen (130.22 nm) and iron (370.19 Nm).

Figure 5.8 is the GDOES profile of the oxidized carbon steel for 4 days and subsequently oxidized for 48 h in low dissolved (LDO) and high dissolved oxygen (HDO). On the basis of elemental profile, it can be divided into four different regions *viz.* Outer oxide, oxide, interface and base material carbon steel. It can be seen that there is increase in iron concentration and decrease in oxygen concentration when we move from oxide to metal in the interface region. The interface zone is not very sharp and it spread from 1.2 s to 1.8 μm. This can be attributed to the surface roughness of the base material as the base materials were polished only up to 600 grit emery papers. Oxide film thickness for the oxidised sample for 4 days at 270 °C was found to be 1.5 μm. the thickness of this oxide film was found to be decreased after exposure in LDO environment at 150 °C whereas there is small increase in the thickness of oxide film when exposed to HDO environment. This may be attributed to formation of hematite on the surface (as confirmed by Raman spectroscopy and XRD) having lower solubility whereas in LDO only magnetite is there which have higher solubility that decreased the thickness of oxide.

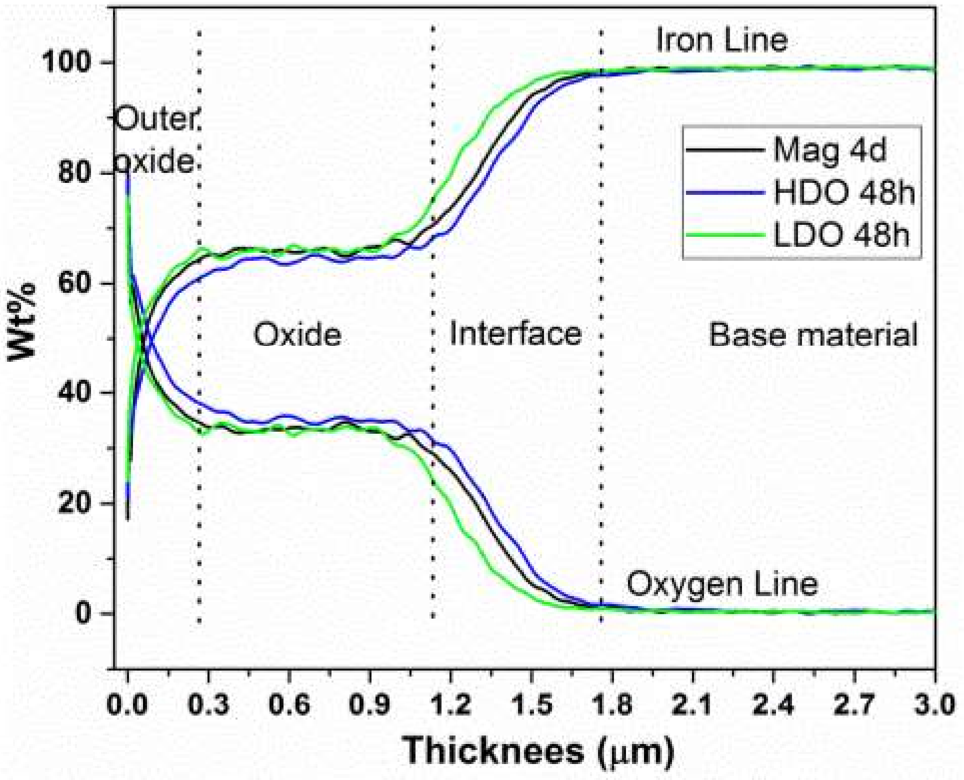

Figure 5.8(a). GDOES depth profile of oxide formed on carbon steel.

Figure 5.8 (b) is the depth profile of oxygen in the oxidised sample for 4 day in de-aerated condition (Mag 4d) at 270 °C and there after oxidised for different duration in HDO condition at 150 °C. surface region shows there is increase in oxygen level for the samples oxidised for 24h and 48h in HDO environment. This is due to formation of hematite (Fe_2O_3) as iron to oxygen ratio in hematite is more than that in magnetite (Fe_3O_4).

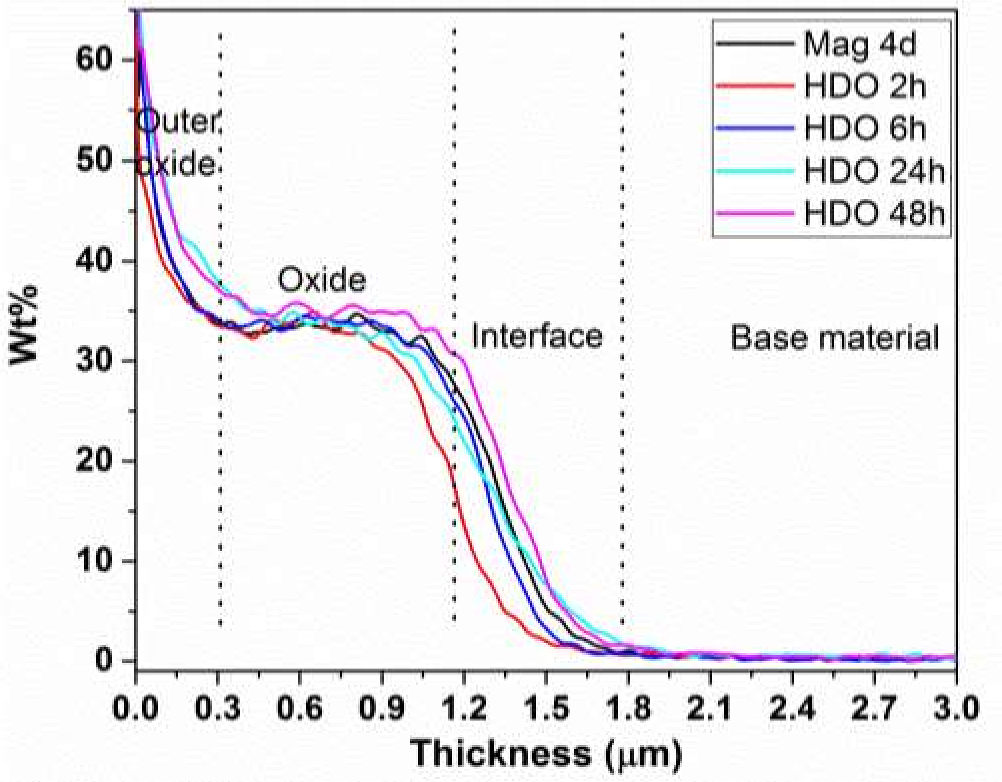

Figure 5.8(b) Depth profile of oxygen in the oxide film formed on carbon steel in different duration in HDO environment.

Weight measurement of the specimen was done after the exposure at 270 °C for 4 days in de-aerated conditions. This sample was again exposed to LDO and HDO conditions at 150 °C for different duration up to 48 h. Weight change is plotted against time for both the environmental condition as shown in figure 5.9. In can clearly be seen that there is a decrease in the weight of specimen for the initial exposure (2 and 6 h) duration. However, the weight decrease in LDO environment is more as compared to HDO environment. After 24 and 48 h exposure at 150 °C in HDO environment weight is found to increase in case of HDO condition but in LDO condition there is further decrease in weight. This may be attributed to formation of hematite on the surface in HDO environment that prevent further dissolution.

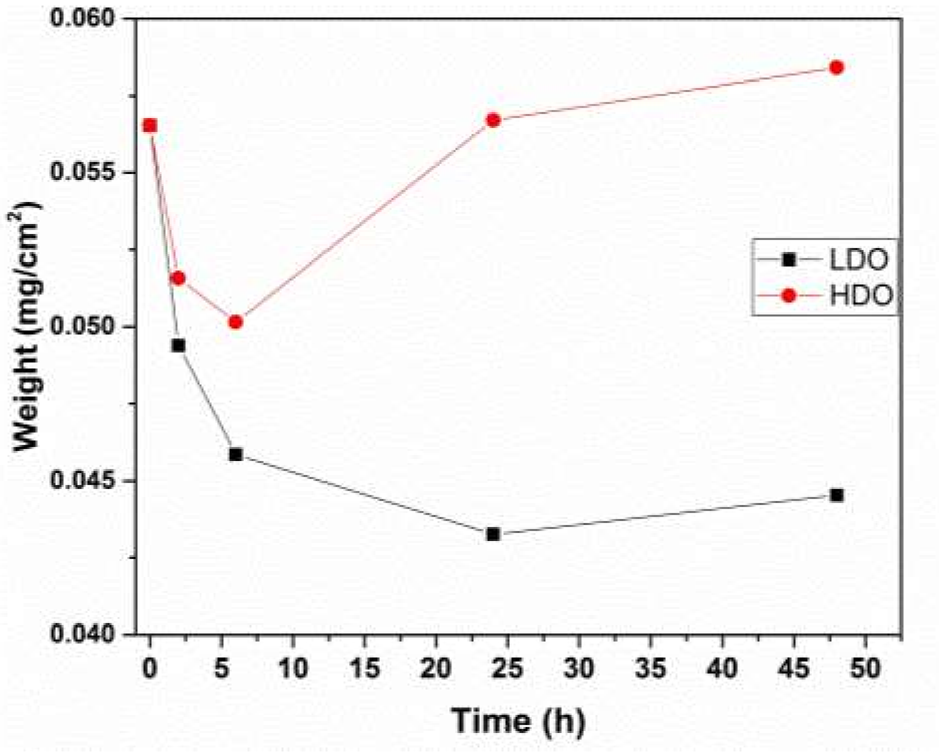

Figure 5.9: Weight change of specimen after exposure in HDO and LDO condition at 150°C.

The results obtained by Raman spectroscopy, XRD, GDOES and weight measurement is in line with each other. Raman spectroscopy and XRD showed the formation of hematite on the surface and GDOES showed the increase in oxygen intensity at the surface due to formation of hematite. Weight measurement showed the increase in weight in the specimen exposed for 24 and 48 h in HDO condition. This was due to formation of hematite which leads to decrease in solubility.

Electrochemical impedance (EIS) measurement was carried in a borate buffer solution of pH 9.2 at room temperature. EIS was performed at OCP in frequency range 10 kHz to 10 mHz and amplitude of the sinusoidal voltage was 10 mV. Figures 5.10 (a) and (b) is the Nyquist and Bode plot of EIS respectively. In these plots the impedance values at high frequency region corresponds to the solution resistance and impedance value in low frequency region corresponds to charge transfer resistance. From Nyquist and Bode plot it is very clearly seen that change transfer resistance is increased with the exposure duration in HDO environment. This is again attributed to formation of hematite in high dissolved oxygen environment. The band gap of magnetite is approximately 0.7 eV and that of hematite is 2.0-2.2 eV. This higher band gap in hematite leads to increase in change transfer resistance.

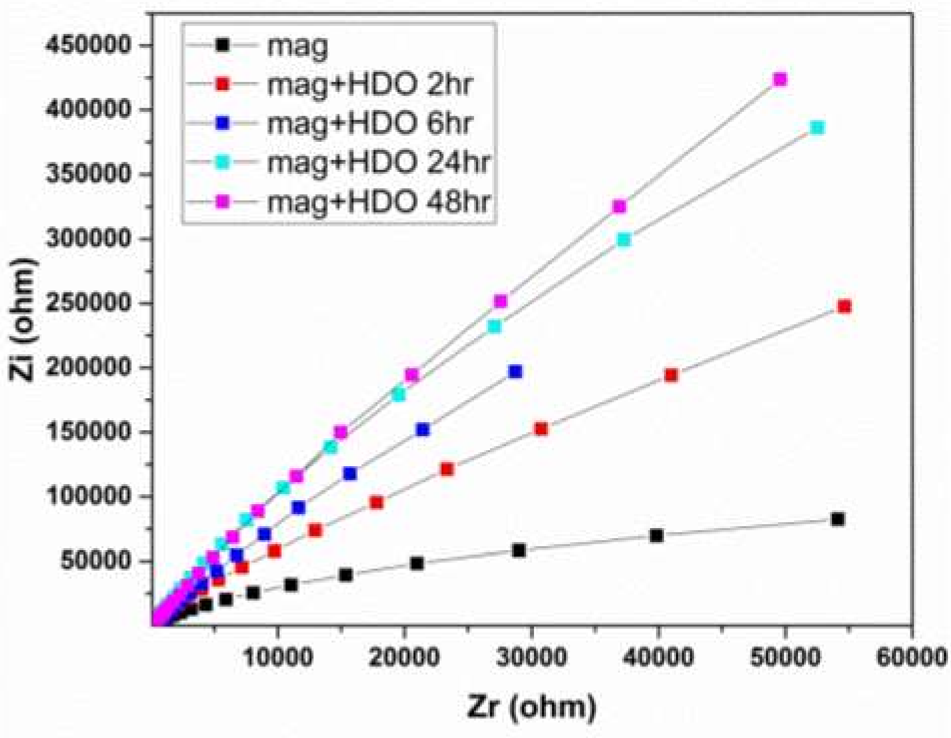

Figures 5.10 (a) Electroshemical impedance sprectra of oxidised carbon steel showing increase of charge transfer resitance with exposure duration in HDO environment (HDO) (Nyquist plot).

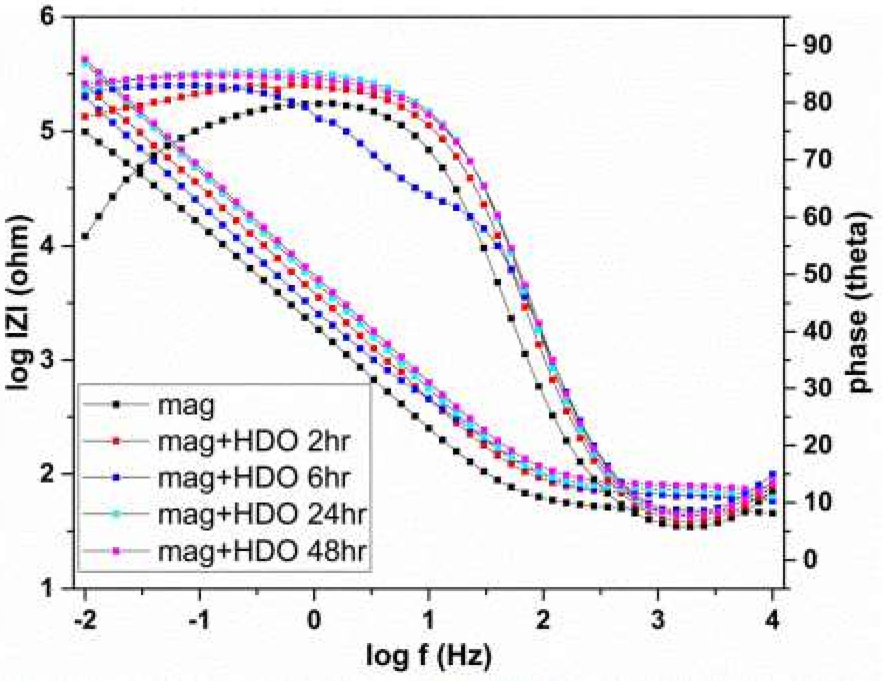

Figure 5.10 (b) Electroshemical impedance sprectra of oxidised carbon steel showing increase of charge transfer resitance with exposure duration in HDO environment (HDO) (Bode plot).

Mott-Schottky analysis was done was done on all the specimen exposed at 270 °C for 4 days (mag) and there after exposed at 150 °C in HDO environment for different duration. For this purpose capacitance was measured in borate buffer solution (pH 9.2) at dufferent potetial from -300 mV_{SCE} to 1000 mV_{SCE} at a step of 50 mV. Capacitance measurement was at at 1000 Hz. Reciprocal of square of capacitance was plottes against potential. this plot is know as Mott-schottky plot. Figure 5.11 is the Mott-Schottky plot of the specimens exposed at 270 °C for 4 days (mag) and there after exposed at 150 °C in HDO environment for different duration.

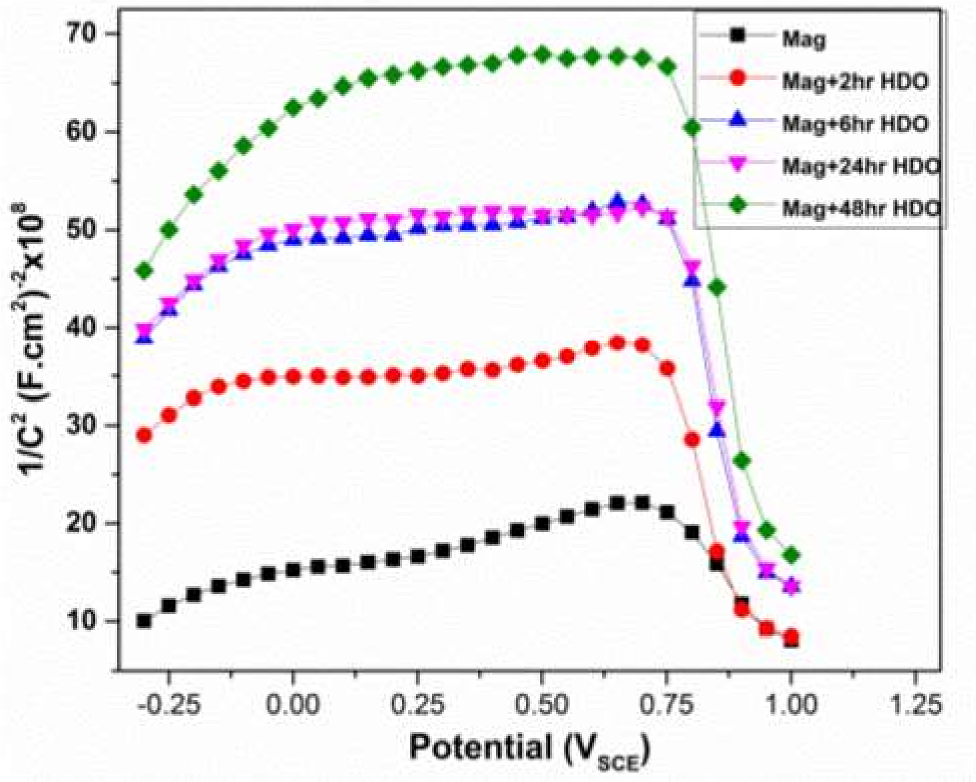

Figure 5.11 Mott-Schottky plot of the specimens exposed at 270 °C for 4 days (mag) and there after exposed at 150 °C in HDO environment for different duration.

Mott-Schottky plot showed the two slopes and is attributed to two donor level in the oxide i.e. deep donor level and swallow donor level. Defect density for each specimen was calculated using Mott-Schottky equation. Details of Mott-Schottky equation is mentioned in this chapter previously. It ac clearly be seen that defect density decreased with the exposure duration in HDO environment as shown in figure 5.12. This implies that the diffusion of ions across the oxide film will become difficult in presence of high DO.

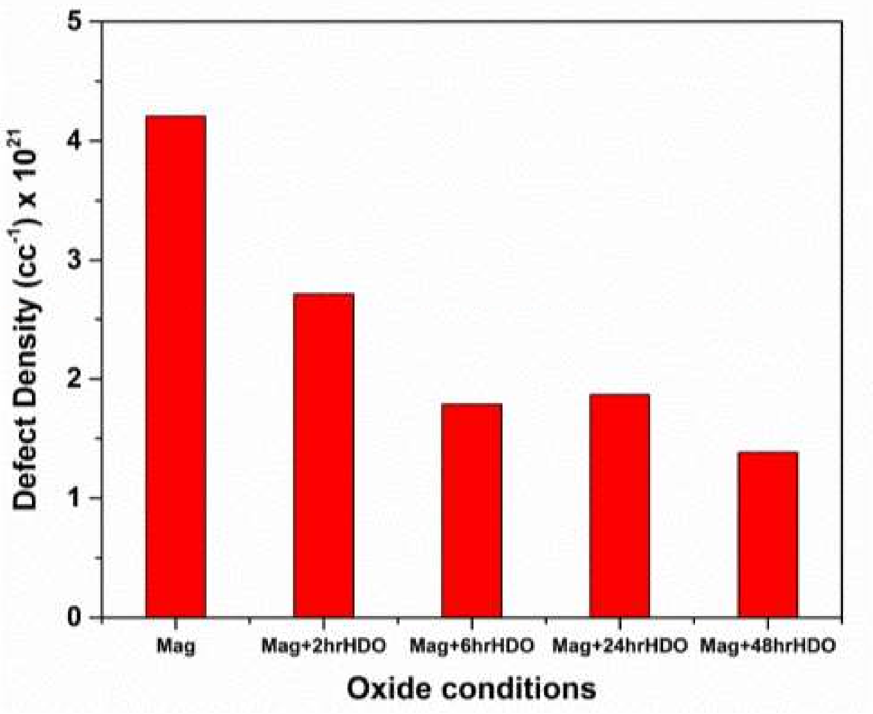

Figure 5.12 Variation in defect density with the exposure duration in HDO environment showing decrease in defect density value with increase in DO level

Hence these results confirm that exposure of pre-existing magnetite film in high DO environment increased the charge transfer resistance and also decreased the defect density. So oxide film becomes more protective in presence of dissolved oxygen. However, this experiment was done for 48 h. the behaviour of oxide film in high DO environment for longer duration need to be established. It is also reported in literature that desired DO to inhibit FAC is dependent of pH. At higher pH, low DO is required [Fujiwara et al., 2008].

Effect of dissolved oxygen was also evaluated by electrochemical noise (ECN) measurement. In this the current noise and potential noise of the sample was measured in LiOH (pH 9.2) solution at 70 °C in three DO level. Figure 5.13 shows the current and potential noise in three dissolved oxygen level. The current noise in low DO level showed high frequency of fluctuation and the amplitude was also high as compared to high DO level. The noise resistance (Rn) is calculated from the standard deviation of potential noise and standard deviation of current noise [Kearns et al., 1966]. The ratio of these gives the value of Rn. The value of Rn will give the corrosion resistance of the material and is generally follows the same trend as obtained by Tafel extrapolation method. It can be clearly seen that Rn value increased with the increase in DO level but when O_2 was purged, it came down slightly (figure 5.14). This result is in good agreement with result obtained by potentiodynamic polarization method and EIS measurement. Hence dissolve oxygen in the above environment increases the corrosion resistance of the material by forming a passive film.

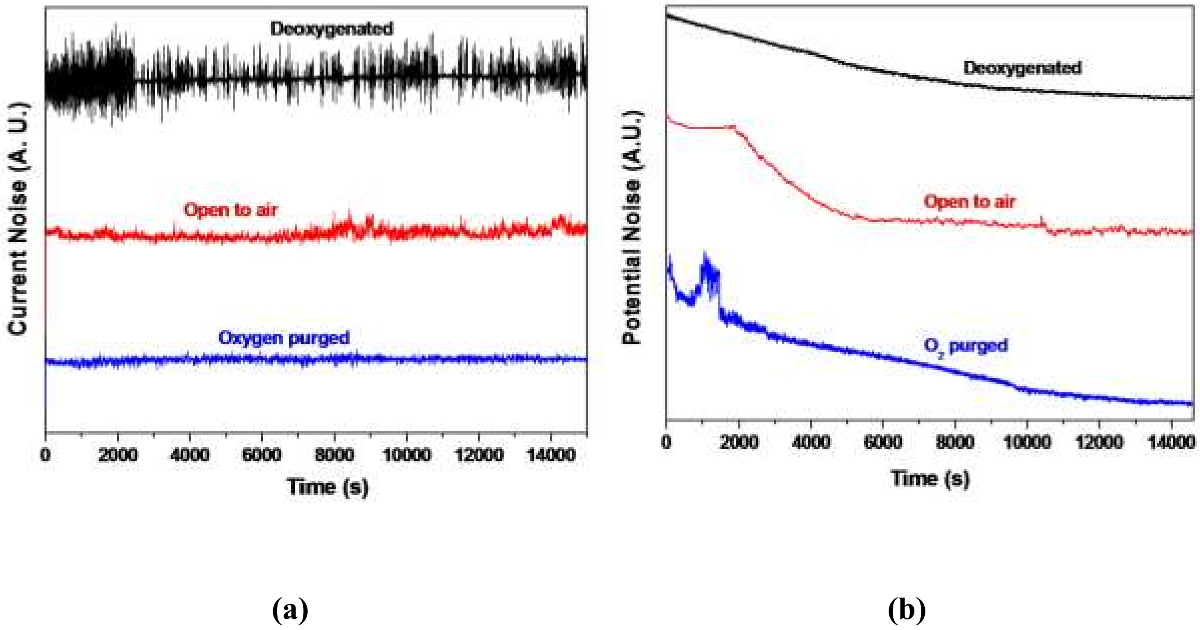

(a) (b)

Figure 5.13 (a) Current noise (b) Potential noise of carbon steel in LiOH (pH 9.2) at 70 °C

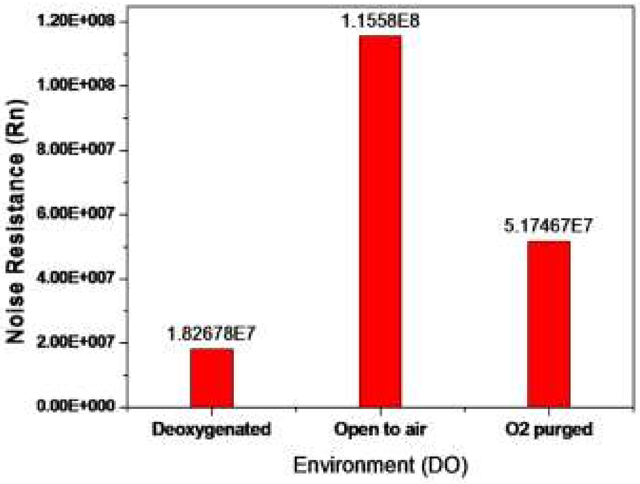

Figure 5.14 Effect of dissolved oxygen on the noise resistance

Above experiments showed that increase in DO level will not increase the corrosion rate. Moreover, increase DO level will modify the nature of oxide film that has better corrosion protection resistance. Hence dissolved oxygen in the environment during certain period of time would protect the component against corrosion. The DO converts the magnetite in to hematite have higher resistance and lower solubility but pure magnetite is not adherent to the base materials. Long term effect of dissolved oxygen on protection nature of oxide needs to be established.

5.4 Highlights

The effect of dissolved oxygen was investigated by electrochemical methods like EIS, potentiodynamic polarization and electrochemical noise method. EIS and potentiodynamic polarization were carried out on magnetite film formed on carbon steel. EIS clearly showed increase in charge transfer resistance due to increase in DO level.

Exposure of magnetite film in high DO environment resulted in the formation hematite of the surface as confirmed Raman spectroscopy, XRD and GDOES. SEM images showed the fine crystals of hematite on the surface. EIS and Mott-Schottky analysis showed the increase in charge transfer resistance and decrease in defect density in the oxide film.

Electrochemical noise measurement also showed increased noise resistance due to increase DO level. Although, there is small increase in corrosion rate when oxygen was purged but this increase is very less and still corrosion rate is lesser than that in de-oxygenated condition. All the experiments established that increase DO level increase the corrosion resistance of the component for the duration of experiment.

Chapter 6

SYNTHESIS AND CHARACTERIZATION OF MAGNETITE POWDER FOR SOLUBILITY STUDY

6.1 Introduction

Carbon steel is used for fabrication of most of the components in the secondary circuit of nuclear power plants and for thermal/fossil fuel based power plants. During the operation with alkaline aqueous process fluid at high temperature and pressure and low dissolved oxygen (DO) concentration, magnetite (Fe_3O_4) film forms on the internal surfaces of pipings and other components [Kain et al., 2008, Kain et al., 2011]. In high velocity flow of liquid/wet steam, magnetite dissolves in the environment at a faster rate [Guimaraes 2003, Poulson 1999]. This high rate of dissolution of magnetite film/base material in the flowing environment is referred as flow accelerated corrosion (FAC). The rate of FAC depends on the solubility of magnetite film in the bulk medium [Betova et al., 2010] (that is dictated by pH of the solution and temperature of operation) and mass transport of corrosion products from the magnetite layer across the boundary layer that develops on the inner surfaces of pipings and other components. The diffusion across the boundary layer is a function of hydrodynamics and temperature of operation [Betova et al., 2010]. There are many reported cases of thinning and failures of primary and secondary components in nuclear power plants (NPPs) due to FAC [Kain 2014, Singh et al., 2012]. The thinning and failures are attributed to enhanced rate of dissolution of magnetite film formed on the internal surface of the components. Solubility of the magnetite in the bulk solution is an important factor of FAC [Betova et al., 2010, Kain, 2014, Singh et al., 2012].

To study the solubility of magnetite, magnetite powders are used by many researchers [Sweeton et al., 1970, Tremaine et al., 1980]. Synthesis of magnetite has been done by many researchers using different routes [Gribanov et al., 1990, Zhuo et al., 2001, Vollath et al., 1997, Zhu et al., 1999, Park et al., 2005, Thapa et al., 2004]. Gribanov et al., [1990] used the colloidal method with ammonium hydroxide as an alkaline agent. They obtained high purity magnetite and avoided the formation of other iron compounds. There are other reports that mentioned the formation of magnetite nano particles by other routes e.g. micro emulsion route [Zhuo et al., 2001] and microwave plasma synthesis technique [Vollath et al., 1997]. Other techniques have been used for the iron oxide nanoparticles synthesis such as sol–gel, freeze-drying, laser pyrolysis and vaporization condensation [Zhu et al., 1999, Park et al., 2005, Thapa et al., 2004]. However, one of the main challenges of these numerous and novel techniques lie in their capacity to obtain a narrow range in particle size together with the desired compositional, structural and crystalline uniformity [Martínez-Mera et al., 2007].

The aim of the present work is to synthesise pure magnetite powder of a specific size (105 – 125 μm) by co-precipitation method. This range of powder size is required for the solubility study of magnetite in a high temperature high pressure circulation loop. For the solubility study, magnetite powder needs to be confined in a high temperature and pressure autoclave using filters on the inlet and outlet sides. Hence nano particles are not suitable for such a solubility study. Only a few researchers have synthesised powder of this size [Sweeton 1970, Tremaine et al., 1980] using iron powders. The present chapter focuses on a novel synthesis route for high purity coarse magnetite powder. The characterization of the magnetite powder was done by scanning electron microscopy (SEM), X-ray diffraction (XRD) and micro laser Raman spectroscopy (MLRS).

6.2 Experimental

6.2.1 Materials

For the synthesis of magnetite powder ferric chloride (iron (III) chloride hexahydrate $FeCl_3.6H_2O$, Merck AR grade) and ferrous chloride (iron (II) chloride tetrahydrate $FeCl_2.4H_2O$, Merck AR grade) were used as salts and ammonium hydroxide (25% NH_4OH) was used as a precipitating agent. Water used in this study was demineralized water (DM water, specific conductivity 0.06 μS/cm at 25 °C).

6.2.2 Synthesis of magnetite powder

The magnetite powder was prepared via chemical co-precipitation method. Co-precipitation method is used by many researchers for the preparation of nano sized magnetite powder [Zhu et al., 1999, Martínez-Mera et al., 2007, Faiyas et al., 2010, Mamania et al., 2016] by precipitating the ferric and ferrous ions in 2:1 ratio. Before dissolving the salts, DM water was de-aerated by purging argon gas for 2 hours. In 500 ml of de-oxygenated water, 9.9415 g (0.1M) of $FeCl_2.4H_2O$ and 27.033 g (0.2M) of $FeCl_3.6H_2O$ were dissolved with slow stirring at room temperature. The pH of the solution was measured after dissolution and was in the range of 2.0 - 2.2. The 25% NH_4OH was added gradually in this solution with continuous stirring and pH was raised to 10.0. The orange colour of the solution immediately turns to black on addition of NH_4OH due to precipitation reaction. This black precipitate was allowed to settle by sedimentation for 1 h and then filtered with Whatman filter paper (Grade 542) using a Buckner funnel and side arm flask attached with a rotary pump. This precipitate was thoroughly washed with DM water to remove all the chloride and dried in the air at room temperature. The co-precipitation reactions can be represented by equations (6.1)-(6.3) [Petcharoen et al., 2012, Zheng et al., 2010].

$$Fe^{2+} + 2OH^- \rightarrow Fe(OH)_2 \quad (6.1)$$

$$Fe^{3+} + 3OH^- \rightarrow Fe(OH)_3 \quad (6.2)$$

$$2Fe(OH)_3 + Fe(OH)_2 \rightarrow Fe_3O_4 + 4H_2O + H_2 \quad (6.3)$$

This dried precipitate was ground into a fine powder. Double stage sieving was done to get the uniform powder size. In this the ground powder was first sieved with mesh no 120 sieve (standard sieve opening 125 μm) and then finally mesh no 140 sieve (standard sieve opening 105 μm) was used. Residual powder on the mesh no 140 sieve was used for characterization.

6.2.3 Sintering of powders

The powder obtained from above process was sintered in an inert atmosphere. For this purpose, oxide powder was compacted using 500 MPa uniaxial pressure for 5 min in a compaction press. Sintering of these compacts (25 mm diameter and ~20 mm length) was done at 1100 °C in inert Ar atmosphere [Jung et al., 2010]. Prior to raising the temperature for sintering, the chamber was flushed with Ar for 30 min to remove all the residual oxygen present. The temperature was raised to 1100 °C at a rate 5 °C/min. Sintering treatment was done for 2 h at 1100 °C then the temperature was brought down to room temperature at a rate of 5 °C/min. The Ar was flushed throughout the process of sintering treatment and during cooling to avoid any incursion of oxygen. The compacts were ground using mortar and pestle. Double stage sieving was done to get the uniform powder size as per section 5.2.2.

6.2.4 Characterization of magnetite powder

Phase identification was carried out by powder XRD in an Inel-make unit (model MPD) with Cr Kα (2.29 Å) radiation operated at 35kV/25mA. A Raman scattering measurement was conducted at room temperature with excitation light of 514.5 nm of an Ar laser. A SEM was used to examine the morphology of the powders and an energy dispersive X-ray spectroscopy (EDS) attached with this SEM was used to establish chemical composition of the powders. XRD, Raman spectroscopy and SEM were carried out for the magnetite powder in as-synthesized condition and also after sintering at 1100 °C for two hour in an inert atmosphere.

6.3. Results and Discussion

6.3.1 Synthesis and characterization of co-precipitated powder

As ferric chloride hexahydrate and ferrous chloride tetrahydrate were dissolved in water, it immediately ionizes and produces ferric and ferrous ions respectively. When the pH of the above solution was raised (by addition of ammonium hydroxide) to alkaline region it forms corresponding hydroxides as per eqns. (6.1) and (6.2) and these hydroxides immediately convert into magnetite as per eqn. (6.3). The as-synthesized magnetite precipitate was very dark (black in colour) and magnetic in nature. Figure 6.1(a) shows the magnetite particles 1 h after precipitation. It was clearly seen that magnetite precipitate settles down after 1 h. Clear water can be seen at the top of the beaker. Magnetic nature of the precipitate is clearly demonstrated in figure 6.1(b). When a magnet was placed near the black magnetite precipitate, the precipitates immediately moved towards the magnet. It was due to magnetic nature of precipitates (magnetite powder). This type of movement of magnetite particle in the magnetite is also shown by Petcharoen et al.,., [2012] and Sakthivel et al.,., [2010]. Since the powder settles down after 1 h, initially decantation method was used for washing the precipitate and for removing the dissolved chloride ion. This decantation process was repeated at least five times and then vacuum filtration was carried out to remove the remaining chloride. During vacuum filtration DM water was added to the precipitate for effective removal of chloride ions.

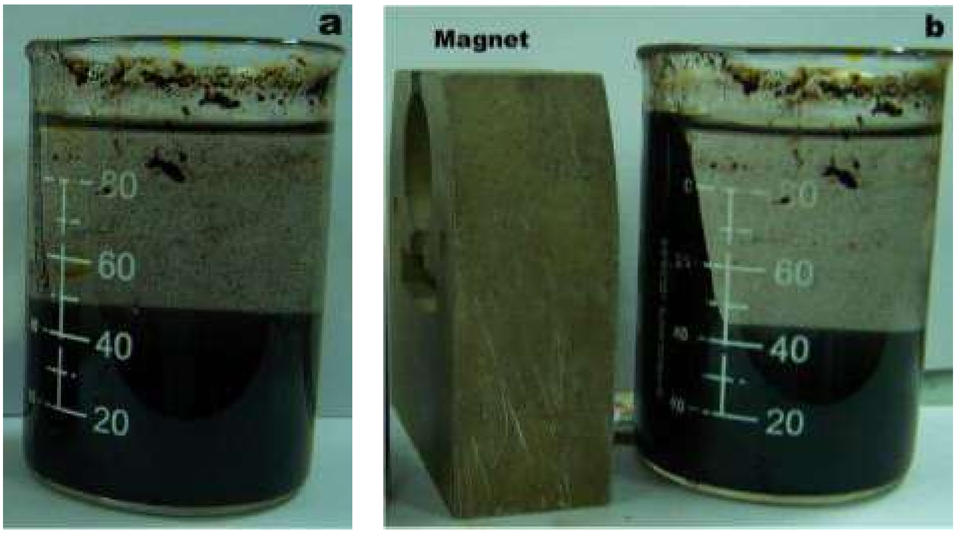

Figure 6.1. (a) Settleing down of black powders and (b) magnetic nature of the precipitates when a magnet is placed next to it.

After filtration, drying, grinding and sieving, the characterization of the powder was carried out. The crystal structure of the oxide powder synthesized was characterized by XRD and is shown in figure 6.2. All the six peaks (marked as M1-M6) at 2θ (hkl) are at 45.51 (220), 54.07 (311), 66.64 (400), 84.23 (422), 90.81 (511) and 101.43 (440) correspond to the magnetite (Fe_3O_4) crystal with cubic spinel structure (PCPDF No 890691). As can be seen in figure 6.2, the peaks for magnetite only are observed and no other peaks of iron oxide like hematite or wustite are seen. The crystal structure of magnetite is a cubic inverse spinel structure. A unit cell of magnetite consists of twenty four Fe (eight ferrous and sixteen ferric) ions and thirty two oxide ions. In these eight ferric ions occupies tetrahedral position (A-position) each with four oxide nearest neighbours and eight ferric and eight ferrous ions at octahedral position (B-position) each with six oxide ions nearest neighbours [Zhu et al., 1999, Cornell et al., 1996, Verwey et al., 1947, Dobson et al., 1970]. The structural formula for the magnetite crystal is referred as $(Fe^{3+})\ [Fe^{3+}Fe^{2+}]O_4$ [Zhu et al., 1999, Cornell et al., 1996, Verwey et al., 1947, Dobson et al., 1970]. Magnetite formed by the co-precipitation method gets easily converted to maghemite (γ-Fe_2O_3) and hematite (α-Fe_2O_3). Characteristic peaks of maghemite and hematite are at (hkl) positions at (113), (210), (213) and (210) respectively [Murbe et al., 2008] and these peaks were not observed in the XRD pattern from the powders obtained in this study (figure 6.2). From the above result it can be inferred that pure magnetite powder without any other phases of iron oxide was synthesized.

In the XRD pattern (figure 6.2), very clear peak broadening can be seen. This may be due to the very fine crystallite size of the powders. In the co-precipitation process nano crystalline magnetite formation is expected [Zhu et al., 1999, Martínez-Mera et al., 2007, Faiyas et al., 2010].

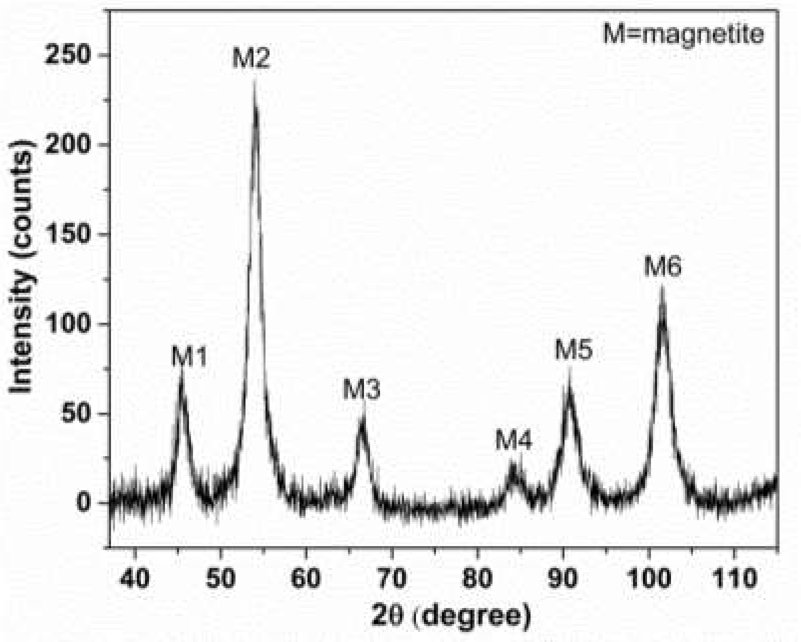

Figure 6.2. XRD pattern of the oxide powders synthesized by co-precipitation method indicating formation of magnetite only

Micro laser Raman spectroscopic characterization was done as a supplementary study to characterize the type of oxide formed. Figure 6.3 is the Raman spectra of the magnetite at two different laser powers (18 mW and 2.5 mW). Characteristic peaks corresponding to hematite (Fe_2O_3) were observed with 18 mW. This result was contrary to the result from XRD where only magnetite was observed. When the laser power was reduced to 2.5 mW, peaks characteristic of only magnetite were seen in the Raman spectra (figure 6.3). Hence at high laser power, due to radiation/heat, the total transformation of magnetite to hematite takes place when the experiment is done in air [Guo et al., 2011]. The characteristics Raman peaks of magnetite and hematite from the literature and Raman peaks of oxide in present study are listed in Table 6.1 [de Faria et al., 1997, Gasparov et al., 2000, Graves et al., 1988, Shebanova et al., 2003, Dunnwald et al., 1989]. It can be seen from the Raman peaks of hematite (figure 6.3) that the peaks have shifted towards lower wave number, as compared to the peaks given in literature [de Faria et al., 1997]. This is attributed to higher laser power. The effect of laser power on the Raman shift has been studied by de Faria et al.,., [1997] where they used laser power of 0.7 mW and 7.0 mW and found that the Raman peaks shifted to lower wave numbers in case of 7.0 mW laser power as compared to the peaks with laser power of 0.7 mW. In the present case Raman peak is further shifted to lower wave numbers. This may be attributed to a still higher laser power of 18 mW.

The magnetite powders synthesized by co-precipitation method have very fine crystallite size as is clear from the broadening of XRD peaks in figure 6.3. Higher laser power very easily converts these fine crystals of magnetite into hematite [Guo et al., 2011].

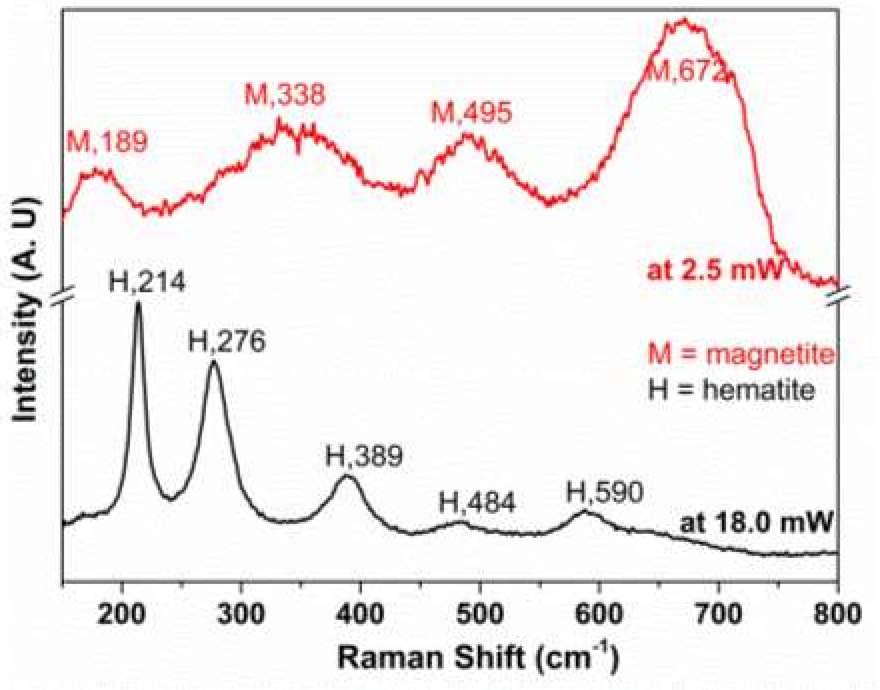

Figure 6.3 Raman spectra of oxide powder synthesized by co-precipitation method done at 18.0 mW and 2.5 mW

Table 6.1 Overview of Raman peaks reported in different studies and in this work.

Compounds	**Raman Shift (cm^{-1})**							**Ref**
Fe_3O_4	189		338		495		672	This work at 2.5 mW
Fe_2O_3	214	276		389	484		590	This work at 18.0 mW
Fe_3O_4	229	295		415		540	668	After sintering,18.0 mW
Fe_2O_3	226.7	292.5		410.9	497.1		611.1	de Faria et al., (0.7 mW) [1997]
Fe_2O_3	219.6	282.7		395.9	492.3		596.0	de Faria et al., (7.0 mW) [1997]
Fe_3O_4	193		308			540	670	Gasparov et al., [2000]
Fe_3O_4	226		336		490	570	706	Graves et al., [1988]
Fe_3O_4	193		306			538	668	Shebanova et al., [2003]
Fe_3O_4		298	319	418	470	550	676	Dunnwald [1989]

The SEM images of the powders are shown in figure 6.4. The SEM images clearly indicate the powder particles are properly crystallized and the big particles are single particles and not an agglomerate of small particles. The particle size distribution is not uniform as can be seen in figure 6.4. To get uniform size of magnetite powder, a double step sieving was done. In the first step, 125 µm sieve and in the second step 105 µm sieve was used to get the particle size in the range of 105 - 125 µm. However it can be seen that even after double step sieving, a uniform particle size could not be obtained, as shown in figure 6.4b. This may be due to breaking of particles into smaller sized particles during sieving. This may be due to weak binding among the powder particles of magnetite.

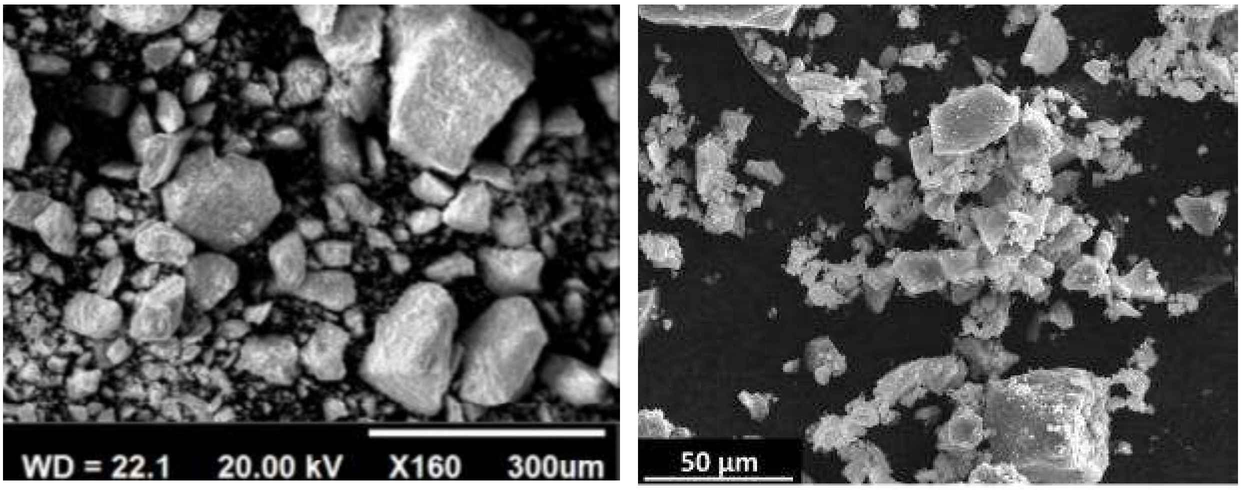

(a) **(b)**

Figure 6.4 SEM image of the magnetite powder (a) before and (b) after sieving showing non uniform distribution of particle size

6.3.2 Efficiency of co-precipitation process

After filtration, drying, grinding and sieving, the collected powder was weighed. The total weight of the powder was found to be 9.853 g. Weight of ferrous chloride tetrahydrate and ferric chloride hexahydrate used for synthesis was 9.9415 g and 27.033 g respectively. The efficiency of the process was calculated on the basis of weight of Fe in salts and weight of Fe in the magnetite formed and collected. The efficiency of the co-precipitation process for synthesis of magnetite was thus established to be 85%. It is possible that during the process of filtration and washing, some fine magnetite powders were lost.

6.3.3 Sintering, grinding, sieving and characterization of powder

To increase the binding and strength of the particles, magnetite powers were sintered as described in section 6.3. After sintering, the pellets obtained were ground into powder and a two-step sieving was done, as described in section 6.2. All the characterization was again performed to check the purity and particle size distribution after sintering, grinding and sieving.

Figure 6.5 shows the XRD of the magnetite powder after sintering at 1100 °C in Ar environment for 2 h, crushing/grinding and sieving as mentioned above. All the peaks corresponding to magnetite were observed after sintering at 1100 °C, grinding and sieving. It may be noted that during sintering of magnetite, oxygen must not be allowed in the system. Even a small amount of oxygen leads to oxidation of magnetite to hematite. In a few cases of sintering trails, some XRD peaks corresponding to hematite were also observed along with magnetite peaks and this was attributed to incursion of oxygen into the sintering set-up that partially converted the magnetite into hematite. It can be seen from figure 6.5 that peaks are sharp (narrow) after sintering and this may be attributed to increased (coarser) crystallite size due to sintering at high temperature and crushing/grinding compared to that obtained from precipitation step directly. From the curve fitting of peaks, full width at half maximum (FWHM) and intensity was determined and these values are given in Table 6.2. Peak broadening value can be seen by FWHM of each peak in Table 6.2.

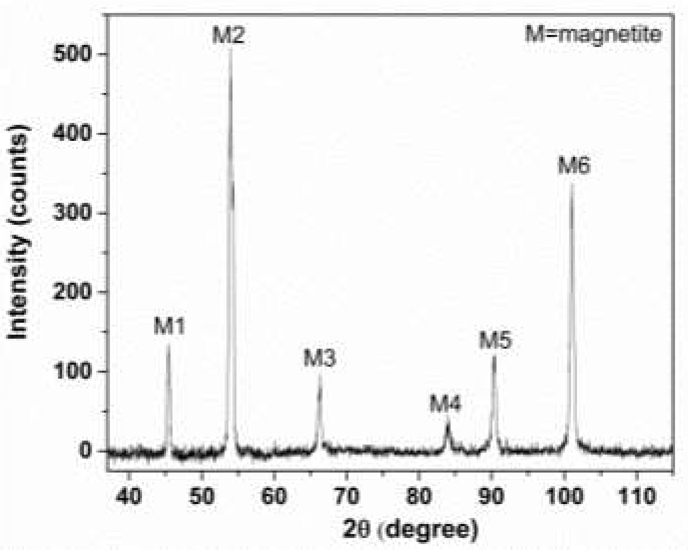

Figure 6.5 XRD of the oxide powder after sintering, grinding and sieving, showing formation of pure magnetite

Table 6.2 Overview of the XRD peaks obtained on the powders before and after sintering, grinding and sieving

Peak	Powder before sintering			Powder after sintering at 1100 °C, grinding and sieving		
	2θ	FWHM	Height	2θ	FWHM	Intensity
M1	45.51	1.63469	58.24111	45.46	0.35753	128.2581
M 2	54.07	1.95516	199.621	53.88	0.64923	453.8748
M 3	66.64	1.59505	39.09085	66.28	0.51629	81.01502
M 4	84.23	1.70595	13.81366	83.94	0.76894	31.92629
M 4	90.81	2.32738	53.30091	90.42	0.59014	115.361
M 6	101.43	2.35329	98.04438	101.05	0.60955	297.9943

Figure 6.6 is the Raman spectrum of the magnetite powder after sintering at 1100 °C, grinding and sieving, done at a higher laser power of 18 mW. It can be clearly seen that the characteristic peaks of magnetite are observed even with a high laser power. Also the peaks remained sharp after sintering. It can be attributed to increased crystallite size due to sintering. Owens et al., [2006] and Slavov et al.,[2010] have shown the peak broadening in the magnetite and hematite. Slavov et al., [2010] showed the FWHM of 80 cm^{-1} for the Raman peak of magnetite nanoparticle at 670 cm^{-1}. Kosacki et al., [2002] studied the effect of grain size of ceria (CeO_2) on the Raman peaks. They showed that the line broadening decreased from 30.3 cm^{-1} to 9.2 cm^{-1} as the grain size increased from 4 nm to single crystal. This behaviour is attributed to the reduction in phonon life-time by the fine microstructure [Kosacki et al., 2002].

Increased crystallite size increases the oxidation resistance of the magnetite powder. So the hematite peaks was not observed even at higher laser power of 18 mW for the powder obtained after sintering, grinding and sieving in contrast to the results shown in figure 6.3 for the powder directly precipitated, ground and sieved.

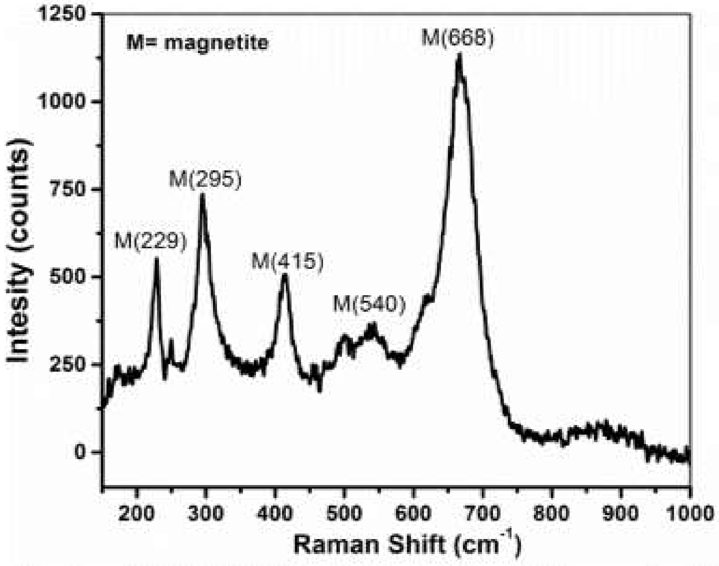

Figure 6.6 Raman spectrum of magnetite powder after sintering at 1100 °C in inert atmosphere; done at 18 mW showing formation of magnetite.

Figure 6.7 (a) and (b) is the SEM image of the magnetite powder after sintering the pellet at 1100 °C, grinding using mortar and pestle and sieving done in two steps. It can clearly be seen that the uniform particle size of approximately 105-125 µm has been achieved. Figure 6.7(c) is the stereomicroscopic image of the oxide powder that also shows the uniform particle size distribution as was shown by SEM.

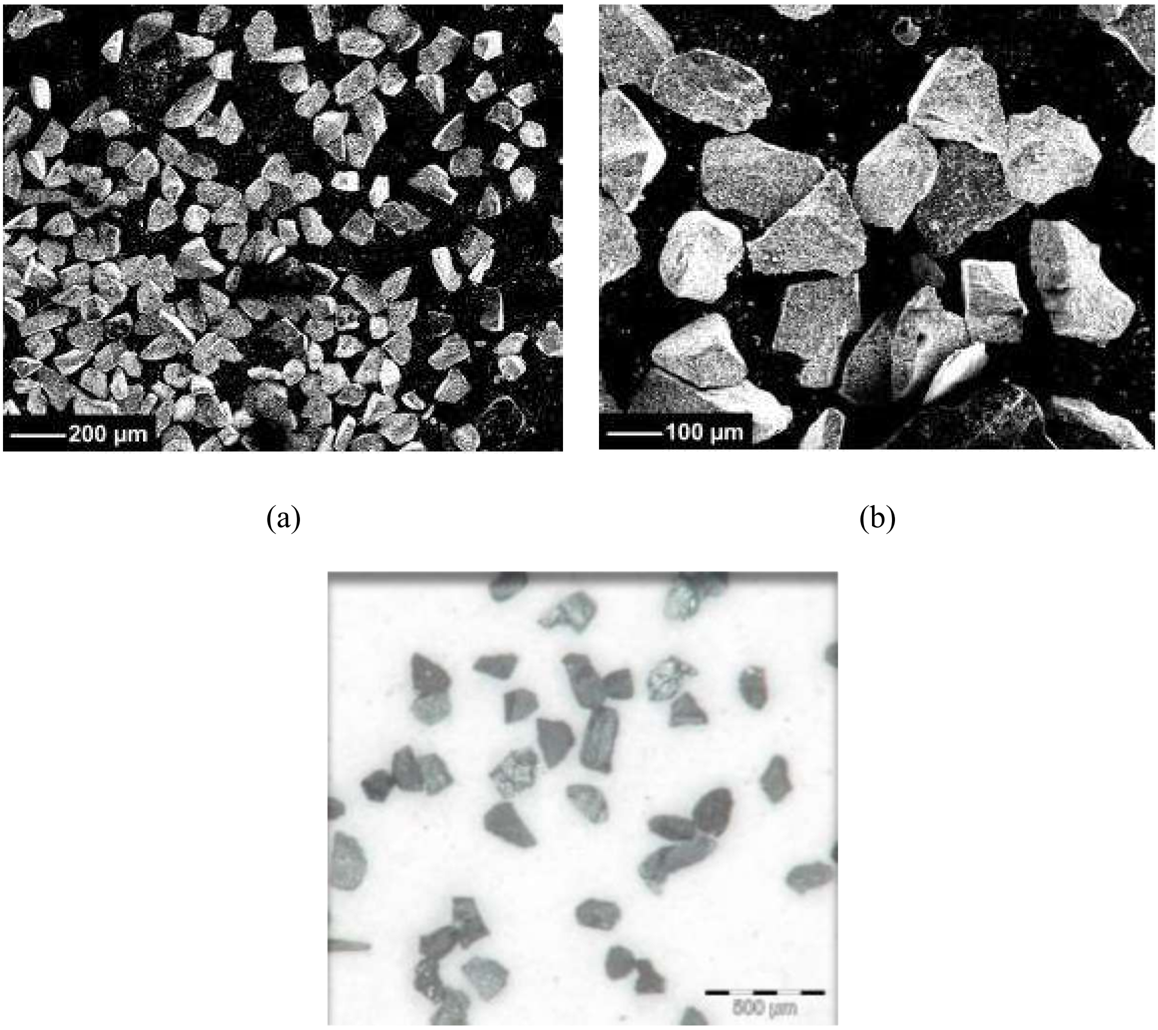

(a) (b)

(c)

Figure 6.7 Magnetite powder obtained after sintering, grinding and two stage sieving showing uniform distribution of particle size, (a) and (b) SEM images and (c) stereomicroscopic image.

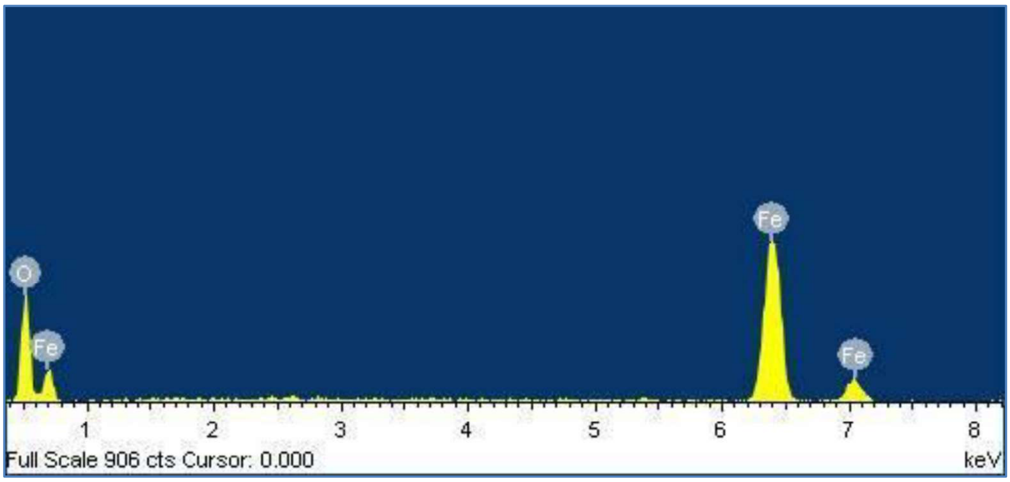

Figure 6.8 EDS result of the magnetite powder showing the presence of iron and oxygen only.

Figure 6.8 shows the energy dispersive spectra of the magnetite powder after sintering at 1100 °C in an inert atmosphere, grinding and sieving. It can be clearly seen that the peaks due to oxygen and iron were obtained. No other peak corresponding to chlorine is obtained which is the most probable impurity from this synthesis process. This clearly indicates that thorough washing during filtration removed all the chloride ions form the system. This is very important for the subsequent use of the magnetite powder e.g. for study of its solubility as it will affect the solubility behavior by changing the environment.

6.4. Highlights

Several studies e.g. the study to establish solubility of magnetite in different aqueous process streams need pure magnetite powder of a required and uniform size. In the present study, magnetite powder was synthesized by co-precipitation method using hydrated ferrous chloride and hydrated ferric chloride as salts in the ferrous to ferric ratio of 1:2. Ammonia hydroxide was used as precipitating agent. These obtained powders were sintered, ground and sieved. Detailed characterization of the powder was done using XRD, Laser Raman spectroscopy and SEM-EDS studies. From the experimental results, the following the following highlights were made:

1. Co-precipitation method was used successfully to synthesize magnetite powder. The efficiency of the co-precipitation process for magnetite powder synthesis was established to be 85%.
2. XRD and Raman analyses showed that pure magnetite powder was formed by co-precipitation, grinding and sieving process.
3. Raman analysis done in air using a high laser power of 18 mW showed presence of hematite while a low power laser of 2.5 mW revealed presence of only magnetite. Hence for characterization of very fine crystallite magnetite powders, only low power laser should be used.
4. Co-precipitation of powders, after grinding and sieving also, did not result in a uniform and narrow range of powders. However, a sintering process is established for these co-precipitated powders followed by its grinding and sieving that produced a uniform range of 105 – 125 μm powder sizes.
5. After the sintering of the powders, grinding and sieving, the high laser power (of 18 mW) also showed the magnetite peaks indicating that the oxidation resistance increased with increased crystallite size.

Chapter 7

SOLUBILITY STUDY OF MAGNETITE POWDER USING A HTHP CIRCULATION LOOP

7.1 Introduction

Solubility of the magnetite film formed on the internal surface of pipeline is a significant parameter of FAC. The solubility limit of metal ions is a function of the pH and temperature of process fluid. Though a given value of pH (at 25 °C) can be obtained by adding various chemicals (e.g. ammonia, ethanolamine (ETA), hydrazine, NaOH, etc.), the pH at the operating temperature would be different as variation in dissociation constants with temperature for each chemical is different. The pH at the operating temperature determines the solubility limit. The solubility limits of magnetite as a function of pH and temperature are available in literature for cases in which pH is adjusted by adding ammonia, NaOH etc. [Sweeton 1970, Tremaine et al., 1980, Betova et al., 2010]. However, some plants use ETA for pH adjustment in the secondary circuit and the solubility limit data for magnetite as a function of temperature and pH adjusted using ETA is not available.

To study the solubility of magnetite a high temperature high pressure loop is required. Magnetite in the form of powder is also needed as it will have a large area and saturation limit of dissolved ions would therefore reach at a faster rate. In the present study, a high temperature and pressure solubility loop was designed and fabricated and solubility of magnetite was studied.

7.2 Experimental

7.2.1 Design and fabrication of HTHP solubility loop

A HTHP loop was designed to study the solubility of oxide in the different environmental condition. The design of loop had two circuits; 1) low pressure circuit to maintain the water chemistry 2) high pressure circuit to expose the magnetite powder in the process water. Low pressure circuit has a low pressure pump and a storage tank with the provision of purging gases and addition of chemical through a peristaltic pump. High pressure circuit has a high pressure pump, pre-heater, autoclave with heater and a back pressure regulator. In this loop all the high pressure and temperature parts are made of a titanium alloy (grade-2).

7.2.2 Water chemistry of the environment

The total de-aeration of the environment is required for the solubility study. Initially Ar/N_2 was purged for 5 day to remove all the dissolved oxygen present in the environment with low pressure/mixing pump on. After this 16 ppm hydrazine hydrate was added to the tank to remove residual dissolved oxygen. Ethanol amine was slowly added to the tank water with monitoring of pH. Addition of ETA was stopped when the required pH was achieved.

7.2.3 Solubility study

Synthesized magnetite powder was kept in the autoclave and high pressure pump was started after closing the autoclave lid. Required pressure in the high pressure line was maintained with high pressure pump and back pressure regulator. Prior to raising the temperature, around 50 litres of water with required chemistry was circulated through loop (the autoclave and pipelines). The temperature of the preheater and autoclave heater was raised to the target temperature. After temperature was reached to the desired value, the samples were collected intermittently after every 1 h. the solubility experiment was carried out for a cumulative 18 h. After collection of the samples, ascorbic acid solution was mixed in the collected water samples to keep all the iron ions in ferrous state. All the samples were analyzed by ion chromatography (IC) system.

7.2.4 Analysis of the samples by ion chromatography

Prior to analysis of the samples, the IC system was calibrated using 20 ppb, 40 ppb and 80 ppb Fe^{2+} standards. In this IC the eluent used is solution of tartaric acid, citric acid and ethylenediamine. Post column reagent (PCR) used is solution 4-(2-Pyridylazo) resorcinol in ammonia and glacial acetic acid. DM water is used for making all the solution. Collected samples were filtered using a syringe filter of 0.45 µm. IC was allowed to equilibrate with eluent and PCR for 30 min and background signal was measured. All the samples were injected one by one for the analysis of ferrous ion content. Injection coil was cleaned with DM water after each and every analysis.

7.3 Results and Discussion

Figure 7.1 shows the schematic design of the high temperature and pressure loop for the solubility study. It has a 300 litre storage tank made of SS 316 and a low pressure pump for mixing of chemicals in the tank. Gas purging system is also for maintaining dissolved gasses in the water. Chemical addition through the peristaltic pump was also provided in the loop. A pressure relief valve is installed on the storage tank to avoid any increase in the pressure of the tank. Schematic of the solubility loop is shown in figure 7.1.

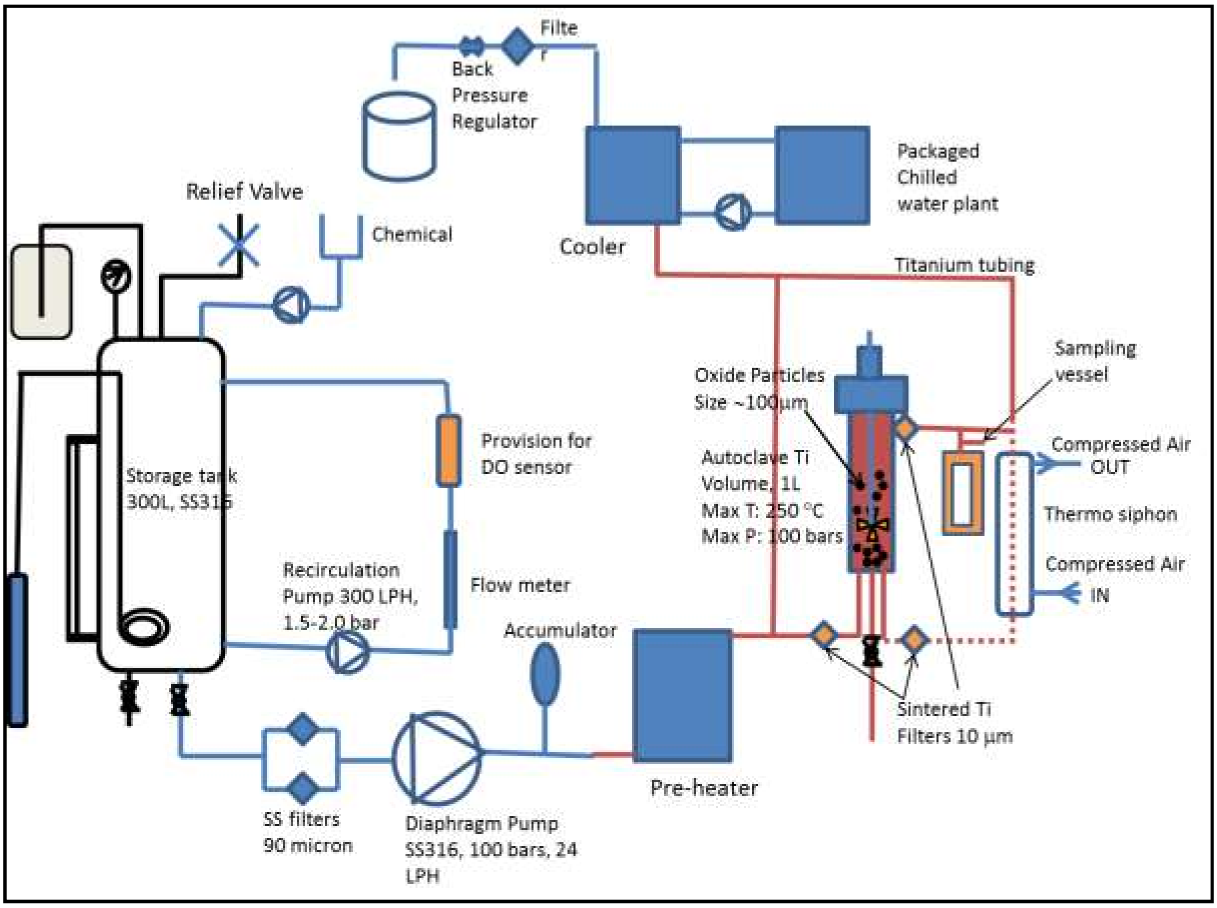

Figure 7.1 schematic of high temperature and pressure loop of solubility study of oxide.

In high pressure circuit of loop a high pressure loop and a back pressure regulator. Pressure in the high pressure circuit is controlled using combination of this HP pump and back pressure regulator. Filters are installed before and after the autoclave in which the magnetite powder is kept. There is a provision for the collection of samples in sampling bulb. The outlet water from the heater is cooled and discharged. Figure 7.2 is the image of the solubility loop.

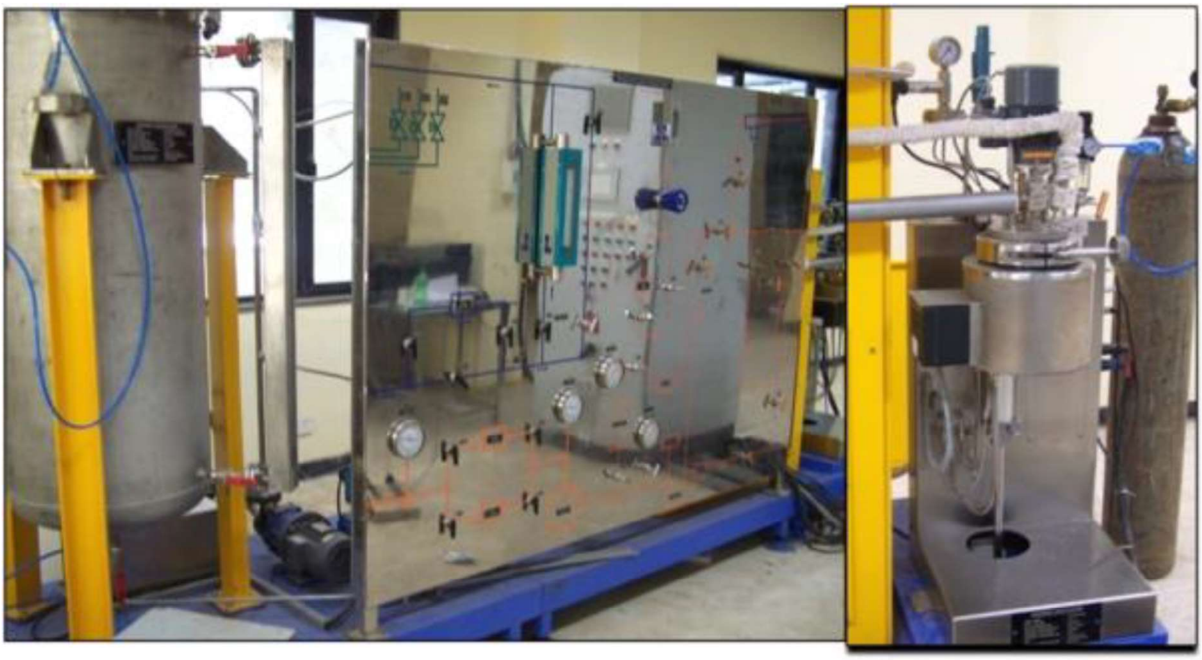

Figure 7.2 High temperature and pressure loop to study the solubility of oxide powder.

All the high temperature and wet parts are made of titanium grade-2 alloy. The reason for using titanium alloy is to avoid interference during analysis of the collected water samples for ferrous ions. Any iron bases alloy like SS will release the iron ions in the process water. The dissolution product of the magnetite powder is also iron ions. So there will be interference during analysis. Hence iron base alloy cannot be used in the high pressure and wet parts.

This loop is designed to study the solubility up to 200 °C. The temperature is maintained with an accuracy of ±2 °C using a preheater and autoclave heater. Before starting the solubility experiment several blank tests were carried out in the simulated secondary circuit environment to remove any loose product and passivation of internal surface of the pipings.

Water chemistry in the tank was maintained in the tank by purging high purity Ar/N_2 for five days. Hydrazine was added to remove any residual oxygen as per equation (7.1).

$$N_2H_4 + O_2 = N_2 + H_2O \quad (7.1)$$

As per the equation 7.1, hydrazine reacts with dissolved oxygen in the water and gives rise nitrogen and water. In the process the dissolved oxygen gets consumed.

Ethanol amine is used for pH adjustment in secondary circuit and affects FAC rate by its effect on resultant HT pH. The effect of ETA on magnetite is mainly due to its resultant pH. ETA was diluted and added to the tank and pH was measured simultaneously. The addition was continued till required value of pH was reached. The amount of ETA required to maintain a particular pH was using figure 7.3. Figure 7.3 gives the volume of ETA per liter of solution, required to obtained a particular pH at room temperature. The data in figure 7.3 is obtained by gradual addition of ETA in one litre of DM water and simultaneous pH measurement.

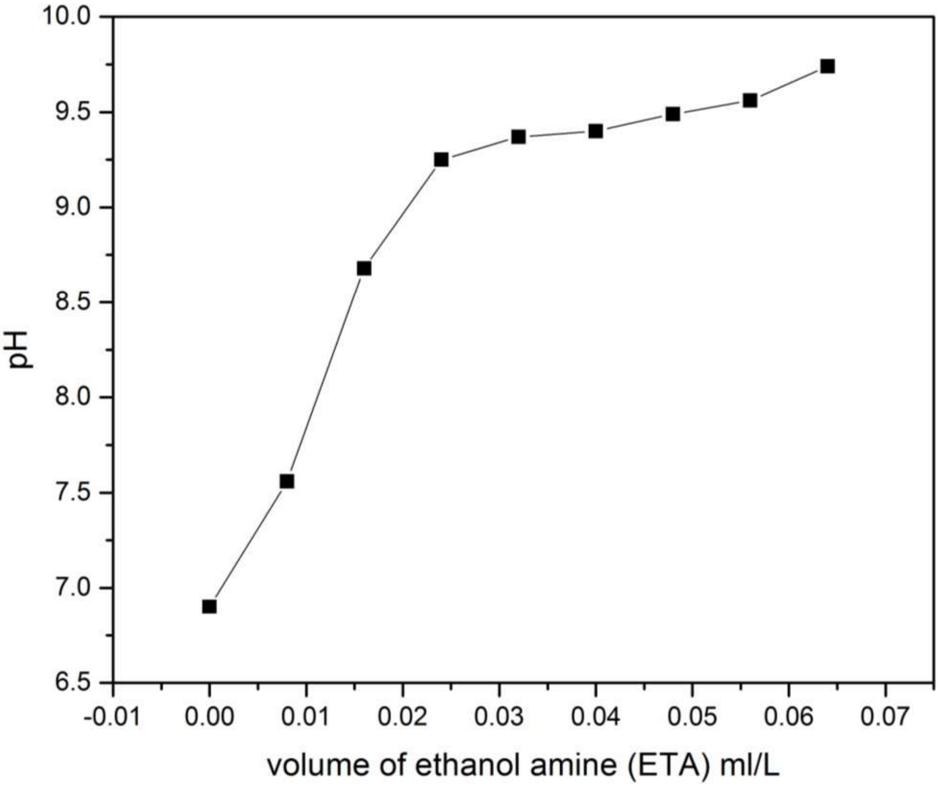

Figure 7.3 Variation of pH value by addition ETA in water.

On the basis of figure 7.3, the amount of ETA required is estimated and added to the tank containing 300 litres of water. But final value is adjusted using a pH meter. Prior to pH measurement, solution in the tank was mixed using a mixing pump to get uniform solution of ETA in DM water. The solubility experiment was carried out at pH 9.5 and temperature 150 °C.

Before measurement of magnetite exposed samples, blank samples with all the water chemistry without magnetite were done. No peaks of iron were detected. Hence it can be inferred that no iron ions from the loop is released in the process water.

Figure 7.4 shows the ion chromatogram of the magnetite exposed in pH 9.5 solution at 150 °C. Ion chromatogram are for the samples collected at different time interval. The peak only due to iron was observed.

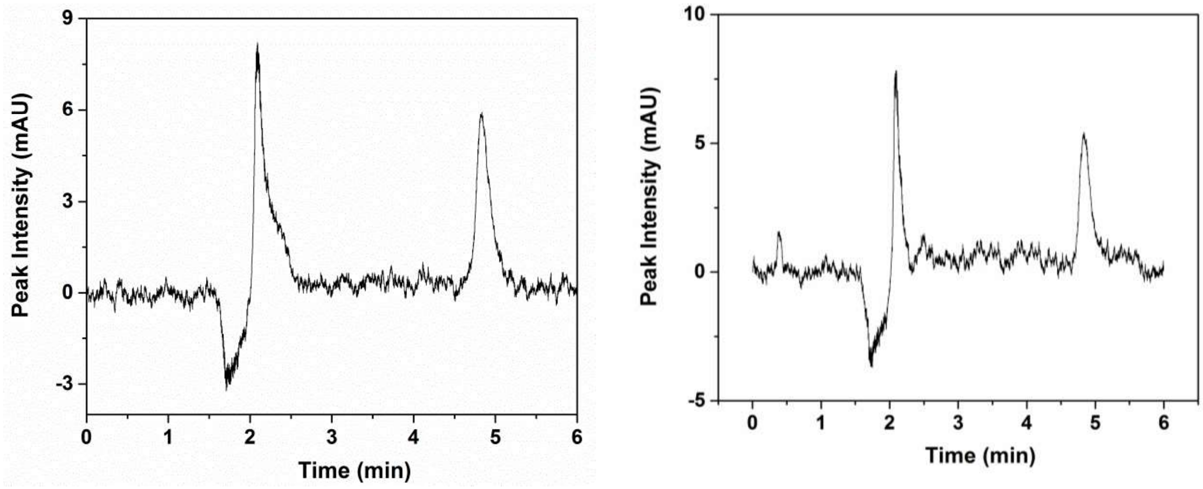

(a) (b)

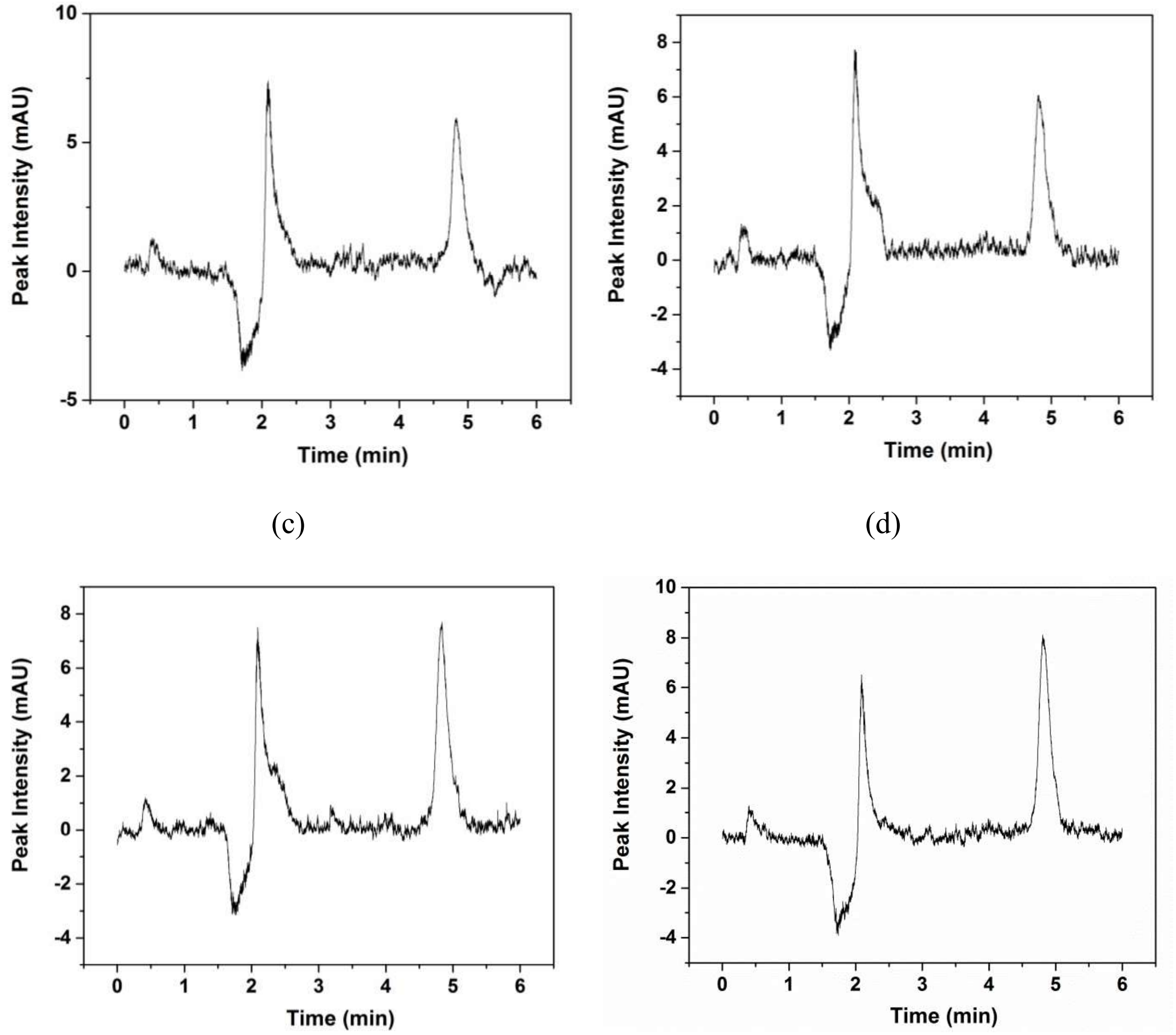

(c) (d)

(e) (f)

Figure 7.4 Ion Chromatogram of the samples collected after (a) 1 h, (b) 2h, (c) 4h, (d) 7h, (e) 8h and (f) 9h exposure.

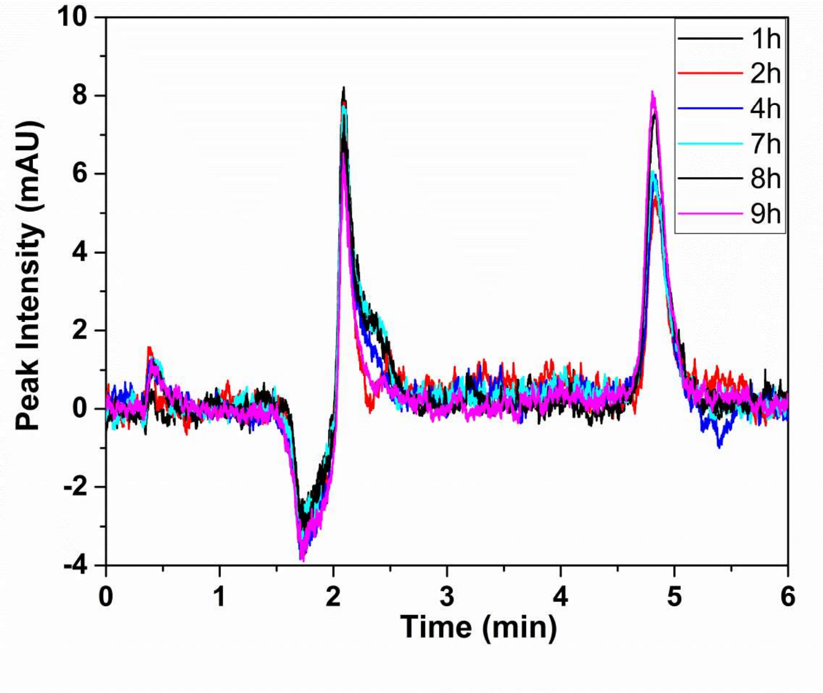

Figure 7.5 Ion Chromatogram of the samples collected after exposure of magnetite in pH 9.5 solution (ETA) at 150 °C.

From the chromatogram and calibration plot, concentration of ferrous ions for each samples were determined. Figure 7.6 shows the concentration of ferrous ion with time of exposure. The concentration of ferrous ion was increased with exposure time. Initially the concentration was found to be 25 ppb which increased to 47 ppb after 18 h.

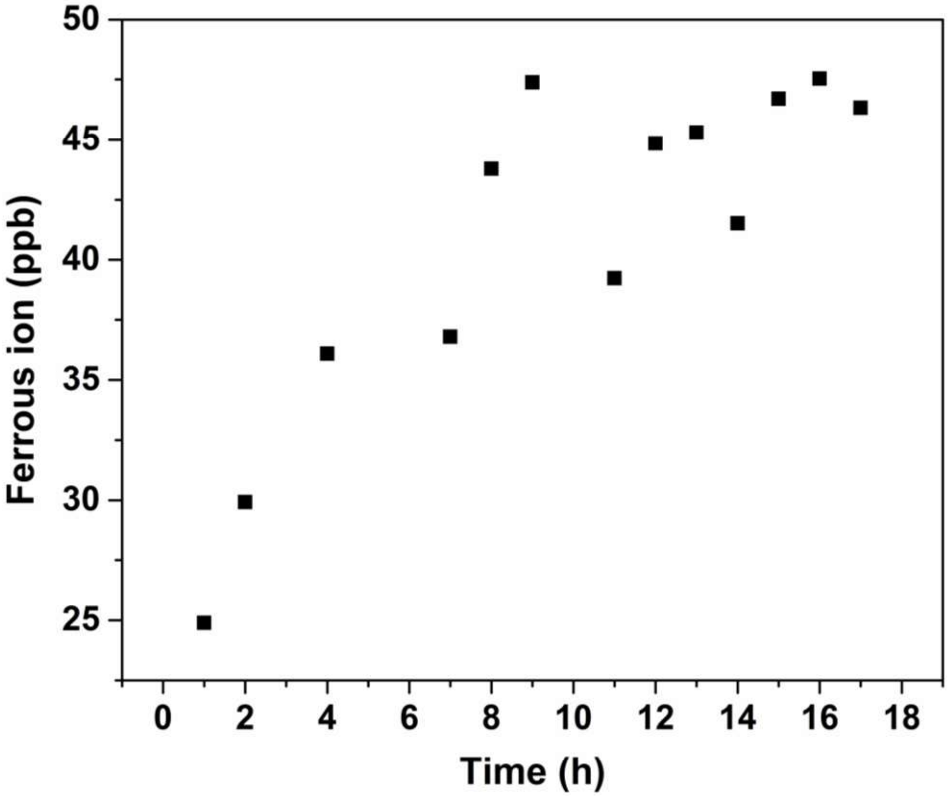

Figure 7.6 variation of ferrous concentration in the samples collected after different time interval.

Dissolution magnetite or hematite involves three principle reactions by which solid oxide released in to an aqueous solution: protonation, reduction and complexation producing ferrous or ferric ions and complexes of ferrous or ferric ions [Schwertmann U., 1991]. In magnetite iron is in ferrous and ferric state ($FeO.Fe_2O_3$). Depending upon the nature of environment (reductive or oxidative) after dissolution iron oxide dissolves as ferrous species (reduction) or ferric species (oxidation) and these processes are called as reductive or oxidative dissolution respectively [Rocchini G. 1994].

7.4 Highlights

A high temperature and pressure solubility loop having all wet and high temperature part made of titanium has been fabricated and successfully tested for its operation and control. Magnetite powder was exposed to 150 °C in pH 9.5 solution maintained by ethanol amine. The solubility experiment was carried for 18 h and samples were analyzed by ion chromatography. The concentration of ferrous ion was increased with exposure time. Initially the concentration was found to be 25 ppb after 1 h which increased to 47 ppb after 18 h. This establishes the test facility and a procedure for measuring the solubility for any given combination of temperature and pH. This work has established a methodology for establishing the optimum pH for lowering FAC rate. This solubility work is an example of such measurement in HTHP loop. Such a correlation with pH requires a large database and it can be established using the methodology highlighted in this thesis.

Chapter 8

CONCLUSIONS

The objective of the thesis were two-fold:- (a) to establish the effect of various environmental parameters., viz; temperature, pH, dissolved oxygen levels and extent of cold working on the oxidation kinetics and nature of oxide formed on carbon steel and (b) to synthesize magnetite powder by co-precipitation method and establish its solubility behavior in simulated secondary circuit environment. The oxidation work was done in autoclaves at temperatures varying from 150 to 300 °C, with DM water having pH adjusted by adding ETA/LiOH, pH variation from 7.0- 10.2, DO levels varying from deoxygenated condition to high DO levels. The material used was carbon steel that was cold rolled from 0 to 30% reduction in thickness. The oxide film formed on carbon steel as well as the synthesized magnetite powder were characterized using various techniques to establish the phases present, defect densities, etc. Following are the main findings of the thesis.

1. Total oxidation/corrosion rate increased with the extent of cold working. Total oxidation/corrosion for the specimen exposed for 20 days increased from 0.50 mg/cm^2 to 0.67 mg/cm^2 as the extent of cold working increased from AR to 30%. The defect density in the oxide film was found to increase with cold working up to 30% reduction and was the main reason for increased oxidation rate. Cold working did not affect the morphology of the oxide film, as formation of outer layer was governed by environmental variables and precipitation of magnetite crystallites on the outer layer of the oxide film. Cold work also did not change the type of oxide formed; magnetite being the only oxide type present on all the cold worked and as-received specimens. Therefore, the extent of oxidation increased and

defect density of the oxide also increased with the extent of cold working of carbon steel. This could have a possible influence on FAC behavior.

2. Increased temperature facilitated the formation of outer layer (precipitated layer) by lowering the solubility of dissolved ions. Intensity and emergence of new XRD peaks with increase in formation temperature confirmed that the thickness of the oxide (magnetite) increased with increase in temperature. This result was in line with the weight gain data. Defect density decreased with increase in formation temperature confirming that the oxide film formed at high temperature is therefore more protective.

3. In high DO condition, there was formation of hematite (over magnetite) as confirmed by GI-XRD and Raman Spectroscopy. EIS confirmed that the oxide film formed in high DO condition had more charge transfer resistance than that formed in low DO condition. Defect density was also found to be less in the oxide formed in high DO condition. Hence, the oxide film (hematite) formed in high DO is more protective (has lower defect density).

4. Magnetite powder of ~100 μm size was synthesized by co-precipitation method followed by sintering and sieving. Sintering and sieving was shown to be a must for ~100 μm size powder synthesis by co-precipitation route. Efficiency of the co-precipitation process was established to be ~85%.

5. Synthesized powder was confirmed to be magnetite using laser Raman spectroscopy. High laser power in air is shown to covert magnetite to hematite. Hence during characterization of magnetite, low laser power should be used.

6. A high temperature, high pressure circulation loop to study the solubility of magnetite powder was fabricated and solubility study of magnetite powder was done. Solubility limit of synthesized magnetite powder of size 100-125 μm at 150 °C and pH 9.5 was established to be ~47 ppb. This approach of analysis would result in establishing the optimum pH to be used (with a given chemical addition) for minimizing FAC rate.

Chapter 9

SCOPE FOR FUTURE RESEARCH

On the basis of work carried out, further studies can be done in future. This study includes the oxide film characterization and solubility study.

- As the solubility of the oxide film also depends on the Redox potential of the environment. Chemical used to maintain the pH would affect redox potential of the environment. Hence oxide film formed using different chemical need to be studied.
- In this thesis, effect of pH on oxide film formation was studied only at two pH values i.e. neutral pH and pH 9.5 (ETA). There is a need to cover a broader range of pH i.e. up to 10.5.
- Solubility of magnetite was established at 150 °C in pH 9.5 solution. Solubility needs to be established in the temperature range 100 to 200 °C and in the pH from neutral to 10.5.
- Synthesis of hematite and its solubility behaviour also needs to be established.

REFERENCES

- Ahmed W.H., Evaluation of the proximity effect on flow-accelerated corrosion, *Ann. Nucl. Energy*, **2010**, 37, 598-605.
- Antunes R. A., de Oliveira M. C. L., I. Costa, Study of the correlation between corrosion resistance and semi-conducting properties of the passive film of AISI 316L stainless steel in physiological solution, *Mater. Corros.*, **2012**, *63*, 586.
- ASM Handbook, 1990, Volume 1 Properties and Selection: Irons, steels and high performance alloys
- ASTM A106 / A106M-15, Standard Specification for Seamless Carbon Steel Pipe for High-Temperature Service, ASTM International, West Conshohocken, PA, 2015,
- ASTM G2 / G2M-06(2011)e1, Standard Test Method for Corrosion Testing of Products of Zirconium, Hafnium, and Their Alloys in Water at 680°F (360°C) or in Steam at 750°F (400°C), ASTM International, West Conshohocken, PA, 2011.
- Atomic energy regulatory board report, 2003, AERB SAFETY GUIDE NO. AERB/NPP-PHWR/SG/D-8
- Avner H. S., Introduction to Physical metallurgy, Second Edition, McGraw-Hill International Edition.
- Beak W. C., Kang T., Sohn H. J., In situ surface enhanced Raman spectroscopic study on the effect of dissolved oxygen on the corrosion film on low carbon steel in 0.01 M NaCl solution, *Electrochim. Acta*, 2001, 46, 2321-2325.
- Betova I., Bojinov M., and Saario T., "Predictive modelling of flow accelerated corrosion-unresolved problems and issues," VTT research report No VTT-R-08125-10, 2010.

- Beverskog B., and Puigdomenech I., Revised pourbaix diagram for iron at 25-300 °C, *Corrosion Science,* 1996, 38, 2121-2135.
- Bhadeshia H. K. D. H. et al.,., Steels: Microstructure and Propery, third edition, 2006
- Birks N. and Meier G. H., Introduction to high temperature oxidation of metals, Edward Arnold, London, 1983.
- Bojinov M., Fabricius G., Laitinen T., Mäkelä K., Saario T., Sundholm G., Coupling between ionic defect structure and electronic conduction in passive films on iron, chromium and iron–chromium alloys *Electrochim. Acta*, **2000**, *45*, 2029-2048.
- Bojinov M., Gaonkar K., Ghosh S., Kain V., Kumar K., Saario T., Characterisation of the oxide layer on carbon steel during hot conditioning of primary heat transport systems in heavy-water reactors, *Corros. Sci.*, 2009, **51,** 1146–1156.
- Cáceres L, Vargas T, Herrera L, Influence of pitting and iron oxide formation during corrosion of carbon steel in unbuffered NaCl solutions, *Corros. Sci.*, 2009a, 51, 971-978.
- Cáceres L, Vargas T, Parra M., Study of the variational patterns for corrosion kinetics of carbon steel as a function of dissolved oxygen and NaCl concentration, *Electrochim. Acta*, 2009b, 54,7435-7443.
- Chao CY, Lin LF, Macdonald DD. A point defect model for anodic passive films. I. Film growth kinetics, *Journal of electrochemical society*, l981, 128, 1187-1194.
- Chexal, B., Flow Accelerated Corrosion in Power Plants, EPRI Report TR-106611-R1, Palo Alto, CA, 1998.
- Cornell R. M., Schwertmann U., The Iron Oxides. Structure, Properties, Reactions, Occurrence and Uses, VCH Verlagsgesellschaft, Weinheim, 1996.
- Cotton FA, Wilkinson, G. Basic Inorganic Chemistry, New York: John Wiley & Sons, Inc., 1976.

- Cubicciotti, D., Flow-assisted corrosion of steel and the influence of Cr and Cu additions, *J. Nucl. Mater*. 1988, 152, 259-264.
- Davenport AJ, Sansone M., High resolution in situ XANES investigation of the nature of the passive film on iron in a pH 8.4 borate buffer. *Journal of the Electrochemical Society* 1995, 142, 725-730
- de Faria D.L.A., Lopes F.N., Heated goethite and natural hematite: Can Raman spectroscopy be used to differentiate them? *Vibrational Spectroscopy,* 2007, 45, 117–121.
- de Faria D.L.A., Silva S. V. and de Oliveira M. T., Raman microspectroscopy of some iron oxides and oxyhydroxides, *Journal of Raman Spectroscopy*, 1997, 28, 873-878.
- Dobson D. C., Linnet J. W., Rahman M. M., Mossbauer Studies of the Charge Transfer Process in the System $Zn_xFe_{3-x}O_4$, *J. Phys. Chem. Solids,* 1970, 31, 2727–2733.
- Dooley R.B., Chexal V.K., Flow-accelerated corrosion of pressure vessels in fossil plants, *Int J Pres Ves Pip*, 2000, **77**, 85-90.
- Dunnwald J., Otto A., An investigation of phase transitions in rust layers using Raman spectroscopy, *Corros. Sci*. 1989, 29, 1167–1176.
- Faiyas A. P. A., Vinod E. M., Joseph J., Ganesan R., Pandey R. K., Dependence of pH and surfactant effect in the synthesis of magnetite (Fe_3O_4) nanoparticles and its properties, *J. Magn. Magn. Mater*. 2010, 322, 400–404.
- Frayne C., Boiler Water Treatment Principles and Practice, Chemical Publishing Co., Inc., New York, 2002.
- Fujimoto S., Tsuchiya H., Semiconductor properties and protective role of passive films of iron base alloys, *Corros. Sci*., 2007, **49**, 195-202.

- Fujiwaraa K., M. Domae, K. Yoneda, F. Inada, T. Ohira, K. Hisamune, Correlation of flow accelerated corrosion rate with iron solubility, *Nucl. Eng. Des.*, 2011, **241**, 4482–4486.
- Fujiwaraa K., Domae M., Ohira, T., Hisamune K., Takiguchi H., Uchida S., and Lister D., Electrochemical measurement of carbon steel under high flow rate conditions and thermodynamic solubility of iron, 16th Pasific Basin Nuclear Conference, Aomari, Japan, Paper ID P16P1048.
- Gaskell D. R., Introduction to thermodynamics of materials, 4th edition, 2009
- Gasparov L. V., Tanner D. B., Romero D. B., Berger H., Margaritondo G., Forro L., Infrared and Raman studies of the Verwey transition in magnetite, *Phys. Rev. B.* 2000, 62, 7939–7944.
- Gerischer H. Remarks on the electronic structure of the oxide film on passive iron and the consequences for its electrode behaviour. *Corrosion Science,* 1989, 29(2/3), 191-195.
- Göhring H., Leineweber A., Mittemeijer E.J., A thermodynamic model for non-stoichiometric cementite; the Fe– C phase diagram, Computer Coupling of Phase Diagrams and Thermochemistry, 2016, 52, 38–46.
- Gomes W.P., Vanmaekelbergh D., Impedance Spectroscopy at Semiconductor Electrodes: Review and Recent Developments, *Electrochim. Acta*, 1996, **41**, 967-973.
- Graves P. R., Johnston C., Campaniello J. J., Raman scattering in spinel structure ferrites, *Mater. Res. Bull.*, 1988, 23, 1651–1660.
- Gribanov N. M., Bibik E. E., Buzunov O. V., Naumov V.N., Physico-Chemical Regularities of Obtaining Highly Dispersed Magnetite by the Method of Chemical Condensation, *J. Magn. Magn. Mater*. 1990, 85, 7–10.

- Guimaraes A. C. F., A new methodology for the study of FAC phenomenon based on a fuzzy rule system, *Ann. Nucl. Energy*, 2003, **30**, 853-864.
- Guo C., Hu Y., Qian H., Ning J., Xu S., Magnetite (Fe3O4) tetrakaidecahedral microcrystals: Synthesis, characterization, and micro-Raman study, *Mater. Charact.*, 2011, 62, 148 – 151.
- Guo H.X., Lu B.T., Luo J.L., Study on passivation and erosion-enhanced corrosion resistance by Mott-Schottky analysis, *Electrochim. Acta*, 2006, 52, 1108–1116.
- Guo X.-P., Tomoe Y., H. Imaizumi, K. Katoh, The electrochemical behavior and impedance characteristics of the passive film on carbon steel in nitric acid solutions, *J. Electroanal. Chem*. 1998, 445, 95 – 103.
- Hamadou L., Kadri A., Benbrahim N., Characterisation of passive films formed on low carbon steel in borate buffer solution (pH 9.2) by electrochemical impedance spectroscopy, *Appl. Surf. Sci.*, 2005, **252**, 1510–1519.
- Higgins R. A., Properties of Engineering Materials, Second edition, Edward Arnold, London, 1994.
- Islam Md. A., Farhat Z. N., Characterization of the Corrosion Layer on Pipeline Steel in Sweet Environment, *J. Mater. Eng. Perform.,* 2015, **24**, 3142–3158
- Iverson W.P., Transient Voltage Changes Produced in Corroding Metals and Alloys, *J. Electrochem. Soc.*, 1968, 115, 617-618.
- Jinlong Lv, Hongyun Luo, Effect of Temperature and Chloride Ion Concentration on Corrosion of Passive Films on Nano/Ultrafine Grained Stainless Steels, *J. Mater. Eng. Perform.*, 2014, 23, 4223-4229.
- Jung Ki-Sok, Laurent de Pierrefeu, Electrochemical characterization of sintered magnetite electrode in LiOH solution, Corros. Sci. 2010, 52, 817-825.

- Kain V., Flow Accelerated Corrosion: Forms, Mechanisms and Case Studies, *Procedia Engineering,* 2014, **86**, 576 – 588
- Kain V., Roychowdhury S., Ahmedabadi P., Barua D.K., Flow accelerated corrosion: Experience from examination of components from nuclear power plants, *Eng. Fail. Anal.*, 2011, **18**, 2028–2041.
- Kain V., Roychowdhury S., Mathew T., Bhandakkar A., Flow accelerated corrosion and its control measures for the secondary circuit pipelines in Indian nuclear power plants, *J. Nucl. Mater.*, 2008, **383**, 86–91.
- Kearns J.R., Eden D.A., Yafee M.R., Fathey J.V., Reichert D.L. and Silverman D.C., "Electrochemical noise measurement for corrosion applications", ASTM STP 1277, 1966; 446-471.
- Khoshnevisan, K., Barkhi, M., Ghasemzadeh, A. Tahami, H.V. Pourmand, S. Fabrication of Coated/Uncoated Magnetic Nanoparticles to Determine Their Surface Properties, *Materials and Manufacturing Processes* **2016**, 31, 1206–1215.
- Kofstad P. High temperature corrosion. London, New York: Elsevier Applied Science, 1988.
- Konig U., Schultze J.W., The examination of the influence of a space-charge layer on the formation kinetics of thin passive films by Schottky-Mott analysis, *Solid State Ionics,* 1992, 53-56, 255-264.
- Kosacki I., Suzuki T., Anderson H. U., Colomban P., Raman scattering and lattice defects in nanocrystalline CeO2 thin films, *Solid State Ionics*, 2002,149, 99– 105.
- Kumar M. K., Gaonkar K. B., Ghosh S., Kain V., Bojinov M., Saario T., Optimisation of the hot conditioning of carbon steel surfaces of primary heat transport system of Pressurized Heavy Water Reactors using electrochemical impedance spectroscopy, *J. Nucl. Mater.,* 2010, **401**, 46–54.

- Li Y, Wu J, Zhang D, Wang Y, Hou B, The electrochemical reduction reaction of dissolved oxygen on Q235 carbon steel in alkaline solution containing chloride ions, *J. Solid State Electrochem.*, 2010, 14, 1667-1673.
- Liang J. Li, L. Min, L. Wang, L. Yang, R. Synthesis of Monodisperse Magnetite Nanocrystals via Partially Reduced Precipitation Method, *Materials and Manufacturing Processes* **2010**, 25, 915–918.
- Lister D.H., Davidson R.D., Mc Alpine E. The mechanism and kinetics of corrosion product release from stainless steel in lithiated high temperature water, *Corrosion Science,* 1987, 27, 113-140
- Luo H., Dong C.F., Cheng X.Q., Xiao K., Li X.G., Electrochemical Behavior of 2205 Duplex Stainless Steel in NaCl Solution with Different Chromate Contents, *J. Mater. Eng. Perform.*, 2012, 21, 1283-1291.
- Mabuchi K., Horn Y., Takahashi H. and Nagayama M., Effect of Temperature and Dissolved Oxygen on the Corrosion Behavior of Carbon Steel in High-Temperature Water, *Corrosion*, 1991, **47**, 500-508.
- Macdonald D. D., Passivity – the key to our metals-based civilization, *Pure Appl. Chem.*, 1999, **71**, 951-978.
- Macdonald D. D., Some personal adventures in passivity da review of the point defect model for film growth, *Russ. J. Electrochem*., 2012, 48, 235 – 258.
- Macdonald D. D., The history of the Point Defect Model for the passive state: A brief review of film growth aspects, *Electrochimica Acta*, 2011, 56, 1761–1772.
- Macdonald, D.D., et. al., The Thermodynamics of Metal-Water Systems at Elevated Temperatures. Part 2: The Iron Water System. AECL-4137.

- Mamania, J.B. Costa-Filhob, A.J. Cornejoc, D.R. Vieirad, E.D. Gamarraa, L.F. Synthesis and characterization of magnetite nanoparticles coated with lauric acid, *Materials Characterization* **2016,** 111, 183–192.
- Mantia F. La, Habazaki H., Santamaria M., Quarto F. Di, A Critical Assessment of the Mott–Schottky Analysis for the Characterisation of Passive Film-Electrolyte Junctions, *Russ. J. Electrochem*., 2010, 46, 1306-1322.
- Martínez-Mera, I. Espinosa-Pesqueira, M.E. Pérez-Hernández, Arenas-Alatorre, R.J. Synthesis of magnetite (Fe_3O_4) nanoparticles without surfactants at room temperature, *Materials Letters* **2007**, 61, 4447–4451.
- Matsumura M., Wall thinning in carbon steel pipeline carrying pure water at high temperature *Mater. Corros.*, **2015**, 66, 688-694.
- Mendili Y. El, Abdelouas A., Bardeau J-F., The Corrosion Behavior of Carbon Steel in Sulfide Aqueous Media at 30 °C, *J. Mater. Eng. Perform*., 2014, **23**, 1350–1357
- Moon J. Ho, Chung H. Ho, Sung Ki W., Kim Uh Ch., Pho Jae S., Dependency of single-phase FAC of carbon and low alloy steels for NPP system piping on pH, orifice distance and materials, *Nucl. Eng. Technol.*, 2005, **37**, 375-384.
- Moon S.M. and S. II, Pyun, The mechanism of stress generation during the growth of anodic oxide films on pure aluminium in acidic solutions, *Electrochim. Acta,* **1998**, *43*, 3117-3126.
- Murbe J., Rechtenbach A. and Topfer J., Synthesis and physical characterization of magnetite nanoparticles for biomedical applications, *Mater. Chem. Phys*., 2008, 110, 426–433.
- Olmedo A. M., Bordoni R., Studies of Oxide Layers Grown at 260°C on A106 B Carbon Steel in Aqueous Medium with Ethanolamine or Morpholine, *Mater. Sci. Appl.*, **2015**, *6*, 783-791.

- Owens F. J. and Orosz J., Effect of nanosizing on lattice and magnon modes of hematite, *Solid State Commun*. 2006, 138, 95–98.
- Park J., Lee E., Hwang N-M., Kang M., Kim S.C., Hwang Y., Park J-G., Noh Han-Jin, Kim Jae-Young, Park Jae-Hoon, Hyeon T., One-Nanometer-Scale Size-Controlled Synthesis of Monodisperse Magnetic Iron Oxide Nanoparticles Angew. Chem. Int. Ed. 2005, 44, 2872-2877.
- Parkinson G. S., Iron Oxide Surfaces, *Surface Science Reports*, 71(2016) 272-365
- Petcharoen, K. Sirivat, A. Synthesis and characterization of magnetite nanoparticles via the chemical co-precipitation method, *Materials Science and Engineering B* **2012,** 177, 421– 427.
- Poulson B., Complexities in predicting erosion corrosion, *Wear*, 1999, 233-235, 497-504.
- Remy F.N., Bouchacourt M., Flow-assisted corrosion: a method to avoid damage, *Nuclear Engineering and Design*, 1992, 133, 23-30.
- Rickert H. Electrochemistry of solids, an introduction. Berlin-Heidelberg-New York: Springer-Verlag, 1982.
- Rihan R.O., Nesic S., Erosion–corrosion of mild steel in hot caustic. Part I: NaOH solution, *Corros. Sci*. 2006, **48**, 2633–2659.
- Robertson J. The mechanism of high temperature aqueous corrosion of stainless steels. *Corrosion Science,* 1991, 32, 443-465
- Robertson J., The Mechanism of High Temperature Aqueous Corrosion of Steel, *Corros. Sci.,* 1989, **29**, 1275–1291.
- Rocchini G., Magnetite stability in aqueous solutions as a function of temperature, *Corrosion Science,* 1994, 36, 2043-2061.

- Rudden M.N, Wilson J., Elements of solid state physics. Chichester: John Wiley & Sons Ltd., 1984.
- Sabol G. P., Dalgaard S. B., The Origin of the Cubic Rate Law in Zirconium Alloy Oxidation, *J. Electrochem. Soc., 1975, 122, 316-317.*
- Sakthivel R., Vasumathi N., Sahu D., Mishra B. K., Synthesis of magnetite powder from iron ore tailings, *Powder Technol*. 2010, 201, 187-190.
- Schwertmann U., Cornell R.M., Iron Oxides in the Laboratory. Wiley-VCH, 2nd.ed. Weinheim, 2000, ISBN 3-527-29669-7.
- Schwertmann U., Solubility and dissolution of iron oxides, *Plant and Soil*, 1991, 130, 1-25.
- Shebanova Olga N. and Lazor P., Raman spectroscopic study of magnetite (FeFe2O4): a new assignment for the vibrational spectrum, *J. Solid State Chem*., 2003, 174, 424–430.
- Shoji T., Lu Z., Takeda Y., Sato Y., presented in 14th Asia Pacific Corrosion Control Conference (APCCC), Shanghai, China, October 21–24, **2006**.
- Sicupira D. C., Cardoso Junior R., Bracarense A. Q., Frankel G. S., Lins V. de F. C., *Mater. Corros.,* **2017**, *68*, 604.
- Simoes A.M.P., Ferrira M.G.S., Rondot B., Study of Passive Films Formed on AISI 304 Stainless Steel by Impedance Measurements and Photoelectrochemistry, *J. Electrochem. Soc*., 1990, **137**, 82–87.
- Singh J. L., Kumar U., Kumawat N., Kumar S., Kain V., Anantharaman S., Sinha A. K., Flow accelerated corrosion of carbon steel feeder pipes from pressurized heavy water reactors *J. Nucl. Mater*., 2012, 429, 226 – 232.

- Sinha P. K., Kumar M. K., Kain V., Effect of microstructure of carbon steel on magnetite formation in simulated Hot Conditioning environment of nuclear reactors, *J. Nucl. Mater.,* 2015, **464**, 20–27.
- Sinha. A. K., Ferrous Physical Metallurgy, Butterworths, Stoneham, USA, 1989
- Slavov L., Abrashev M. V., Merodiiska T., Gelev Ch., Vandenberghe R. E., Markova-Deneva I., Nedkov I., Raman spectroscopy investigation of magnetite nanoparticles in ferrofluids, *J. Magn. Magn. Mater*., 2010, 322, 1904–1911
- Smith C.L., Shah V.N., Kao T., Apostolakis G., NUREG/CR-5632: US Nuclear Regulatory Commission, **2001**.
- Stratmann M., Muller J., The mechanism of the oxygen reduction on rust-covered metal substrates, *Corros. Sci.*, 1994, 36, 327-359.
- Styrikovich, M.A., et.al., Solubility of Magnetite in Boiling Water at High Temperature, *Teploenergetika*, 1971, 18, 82.
- Subramanian V., Chandran S., Subramanian H., Chandramohan P., Bera S., Rangarajan S., Narasimhan S.V., Electrochemical characterization of oxide formed on chromium containing mild steel alloys in LiOH medium. Materials Chemistry and Physics 145 (2014) 499-509
- Subramanian V., Chandran S., Subramanian H., Chandramohan P., Bera S., Rangarajan S., Narasimhan S.V., Electrochemical characterization of oxide formed on chromium containing mild steel alloys in LiOH medium, *Mater. Chem. Phys*., 2014, 145, 499 – 509.
- Sweeton F. H., Baes C. F., The solubility of magnetite and hydrolysis of ferrous ion in aqueous solutions at elevated temperatures, *J. Chem. Thermodynamics*, 1970, 2, 479-500.

- Tapping R.L., Materials performance in CANDU reactors: The first 30 years and the prognosis for life extension and new designs, *J. Nucl. Mater.*, **2008**, *383*, 1-8.
- Thapa Deepa, Palkar V.R., Kurup M.B., Malik S.K., Properties of magnetite nanoparticles synthesized through a novel chemical route, *Mater. Lett.* 2004, 58, 2692-2694.
- Tremaine, P. R., LeBlanc, J. C., The Solubility of Magnetite and the Hydrolysis and Oxidation of Fe^{2+} in Water to 300 °C, *J. Solution Chem.*, 1980, 9, 415-442.
- Trevin S., FAC in Nuclear Power Plant Components in Nuclear Corrosion Science and Engineering, Damien Feron, Woodhead Publishing, Cambridge, UK, **2012.**
- Verwey E. J. W., Heilmann E.L., Physical Properties and Cation Arrangement of Oxides with Spinel Structures I. Cation Arrangement in Spinels, *J. Chem. Phys.*, 1947, 15, 174–180.
- Vollath D., Szabó D.V., Tyalor R.D., J.O. Willis, Synthesis and magnetic properties of nanostructured maghemite, *J. Mater. Res.*, 1997, 12, 2175-2182.
- Watanabe, Y., Hiroshi, A., Cr effect on FAC rate and its correlation with oxide layer characteristics, FAC2010 proceedings, Lyon 2010.
- Wielant J., Goossens V., Hausbrand R., Terryn H., Electronic properties of thermally formed thin iron oxide films, *Electrochim. Acta*, 2007, **52**, 7617–7625.
- William D. and Callister, R., Fundamentals of Materials Science and Engineering, Fifth Edition, John Wily & Sons Inc., USA, 2001.
- Zeng Y.M., Luo J.L., Norton P.R., study of semiconducting properties of hydrogen containing passive films, *Thin Solid Films* 2004, 460, 116–124.
- Zhang L., Macdonald D.D., On the transport of point defects in passive Fims, *Electrochim. Acta*, 1998, **43**, 679-691.

- Zheng Y.Y., Wang X.B., Shang L., Li C.R., Cui C., Dong W.J., Tang W.H., Chen B.Y., Fabrication of shape controlled Fe3O4 nanostructure, *Mater. Charact.*, 2010, 61, 489 – 492
- Zhu M., Du C.W., A New Understanding on AC Corrosion of Pipeline Steel in Alkaline Environment, *J. Mater. Eng. Perform.,* 2016, **26**, 221-228
- Zhu X. L., Lu X. F., Ling X., A novel method to determine the flow accelerated corrosion rate in the elbow *Mater. Corros.,* **2013**, 64, 486-492.
- Zhu, Y. Wu, Q. Synthesis of magnetite nanoparticles by precipitation with forced mixing, *Journal of Nanoparticle and Research* **1999**, 1, 393-396.
- Zhuo Z.H., Wang, J. Liu, X. Chan, H.S.O. Synthesis of Fe_3O_4 nanoparticles from emulsions, *Journal of Materials Chemistry* **2001**, 11, 1704.